Spectral Characterization of Cytochromes P450 Active Sites Using NMR and Resonance Raman Spectroscopy

Remigio Usai
Marquette University

SPECTRAL CHARACTERIZATION OF CYTOCHROMES P450 ACTIVE SITES USING NMR AND RESONANCE RAMAN SPECTROSCOPY

by

Remigio Usai,
BSc. Chemistry (Major) and Biochemistry (Major)
University of Zimbabwe, 2001

A Dissertation submitted to Faculty of the Graduate School,
Marquette University,
in Partial Fulfillment of the Requirements for
the Degree of Doctor of Philosophy

Milwaukee, Wisconsin

December 2017

ABSTRACT

SPECTRAL CHARACTERIZATION OF CYTOCHROMES P450 ACTIVE SITES USING NMR AND RESONANCE RAMAN SPECTROSCOPY

Remigio Usai, BSc.

Marquette University, 2017

The Cytochrome P450 (P450s) has been the subject of intense research for over six decades. An efficient approach for isotopic labeling of the prosthetic group in heme proteins was exploited to produce an analogue of the soluble bacterial cytochrome P450cam (P450cam) that contains a ^{13}C labeled-protoheme prosthetic group. HU227 strain of *E. coli*, which lacks the δ-aminolevulinic acid (δ-ALA) synthase gene, was employed in the heterologous expression of P450cam harboring a prosthetic group labeled with ^{13}C at the C_m and C_α positions by growing cells in the presence of [5-^{13}C] δ-ALA, which was synthesized in four steps from [2-^{13}C] glycine. NMR spectroscopy was used to confirm labelling of the hemes at the C_m and C_α positions. This system was utilized as proof of principle for the strategy of defining active site structure in cytochrome P450cam, including proton-to-proton distances on bound substrates, using NMR methods[1]. Such data are potentially of significant use in furnishing necessary experimental restrictions in docking routines, which are commonly employed in determining the relative affinities of drug candidates. 2D NOESY was employed and resonances assigned for the ^{13}C labeled reference positions on heme and substrate. To confirm these resonance assignments on camphor, a substrate analogue, norcamphor was used.

In another project, though it's widely accepted that a highly reactive Fe(IV)=O π-cation radical, compound I, facilitates the oxidation of relatively inert hydrocarbons, spectroscopic characterization of this putative intermediate has eluded detection under turnover conditions, presumably due to its very short lifetime. Chemically inert substrates of P450s have been utilized in a novel approach to capture and stabilize this transient intermediate and characterize it with resonance Raman (RR) spectroscopy coupled with cryoradiolysis studies. Specifically, perfluorodecanoic acid was utilized as an inert surrogate substrate of a thermophilic cytochrome P450 designated CYP119 which was reported to possess a stable compound 1[2]. Clearly, the presence of an inert substrate at low temperatures may prolong the lifetime of Compound I, allowing characterization by UV-visible and possibly RR and cryoradiolysis methods.

ACKNOWLEDGEMENTS

Remigio Usai, BSc.

I would like to express my heartfelt gratitude to Dr. Kincaid for providing me the opportunity to do research and his continued guidance mostly through group meeting sessions, support and patience throughout my entire time in his research group. I will forever be grateful for his guidance and mentorship during my time at Marquette University.

I would also like to thank my Committee members, Professors Michael D. Ryan, Daniel S. Sem and Adam Fiedler for enlightening discussions and insightful comments throughout my studies. I would also like to share my gratitude to Professor Michael D. Ryan for kindly offering his UV-vis instrument and glove box for use in my research. Also thanks to Professor Daniel S. Sem for giving me the opportunity to do some research on Cytochrome P450 2D6 in his lab where I met Professor Robert Burlage, a molecular Biologist who helped me a lot to jumpstart the transformation and purification of 2D6. I would also like to thank Dr. Chris Dockendorff for some helpful discussions on organic synthesis. I would also want to thank Dr. Cai Sheng for helpful contributions and technical assistance in NMR spectroscopy. Special thanks are due to all members of our research group, former and present Dr. K. Czarnecki, Dr. Mak Piotr, Dr. Daniel Kaluka, Dr. Ying Wang, Dr. Qianhong Zhu, Dr. Yilin Liu, Yuanqi Jing for the continued discussions. Without this wonderful crew, I would not have reached this point.

Finally, I dedicate this thesis to my family in Zimbabwe, my mother Margaret Chiranda and my late father Paul Madziwanzira Chiranda, my wife Alice Marufu Usai, my beautiful daughters Munashe, and the twins Chido and Chiedza Usai for their love, encouragement and support even though they were so many miles away from me. Their support and love gave me the guts to keep going. It would not have been possible without these wonderful souls. And above all, with a lot of boulders standing along the way, I thank the almighty God for the gift of life and the gift of all the wonderful people around me along this journey.

TABLE OF CONTENTS

LIST OF TABLES

TABLE OF FIGURES

CHAPTER 1

GENERAL INTRODUCTION

1.1 Cytochromes P450

1.1.1 Heme proteins

Heme proteins are metalloproteins that contain heme prosthetic group or closely related structural analogues. There are 4 types of hemes namely heme a, b, c and d [3,4] shown in Figure 1 below:

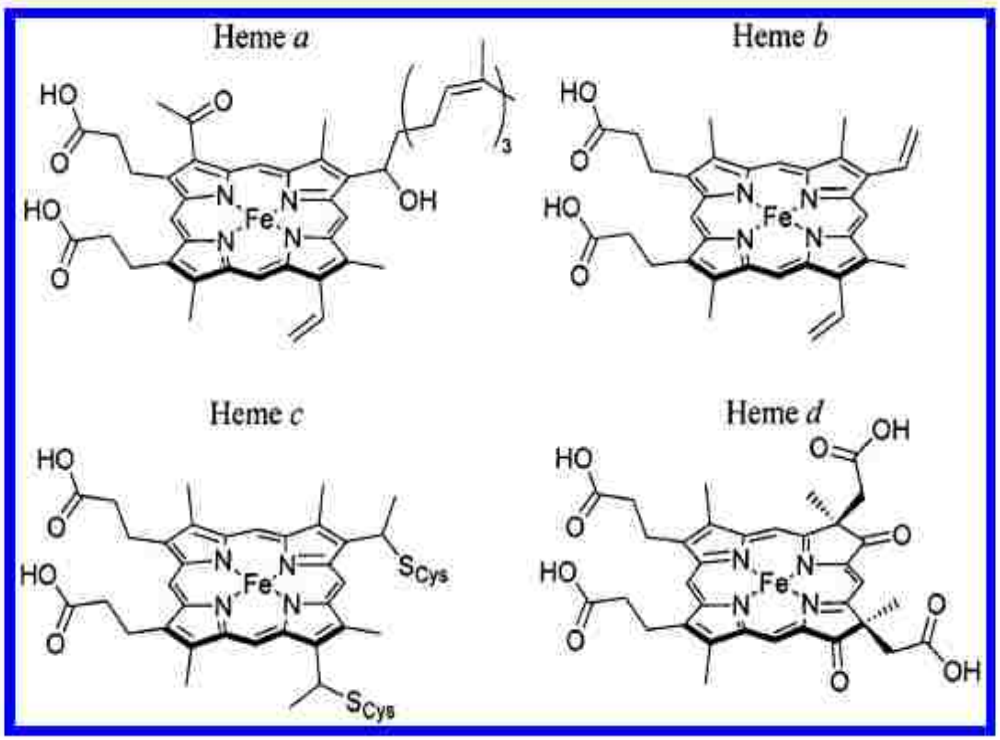

Figure 1 Chemical structures of four commonly occurring natural hemes a, b, c and d.[3,4,5]

The four individual pyrroles are labeled 1-1V. Heme b is by far the most common and its molecular structure and labeling of the heme is shown in Figure 2 below:

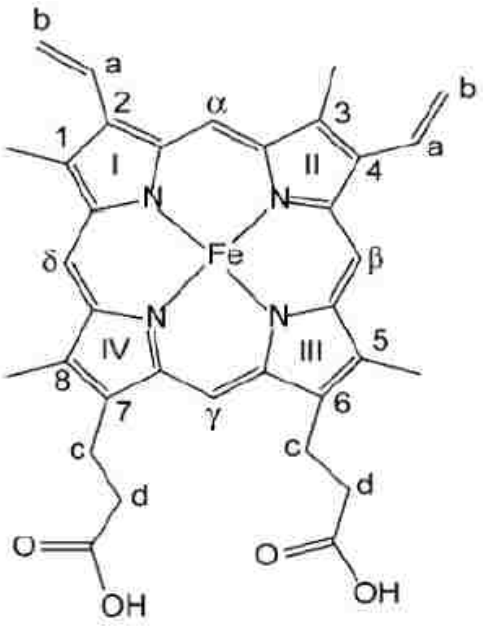

Figure 2 Molecular structure and labeling scheme of heme b.

They are virtually ubiquitous in all forms of life and exhibit remarkable functional diversity. The functions of heme proteins include reversible O_2 transport and storage[6] (hemoglobin and myoglobin respectively), reversible electron transfer[7] (cytochrome b_5), nitric oxide transport (nitrophorin) and catalysis of redox reactions[8] (nitric oxide synthase, peroxidase and cytochromes P450). Heme proteins have a variety of catalytic properties and the most fascinating is cytochrome P450s.

1.1.2 Discovery of P450

In 1955 Axelrod[9] and Brodie[10] first discovered the oxygenase enzyme system in endoplasmic reticulum of the liver. In 1958, Garfinkel[11] and Klingenberg[12] reported the special CO bound pigment in liver microsomes showing a strong Soret absorption maximum near 450 nm in the UV absorption spectrum as shown in **Figure 3** below. The discovery of cytochrome P450s is usually credited to Klingenberg who first reported that an intense absorption band near 450 nm[12] is formed when carbon monoxide is added to reduced rat liver microsomes by either diphosphopyridine nucleotide (DPNH) or dithionite. Therefore the name P450 coined for these enzymes is derived from the intense electronic absorption band of the ferrous CO adducts that maximizes near 450 nm[13]. CO binds to the heme, producing the unusual Soret, and inhibiting enzyme function, it would be useful to ascribe structure to the axial ligands in the ferrous cytochrome P450-CO complex.[14] From these early studies of P450s, research on P450s continued to increase and more enzymes discovered yearly. The generally agreed mechanism or catalytic cycle for P450s is shown in Scheme 1 below. Most of the intermediates have been characterized and resonance Raman (rR) which is described below has played a significant role in these studies.

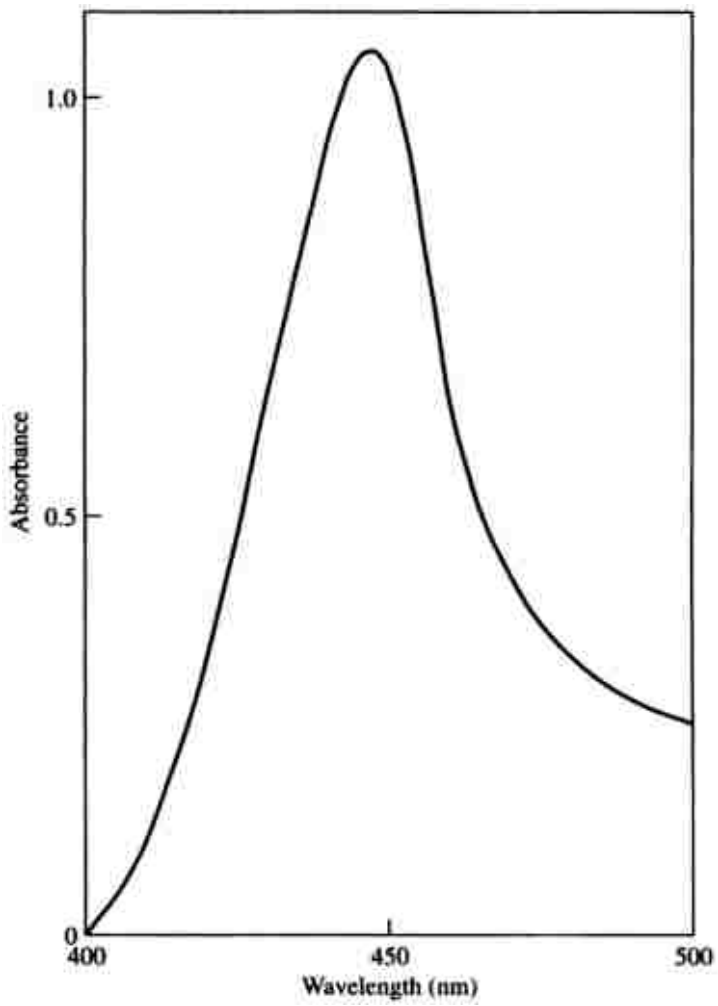

Figure 3 Absorption spectrum of Cytochrome P450-CO complex showing characteristic Soret peak at about 450 nm [11, 12]

1.1.3 Cytochromes P450

Cytochromes P450 (CYP, P450) are heme proteins with a cysteine thiolate axial ligand on the proximal side of the heme. Cytochromes P450 can efficiently catalyze the most difficult of reactions known to occur in biological systems, including: hydroxylation of very difficult inactivated hydrocarbon C-H bonds[15, 16, 17] using molecular oxygen. These metalloenzymes activate molecular oxygen and insert one of the oxygen atoms between the C-H bonds of the inert hydrocarbon, whereas the other oxygen is reduced to

water as shown in the general Equation **1** below. This superfamily represents the largest family of all proteins listed in the gene data banks.[18, 13]

Equation 1 General reaction of monooxygenation by cytochromes P450

$$R_3C\text{-}H + O_2 + 2e^- + 2H^+ \rightarrow R_3C\text{-}OH + H_2O$$

The study of cytochrome P450s is one of the most popular research topics in biochemistry and molecular biology due to due to their importance in medicine and biotechnology. Other application fields and P450 research areas are shown in **Figure 4** below.

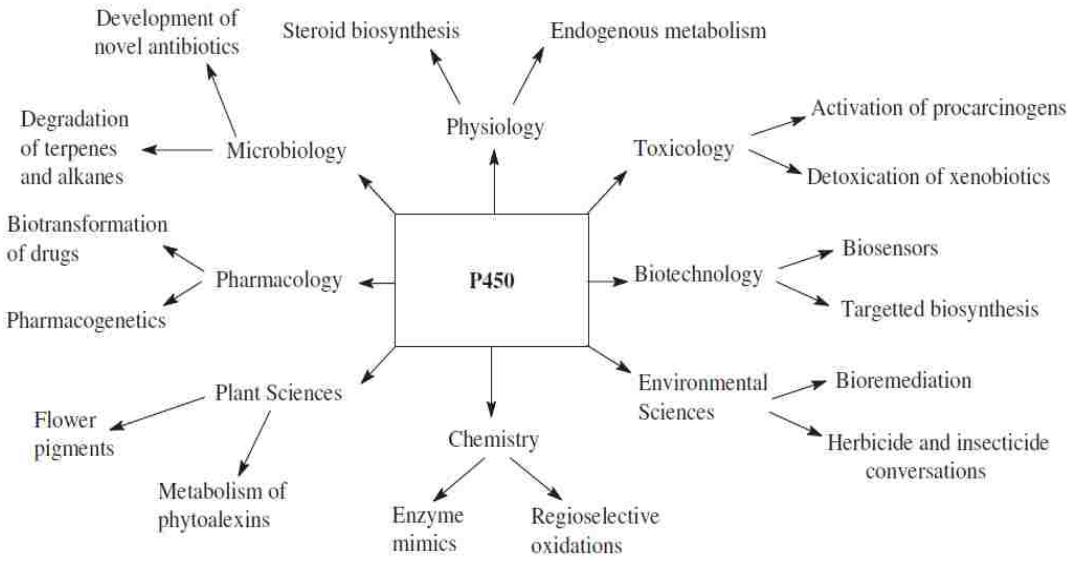

Figure 4 P450 research fields showing various inter-relationships between them.[19,20] The scheme is not intended to be comprehensive but to give the reader a flavor of the broadness of the P450 field.

1.1.4 The P450 catalytic cycle

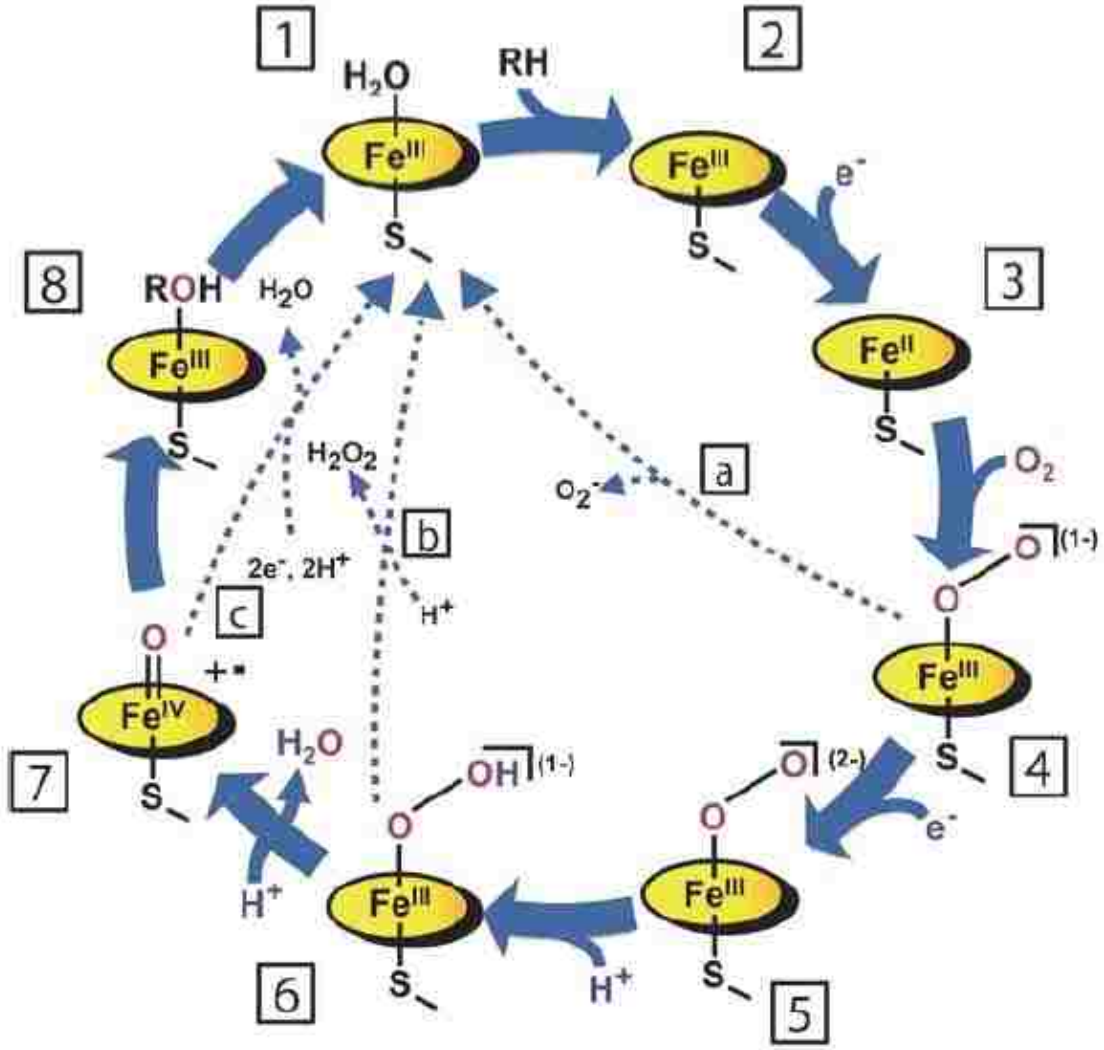

Scheme 1 Cytochrome P450 catalytic cycle[21]

The generally accepted catalytic cycle for P450s is shown in Scheme 1 above[21]. The cytochromes P450 perform this impressive chemistry utilizing the highly-concerted steps. The resting state of the enzyme is the substrate free and the heme iron is in the ferric state with five d-electrons in a low spin ((S = ½) configuration. This low spin is due to a large ligand field contributed by the axial cysteine thiolate (fifth ligand) and an

axially coordinated water molecule (sixth ligand).[8] The low spin is due to the electric field of the protein and not an intrinsic feature of the water complex.[22] The substrate binds to the six-coordinate (6C) ferric resting state [1]. Different substrates cause different percentage conversion from 6cLS to 5cHS. The substrate binding displaces the water cluster coordinated as the sixth ligand to the heme resulting in weakening of the ligand field hence converts it to high-spin (5cHS) (S = 5/2) electronic configuration. The 5cHS ferric substrate bound form [2] exhibits a more positive reduction potential (increasing from -330 mV to -173 mV) hence easily reduced to a ferrous species [3]. The electron for the reduction is passed from NADPH via a redox partner to the heme iron being reduced to the ferrous iron while still in high-spin state. Molecular oxygen binding to ferrous species forms an oxy-P450 species, which is more properly formulated as ferric superoxo intermediate [4]. A second electron transfer event results in reduction of the oxy P450 complex resulting in the formation of a nucleophilic peroxo intermediate ($Fe\text{-}O\text{-}O^{-}$) [5], which is easily protonated (from surrounding amino acid residues or water molecule) to the distal (terminal) oxygen atom to form the ferric hydroperoxo intermediate (Fe-O-O-H) [6]. Another protonation step results in cleavage of the O-O bond forming a water molecule and the very reactive π-radical cation species compound I [7] which catalyzes the oxygen insertion into the inert C-H bond to form the product ROH and reforms the resting form of the enzyme. The rR work has concentrated more on two sub-classes of P450s, bacterial and mammalian which are briefly described below:

1.1.5. Bacterial P450s

Bacterial P450s have been extensively studied because they are soluble, relatively stable and easily expressed. Most studied of these is cytochrome P450cam originally from *Pseudomonas putida* which is shown in Figure 5 below and its redox components has served as a model of these bacterial P450s with the goal of improving our understanding of cytochrome P450 structure and function[8, 23]. Another important bacterial protein studied is CYP102 which utilizes a fused mammalian-like diflavin reductase, therefore serving as a good mimic of mammalian P450s[8,23]. Also, well studied of bacterial cytochromes P450 is the thermophilic CYP119 which is also very soluble and has a high identity in the heme binding region with mammalian P450s consisting of a conserved cysteine for heme coordination and conserved threonine which facilitate coordination of a water ligand to the ferric heme, binding of oxygen to ferrous prosthetic group, and cleavage of the bound dioxygen molecule to give the final oxidizing species[24,25].

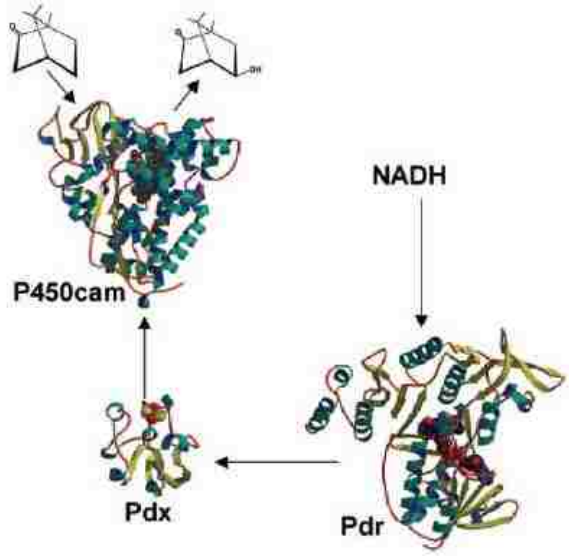

Figure 5 The structures of all three redox components of P450cam[26]

1.1.6. Mammalian P450s

The mammalian cytochrome P450s participate in a vast array of important physiological functions and are responsible for the metabolism of xenobiotics, including drugs and exogenous pollutants, as well as biosynthesis of steroids, fatty acids and vitamins.[8, 23, 27] Majority of these enzymes are very important for human health including CYP3A4 and CYP2D6. Cytochrome P450 2D6 is of great interest since it metabolizes about 20 % of known drugs.[28] Mammalian proteins are divided into drug metabolizing and steroidogenic P450s.

1.1.6.1 Drug Metabolizing P450s

These are enzymes involved in human drug metabolism due to their high levels of expression and broad substrate specificity, ≈75 % of available drugs are processed by these enzymes, with CYP3A4 and CYP2D6 having the largest contribution (45 % and 20 %, respectively). These enzymes generally have a malleable pocket, allowing one enzyme to catalyze a wider spectrum of substrates.[8, 23, 27]

1.1.6.2. Steroidogenic P450s

Approximately a quarter of the human P450s are involved in synthesis and modification of steroids. These P450s have more rigidly organized active sites and that accept a limited number of substrates but carry out highly stereo- and regioselective transformations.[8, 23] Major examples of steroidogenic P450s include CYP11A1, CYP17, and CYP19.

The study of intermediates discussed in the catalytic cycle is very difficult due to the high instability of the intermediates that will not accumulate to a useful extent. This has led to researchers developing many great techniques for stabilization of unstable intermediates and overcome these challenges.

1.1.7 Stabilization of unstable intermediates.

1.1.7.1 Rapid mixing methods

Important to understanding of P450 mechanisms of oxygenation was finding that artificial oxidants, such as H_2O_2, can be used in the place of reducing equivalents and oxygen for oxygenation of substrates.[29, 30] Studies were done with rapid freeze quench or cryogenic quenching techniques to study the intermediates.[31, 30]

1.1.7.2 Stopped flow techniques

Stopped flow studies using m-chloroperoxybenzoic acid (m-CPBA) revealed a spectral intermediate similar to what was expected for compound I in both P450cam[32, 33]and the thermophilic P450, CYP119.[34, 35] Similar studies have been employed by Ballou and coworkers[36, 37] to directly observe compound I. The compound I was generated by rapidly mixing the substrate free protein with m-chloroperoxybenzoic acid.

1.1.7.3 Cryoradiolysis

The cryoradiolysis approach which was pioneered by Martyn Symons and coworkers (1980s) and refined and used extensively by Hoffman, Sligar[38] and coworkers (1990-present), the intermediates along the catalytic cycle can be studied. The technique

involves irradiation of sample (at liquid nitrogen temperature) with ^{60}Co irradiation. This technique will be discussed in more detail later in chapter 3.

1.1.8 Optical properties of cytochromes P450

Nature has chosen heme as a cofactor for a wide range of heme proteins including cytochrome P450s. The iron-porphyrin complex intensely absorbs in the visible region hence proteins can be monitored by absorption spectroscopy. Moreover, heme proteins provide resonance Raman spectra because of high resonance enhancement of the chromophore when excitation line is tuned near the electronic transitions. The extended aromatic porphyrin ring gives rise to low-lying π-π^* electronic transitions that are excited with visible lasers[39,40].

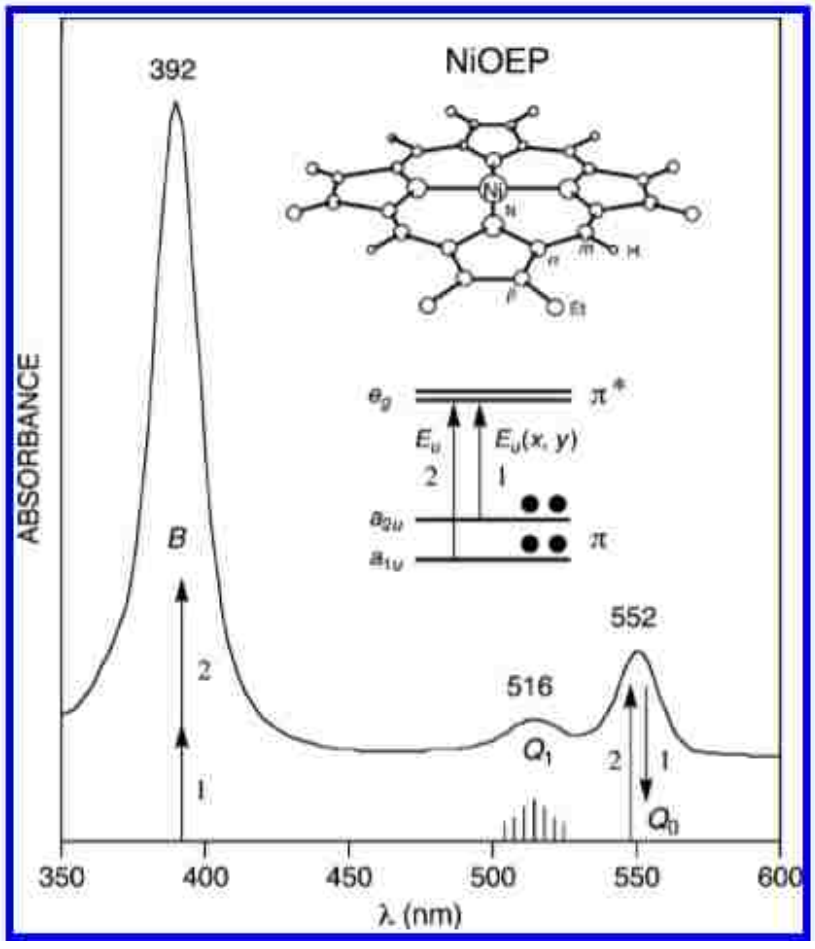

Figure 6 Absorption spectrum of NiOEP (OEP = octaethylporphyrin).[41, 40]

Figure 6 above shows the absorption spectrum of NiOEP, illustrating the typical spectral signature of a metalloporphyrin: the intense Soret (or B) band near 400 nm, and a pair of weak bands near 520 nm and 550 nm called Q_1 (or α) and Q_0 (or β) bands respectively. In idealized D_{4h} symmetry of the tetrapyrrolle ring, the lowest unoccupied molecular orbitals π^* (LUMO) are degenerate and have e_g symmetry while the highest occupied molecular orbitals π (HOMO) are of a_{1g} and a_{2u} symmetries. The two HOMOs have nearly similar energy and there is large interaction between the orbital excitations: $a_{1g} \rightarrow e_g$ and $a_{2u} \rightarrow e_g$ the transition dipoles adding up for the intense Soret band (392 nm) and nearly canceling out for the weaker Q_0 transition (552 nm). About 10 % of the B band intensity is borrowed by the Q transition, producing the Q_1 vibronic side band at 516 nm[40].

1.2 Raman Spectroscopy of heme proteins

Raman spectroscopy is a technique discovered by an Indian scientist C. V. Raman in 1928[42, 43]. This technique is used to study vibrational modes. It is done by scattering light from an intense source, in modern times a laser. In Raman spectroscopy, the sample is irradiated by an intense laser in the UV-visible region (ν_o) and the scattered light is observed usually in the direction perpendicular to the incident beam. The scattered light consists of two forms namely: Rayleigh scattering (strong and has same frequency as the incident beam (ν_o)) and Raman scattering (very weak and has frequencies (ν_o) ± (ν_m), where ν_m is the vibrational frequency of the molecule). If an incident photon encounters a molecule that is in the ground vibrational state (v_0), then it loses energy and can be scattered as a low energy photon. This is called Stokes Raman scattering. Contrary to that, if an incident photon encounters a molecule that is already in the excited vibrational state (v_1), then it can gain energy from the molecule and be scattered as a high-energy photon. This is called anti-Stokes Raman scattering, see **Figure 7** below. According to the Boltzmann distribution, the excited vibrational states are not well populated at room temperature and this population diminishes as the energy of the vibrational states increases. Therefore, observations are made on the Stokes Raman bands. Scattered light is focused by collection lens and focused onto the entrance slit of the single monochromator equipped with a CCD detector.

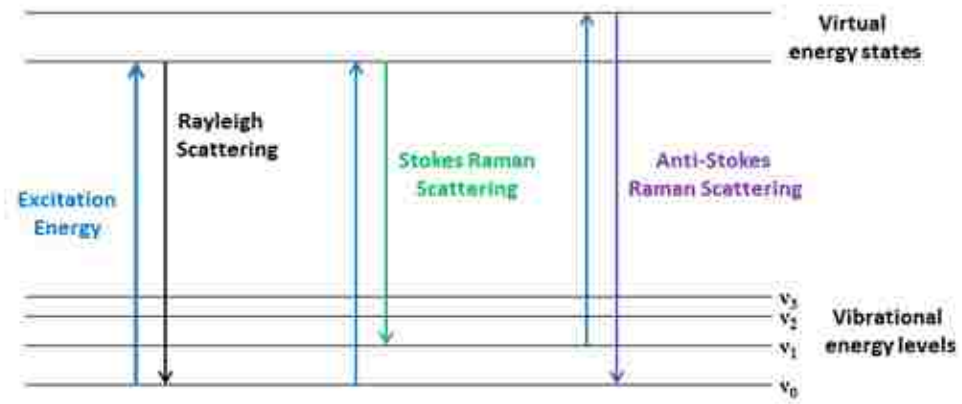

Figure 7 Schematic representation of the Raman Effect

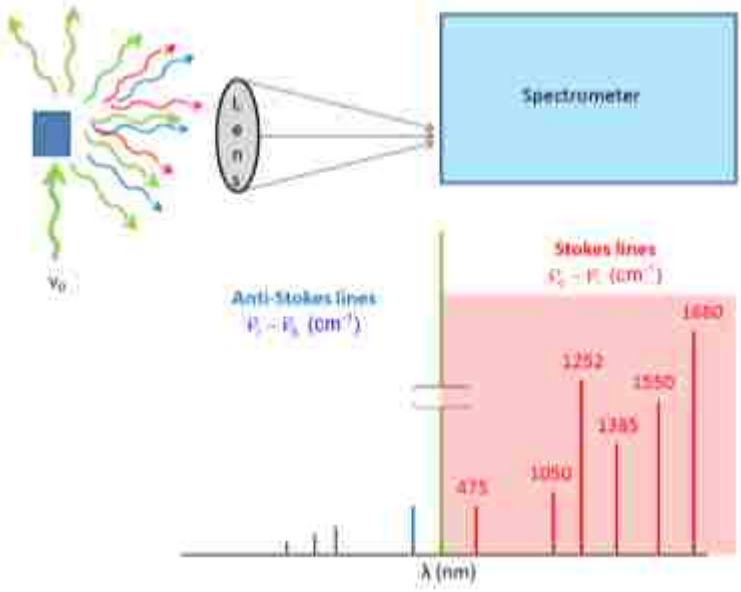

Figure 8 Raman scattering spectroscopy

Raman scattering is a very weak process with very low probability of photon and molecular energy exchange, thus requires a very high concentrated sample, i.e. molar range. The sensitivity issue is the major disadvantage of conventional Raman

spectroscopy and is largely overcome by using resonance Raman spectroscopy which is discussed next.

1.2.1 Resonance Raman spectroscopy

Instrumentation

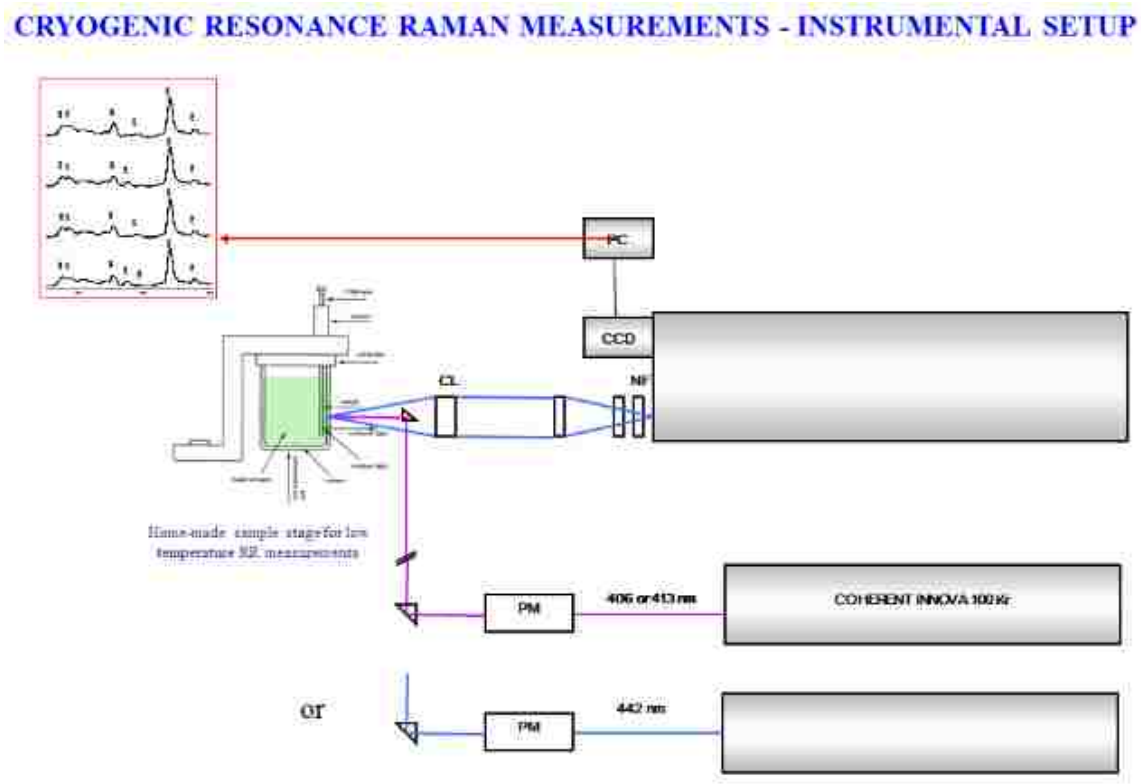

Figure 9 Schematic diagram and view of a cryogenic resonance Raman instrument setup, collimating lens (CL), notch filter (NF), and Charge coupled device (CCD).

Resonance Raman spectroscopy involves use of excitation lines whose excitation frequency approaches the energy of the electronic transition of the target chromophore. The technique is well suited for studying complex biological molecules like heme proteins inasmuch as it permits active site interrogation owing to its ability to selectively enhance vibrational modes of the chromophoric heme prosthetic group.[44] This powerful spectroscopic tool has long been established as an exquisite probe of active site structure for a wide range of heme proteins and enzymes.[44–46] The technique offers a major

advantage over IR spectroscopy in that there is no interference from water making it a method of choice for studying vibrational properties of proteins, samples of which are typically in aqueous buffers. The vibrational modes of the prosthetic heme group buried in the active site of these large biological polymers are selectively enhanced by exploiting laser (excitation) lines which are in or near resonance with the Soret or Q bands electronic transitions.

Isotopic labeling (^{15}N, ^{13}C and ^{2}H) of high symmetry model compounds, such as metal complexes of tetraphenylporphyrin (H_2TPP), octaethylporphyrin (H_2OEP), etioporphyrins (H_2(EtioI)) and (H_2(EtioIII), has been used to unambiguously assign heme core vibrational modes.[47,48] If each peripheral substituent of the iron protopophyrin IX complex is considered as an atom, the heme has D_{4h} symmetry having a total of 37 atoms and 105 vibrational modes. The modes consist of 71 in-plane (ip) modes (2N-3) (where N=37 atoms) and 34 out-of-plane (oop) modes (N-3) and are classified as follows:

Equation 2 Heme vibrational modes

$$\Gamma_{ip} = 9A_{1g} + 8A_{2g} + 9B_{1g} + 9B_{2g} + 18E_u$$

$$\Gamma_{oop} = 3A_{1u} + 6A_{2u} + 5B_{1u} + 4B_{2u} + 8E_g$$

Only the g (gerade, meaning even) are Raman active hence of the 71 in-plane vibrational modes 35 (g symmetry) are Raman active whereas 18 (E_u) (ungerade, meaning uneven) are infrared active.

Most applications have focused on the so-called marker bands in the high frequency region, which effectively document oxidation and spin states of the central iron, in addition to providing a reliable indicator of heme core size.[45,47] The oxidation

marker band (ν_4), occurring at ~1360 cm^{-1} in Fe(II) and ~1375 cm^{-1} in Fe(III) species, is ascribable to the pyrrole ring symmetric stretch, which is very sensitive to the oxidation state of the central iron. The so-called spin state marker bands (ν_2, ν_3 and ν_{10}) report on the core size and spin state of the iron center (Table 1).

Table 1 Assignment and frequencies of in-plane vibrational modes of some nickel porphyrin complexes[45]

Symmetry	ν_i	Description	NiOEP	NiP	NiTPP
A_{1g}	ν_1	$\nu(C_m\text{-}X)$	[3041]	[3042]	1235
	ν_2	$\nu(C_\beta C_\beta)$	1602	1575	1572
	ν_3	$\nu(C_\alpha\text{-}C_m)_{sym}$	1520	1459	1470
	ν_4	ν(Pyr half ring)$_{sym}$	1383	1376	1374
	ν_5	$\nu(C_\beta\text{-}Y)_{sym}$	1138	[3097]	[3097]
	ν_6	ν(Pyr breathing)	804	995	1004
	ν_7	δ(Pyr def)$_{sym}$	674	731	889
	ν_8	ν(Ni-N)	360/343	369	402
	ν_9	$\delta(C_\beta\text{-}Y)_{sym}$	263/274	1066	1079
B_{1g}	ν_{10}	$\nu(C_\alpha\text{-}C_m)_{asym}$	1655	1650	1594
	ν_{11}	$\nu(C_\beta C_\beta)$	1577	1505	1504
	ν_{12}	ν(Pyr half ring)$_{sym}$	1331	1319	1302
	ν_{13}	$\delta(C_m\text{-}X)$	1220	1185	238
	ν_{14}	$\nu(C_\beta\text{-}Y)_{sym}$	1131	[3097]	[3097]
	ν_{15}	ν(Pyr breathing)	751	1003	1009
	ν_{16}	δ(Pyr def)$_{sym}$	746	730	846
	ν_{17}	$\delta(C_b\text{-}Y)_{sym}$	305	1060	784
	ν_{18}	ν(Ni-N)	168	237	277
A_{2g}	ν_{19}	$\nu(C_\alpha\text{-}C_m)_{asym}$	1603	1611	1550
	ν_{20}	ν(Pyr quarter ring)	1394	1354	1341
	ν_{21}	$\delta(C_m\text{-}X)$	1307	1139	[257]
	ν_{22}	ν(Pyr half ring)$_{asym}$	1121	1005	1016
	ν_{23}	$\nu(C_\beta\text{-}Y)_{asym}$	1058	[3087]	[3087]
	ν_{24}	δ(Pyr def)$_{asym}$	597	806	828
	ν_{25}	δ(Pyr rot.)	551	429	560
	ν_{26}	$\delta(C_\beta\text{-}Y)_{asym}$	[243]	1317	1230
B_{2g}	ν_{27}	$\nu(C_m\text{-}X)$	[3041]	[3041]	1269
	ν_{28}	$\nu(C_\alpha\text{-}C_m)_{sym}$	1483	1504	[1481]
	ν_{29}	ν(Pyr quarter ring	1407	1368	1377
	ν_{30}	ν(Pyr half ring)$_{asym}$	1160	1003	1004
	ν_{31}	$\nu(C_\beta\text{-}Y)_{asym}$	1015	[3088]	[3087]
	ν_{32}	δ(Pyr def)$_{asym}$	938	819	869
	ν_{33}	δ(Pyr rot.)	493	435	450
	ν_{34}	$\delta(C_\beta\text{-}Y)_{asym}$	197	1193	1191
	ν_{35}	δ(Pyr tranl.)	144	197	109
E_u	ν_{36}	$\nu(C_m\text{-}X)$	[3040]	[3042]	[1254]
	ν_{37}	$\nu(C_\alpha\text{-}C_m)_{asym}$	[1637]	1624	[1586]
	ν_{38}	$\nu(C_\beta C_\beta)$	1604	1547	[1552]
	ν_{39}	$\nu(C_\alpha\text{-}C_m)_{sym}$	1501	1462	[1473]
	ν_{40}	ν(Pyr quarter ring)	1396	1385	[1403]
	ν_{41}	ν(Pyr half ring)$_{sym}$	[1346]	1319	[1331]
	ν_{42}	$\delta(C_m\text{-}X)$	1231	1150	[233]
	ν_{43}	$\nu(C_\beta\text{-}Y)_{sym}$	1153	[3097]	[3097]
	ν_{44}	ν(Pyr half ring)$_{asym}$	1133	1033	[1003]
	ν_{45}	$\nu(C_\beta\text{-}Y)_{asym}$	996	[3087]	[3100]
	ν_{46}	δ(Pyr)$_{asym}$	927	806	[864]
	ν_{47}	ν(Pyr breathing)	766	995	[1023]
	ν_{48}	δ(Pyr)$_{sym}$	605	745	[895]
	ν_{49}	δ(Pyr rot.)	544	366	[512]
	ν_{50}	ν(Ni-N)	[358]	420	[436]
	ν_{51}	$\delta(C_b\text{-}Y)_{asym}$	328	1064	[1093]
	ν_{52}	$\delta(C_\beta\text{-}Y)_{sym}$	263	1250	[1213]
	ν_{53}	δ(Pyr transl)	212	282	[306]

1.2.2 RR spectroscopy of cytochrome P450

Resonance Raman studies of wild type P450cam (CYP101) and mutants has been extensively studied to understand structure/ function relationships. Most of the assignments of Raman bands for P450s have been done based on model compounds.[49,50,47] The oxidation state marker band, ν_4 is around 1373 cm^{-1}, characteristic of the ferric (FeIII) state.[51,52] The spin state marker bands are ν_3, ν_2 and ν_{10} which occur around 1503 cm^{-1}, 1583^{-1} and 1638 cm^{-1} respectively for 6cLS. Substrate binding results in the shift of the spin state marker bands, ν_3 and ν_2 to 1488 cm^{-1} and 1566 cm^{-1} for 5cHS species.

Table 2 Cytochrome P450cam heme core marker bands. Adapted from ref [53].

Form	Oxidation state	Coordination and spin state	ν_4	ν_3	ν_2	ν_{10}
		P450				
P450 SF	Fe(III)	6cLS	1373	1503	1584	1637
P450 SB	Fe(III)	5cHS	1372	1488	1570	1623
P450 SF	Fe(II)	5cHS	1345	1468	1563	1601
P450 SB	Fe(II)	5cHS	1345	1466	1564	1601
P450 SB	Fe(II)–CO	6cLS	1371	1497	1588	
		P420				
P420 SF	Fe(III)	6cLS	1374	1503	1588	1629
		5cHS		1491	1572	
P420 SB	Fe(III)	6cLS	1374	1503	1588	1629
		5cHS		1491	1572	
P420 SF	Fe(II)	6cLS	1361	1493	1583	1620
		5cHS		1470	1560	1603
P420 SB	Fe(II)	6cLS	1361	1493	1583	1620
		5cHS		1470	1560	1603
P420 SF	Fe(II)–CO	6cLS	1372	1498	1583	1626

1.2.3 Metal ligand interactions in heme proteins

Heme proteins are capable of binding various exogenous diatomic ligands; e.g., CO, O_2, NO and CN^- with differing geometries ranging from linear to bent configurations. Clearly, the ligand of most interest in P450 chemistry is dioxygen, including its reduced peroxo- and hydroperoxo- intermediates (scheme 1). Unfortunately, most of oxygenated intermediates are unstable and therefore difficult to trap and spectroscopically characterize. To better understand the chemical environment of the P450 distal pocket, RR spectra are acquired with other more stable, diatomic ligand complexes of P450, including CO, NO and CN^-. The Fe-X-Y fragments can interact with the distal pocket polar residues and be distorted by steric interactions with non-polar distal pocket residues, thus mimics physiologically relevant oxy complexes.

The bonding between the metal center and a diatomic molecule, XY, involves σ and π interactions. The XY molecules have vacant or partially unoccupied π^* orbitals that match well with the filled d_π orbitals of the central metal ion (Fe). This orbital geometry results in the Fe-XY π back-bonding, where donation of electron density from Fe ion to XY in the $d\pi$-π^* system occurs. Due to this back-bonding, the Fe-X bond becomes stronger while X-Y bond becomes weaker.[21]

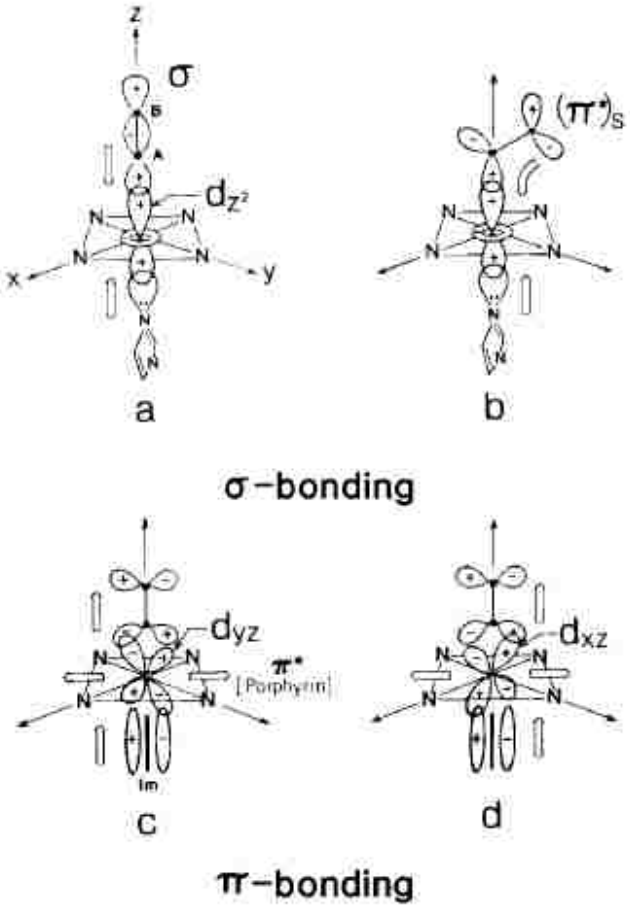

Figure 10 Schematic representation of σ- and π- bonding in porphyrin[54, 55]

1.3 NMR Spectroscopy of heme proteins

NMR is a very useful technique for investigating structure-function relationships in metalloproteins. NMR is used to investigate the electronic environment and physical structure of the heme and its protein environment for several oxidation/ spin states of the protein.

Experimental distance restraints data obtained from proton-proton NOEs (Nuclear Overhauser effect) are the primary data used to define the secondary and tertiary structure of a protein. NOEs arise from through space dipole-dipole interactions of nearby protons, rather than through bond interactions. Therefore, distances of protons nearby in space, ≤ 5Å can be derived even though the protons may be on residues far away in the primary sequence of the protein. The intensity of the NOE cross peak is proportional to the inverse of the sixth power of the distance between the two nuclei due to averaging caused by rotational motion.

NMR can be applied to molecules for which no single crystal structures are available. Comparison can also be made from the solution state structure derived from NMR spectroscopy and the X-Ray crystal structure i.e. the methods complement each other.[56] NMR of protein solution can be employed to help the assignment of heme or amino acid proton signals and consequently determine the 3D structure from solution state of protein hence complement X-Ray diffraction data. NMR as a tool has much to offer for all hemeproteins. The NMR spectra of paramagnetic hemes show some hyperfine shifted regions easy for analysis e.g. the hyperfine shifted regions are very well resolved and outside the diamagnetic region (0-10 ppm window). However paramagnetic hemes have large linewidths in high spin forms but reduced linewidths in low spin forms.

Studies with a paramagnetic heme ferric-CN (low spin) were done in our lab and will be discussed briefly. It is noted that diamagnetic heme protein signals exhibit less line broadening, however the window is in the strongly overlapped region only showing little except that the protein is folded[57].

In high resolution NMR experiment an NMR tube containing the sample solution of interest is placed in a magnetic field B_0 and then subjected to irradiation by one or several of radio-frequency (rf) pulses, B_1, B_2 or B_3 as shown in **Figure 11**. Under the influence of B_0 the nuclear spins are polarized and net macroscopic magnetization (M_0) is along the Z axis. B_1 applied along the X axis causes a torque on M_0. The corresponding free induction decay (FID) is recorded during a period of ≈ 1 s, and the NMR spectrum is obtained by Fourier transform (FT) of the FID.

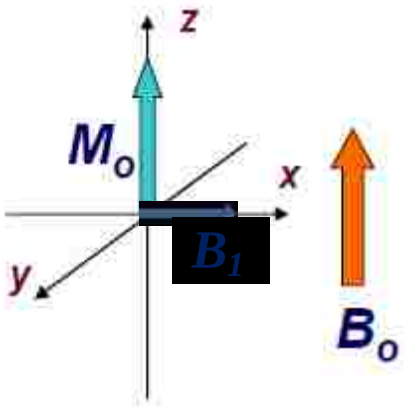

Figure 11 NMR signal obtained after application of a magnetic field

1.3.1 The Nuclear Overhauser effect (NOESY)

NOESY refers to the fractional change in intensity of one NMR line when another resonance is irradiated in a double irradiation experiment (cross polarization of nuclear spins). Nuclear Overhauser effects are due to dipolar interactions (through space interactions) between different nuclei and are correlated with the inverse of the sixth power of the internuclear distance[58], where r is radial distance from the proton of origin. (see expression below)

NOE signal $\propto 1/r^6$

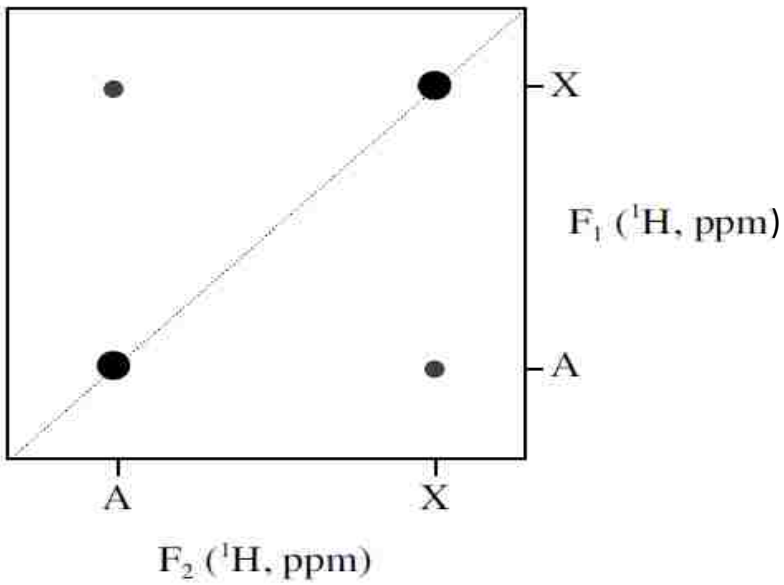

Figure 12 Simple 2D NOE spectrum

Figure 12 above shows diagonal peaks and a cross peak obtained from protons which are less than 5 Å in space. Diagonal peaks have the same frequencies in both F1 and F2 dimensions and they arise from coherence that is not transferred between spins during the mixing period.[59] Cross peaks have different frequencies in F1 and F2

dimensions and result from the transfer of coherence from one spin to the other during mixing period of the experiment. Correlation between those protons close in space is indicated by a cross peak and the peak intensity is inversely proportional to the distance between the protons as described above.

NOESY is the main technique employed to determine distances between protons attached to labeled ^{13}C positions and protons on the substrate or on protein residues. To get distances a comparison of intensity of cross-peak with a reference pair of atoms of known separation distance is the easiest way to use:

$$\eta_A\{B\}/\eta_X\{Y\}=r^{-6}_{AB}/r^{-6}_{XY}$$

where distance of XY is found relative to known reference distance AB.[60]

^{13}C filtering helps eliminate thousands of other resonances and see only resonances from protons we care about in the active site. Labeling is necessary to enable labeled carbons to act as marker positions thus filtering can be done using protons attached to these reference positions. One of the initial aims of my work was to generate camphor deuterated at 5n and 5x positions to be used to check NOE signals in experiments done previously done in our lab and these efforts are described, though recently another approach to verify this effect has been undertaken, as described below.

The first project involves NMR studies including NOE of P450cam which is labeled all methine carbons as proof of principle that experimental parameters can be obtained. The preparation of labeled samples will be discussed incorporating a method described in Mario Rivera's[61] paper of 2006. The approach involves using aminolevulinic acid (ALA) labeled ^{13}C at the 4-position. This approach makes it possible to supplement ^{13}C labeled ALA in some forms of bacteria which lack the ALA synthase gene hence the labeled ^{13}C is incorporated into the heme during protein expression. In the present work, focus was placed on using the Huber strain HU227 which was donated as a kind gift from Dr. Raner[62] from the University of North Carolina at Greensboro. Transformation and expression of P450cam will be done using the mutant form of *Escherichia coli (E. coli)* HU227 which is unable to produce aminolevulinic acid (ALA) naturally. This *E. coli* strain has a mutation in the hemA gene which encodes for glutamyl-tRNA[63]. Glutamyl tRNA is required for biosynthesis of ALA, which is the precursor in the biosynthesis of heme. Therefore, by supplementing labeled ALA it is possible for high level incorporation of labeled ^{13}C into the heme.

However to get the labeled ALA, the method outlined mainly in Kajiwara's paper[1] was used starting with labeled glycine and protecting the reactive amine by use of Phthalic anhydride, activating the acetic acid to acetyl chloride, coupling reaction and hydrolysis to remove the protecting group. This is discussed in more detail in chapter 2. Once the methine carbons are labeled, ^{13}C NOE filtered experiments were employed to get resonances from the protons on reference ^{13}C labeled carbons and protons on the substrate. This technique allows us to calculate distances between protons hence important experimental data obtained which can be used to refine docking parameters.

1.4 Specific issues to be addressed in this work

1.4.1 Utility of NMR in mapping active site of substituted hemes e.g. cytochromes P450

Docking of substrates to the active site of P450s is an active research area for pharmaceutical chemists, whereby the substrate or inhibitor is docked into the active site of the enzyme to see the most energetically favorable structure. However, there is a deficiency of experimental evidence to use for the docking studies. The goal of this first project is to use NMR with labeled heme to provide distances between substrate and sites within the enzyme which contain isotopically labeled heme groups.

A lot of substrates have been docked into the active site of the enzyme. However, there is no direct experimental evidence for the binding form of the enzyme. Use of NMR will possibly help to get some distances from specifically labeled sites on the heme groups and some nearby protons from the substrate, hence refining the docking parameters. P450cam labeled with isotopically labeled heme will be used as the proof of principle method for the studies. Previous studies in our lab had provided preliminary evidence that we can obtain distances from labeled heme to the substrate hence to complete this project, initial efforts were made to synthesize 5,5'-d_2 camphor in order to confirm assignments made. As will be seen, many difficulties were encountered and one reasonable alternative option, to employ structural analogues of camphor to confirm these results, have now been pursued.

1.4.2 Utilization of fluorinated substrates to stabilize Compound 1 intermediates of cytochromes P450 (CYP119)

Cytochromes P450 bind and cleave dioxygen to generate a potent intermediate (compound I) capable of hydroxylating relatively inert hydrocarbon substrates. The compound I form of CYP 119 has been reported to be more stable as compared to other P450s rendering this bacterial P450 an attractive choice in employing chemically inert substrates to stabilize this rather fleeting intermediate. Stabilization of these forms will possibly facilitate their characterization with resonance Raman spectroscopy. Also, studies of oxy complexes of CYP 119 will be done including cryoradiolysis of the oxy samples to study intermediates in the catalytic cycle for CYP119 including oxy, hydroperoxo and, most importantly, compound I.

CHAPTER 2

UTILITY OF NMR IN MAPPING ACTIVE SITE OF SUBSTITUTED HEMES

e.g. CYTOCHROMES P450

2.1 Introduction

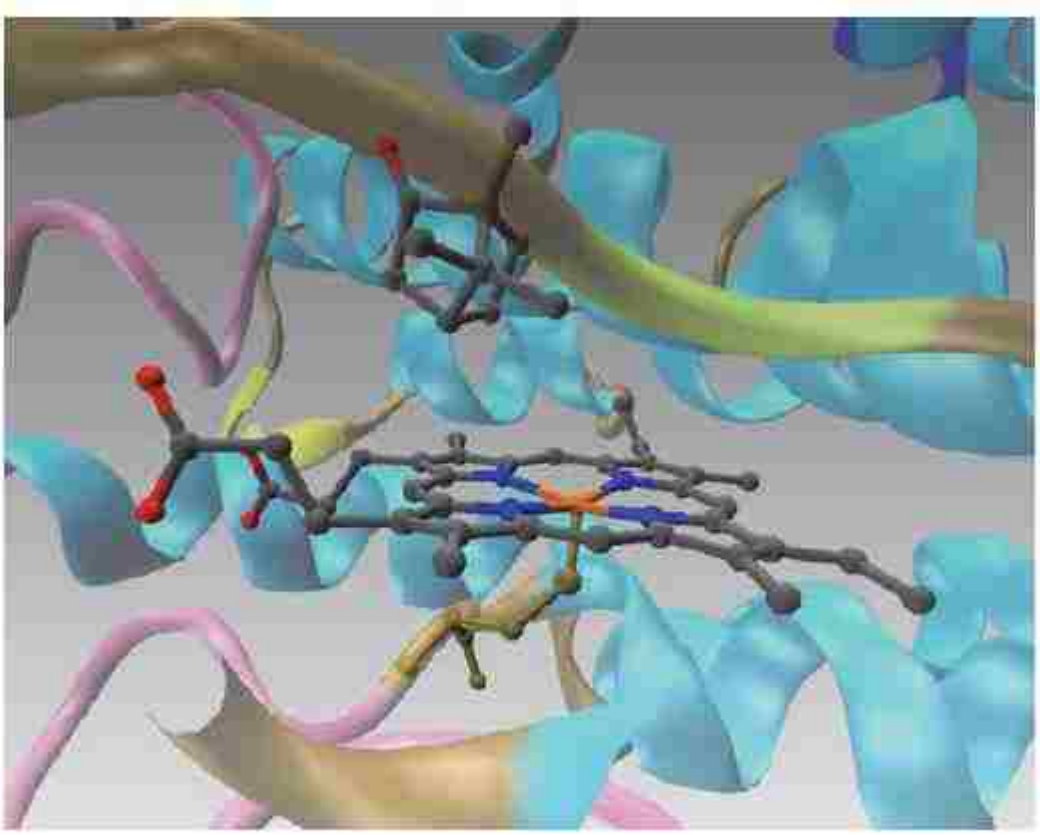

Figure 13 The active site of camphor bound cytochrome P450cam[64] (Adapted from reference 64, PDB 2CPP)

A very important issue of general interest is understanding how various substrates interact with the proteins. A lot of research in the previous decades has focused on

studying drug metabolizing enzymes, specifically drug metabolizing cytochromes P450. The main goal includes understanding how substrates can fit into various P450s; i.e., gaining detailed information about how various substrates, including pharmaceuticals and pollutants, interact with drug metabolizing P450s.

One practical application of these studies is in drug design, where possible drug candidates are pre-screened using docking studies (a computer-based approach for identification of bound conformation of substrates and prediction of binding affinity). There are a lot of possible conformations in which substrates fit into active sites (especially for promiscuous drug-metabolizing enzymes which metabolize more than one substrate) hence if some experimental parameters are known will restrict docking results. Therefore, the goal of this work is to figure out how to get distances of a given substrate in the pocket. One way to get distances is to use two-dimensional Nuclear Magnetic Resonance (2D NMR) spectroscopy, specifically Nuclear Overhauser Effect spectroscopy to find distances between nearby protons. The main challenge for the method is that it picks thousands of these proton-proton resonances since proteins are very large polypeptide chains with thousands of protons. Hence one way to overcome this challenge is to focus only at a few protons we care about near the active site by labeling heme with ^{13}C at some definite positions hence look at resonances from protons on the labeled anchors. This will enable ^{13}C-filtering hence looking at only resonances from labeled positions on heme and other protons near the active site using this methodology. To incorporate ^{13}C into the heme simple bacterial expression system Cytochrome P450cam will be used as proof of principle.

Bacterial P450s

The cytochromes P450 are typically present in large numbers in eukaryotic cells than prokaryotic cells. However, bacterial P450s can be easily expressed and purified, they are soluble and relatively stable than mammalian P450s hence most of the understanding of P450 structure and mechanism was gained mainly using bacterial enzymes. Cytochrome P450cam (CYP101) originally obtained from *Pseudomonas putida* and now expressed in *E. coli* systems will be used in this work. Cytochrome P450cam has been expressed in our lab before but our interest was to incorporate the ^{13}C label. Locally there is a strain of bacteria (HU227-a kind gift from Professor Raner, G. M. (The University of North Carolina at Greensboro) which cannot make its own aminolevulinic acid (ALA, a heme-precursor). HU227 strain of bacteria was used, supplementing the growth medium with 5-^{13}C ALA.

2.1.1 Synthesis of [5-^{13}C] δ-Aminolevulinic acid (ALA)

ALA is the first common precursor in the tetrapyrrolle biosynthetic pathway, leading to hemes, chlorophylls, vitamins etc. There have been several methods reported for the synthesis of ALA but these suffer from disadvantages of multi-step routes, low yields and inconvenient purification resulting in high cost of synthesis of both unlabeled and labeled ALA. Here we report an efficient approach to synthesize ALA using labeled glycine.

ALA can be synthesized starting with glycine, a cheap chemical from Sigma Aldrich. For practice the unlabeled glycine was used to form unlabeled ALA. Since we are interested in incorporating a ^{13}C label, 2-^{13}C glycine was used to form [5-^{13}C] δ-ALA. Aminolevulinic acid (ALA) was synthesized in four steps by the condensation of glycine and phthalic anhydride, followed by the conversion to the chloride, coupling reaction with a three-carbon unit and hydrolysis. This was adapted from previously published procedures[1, 65] with minor modifications.

2.1.2 Expression of [5-^{13}C] δ-ALA P450cam

The expression of [5-^{13}C] δ-ALA P450cam is essentially like the expression of wild type P450cam, with only one exception that 20 mg/L of [5-^{13}C] δ-ALA is supplemented to the growth medium. Since HU227 strain of *E. coli* cannot make its own ALA, the labeled ALA is taken up and forms the labeled heme as described in Figure 16 below. Cytochrome P450cam is used as proof of principle, see **Figure 14** below

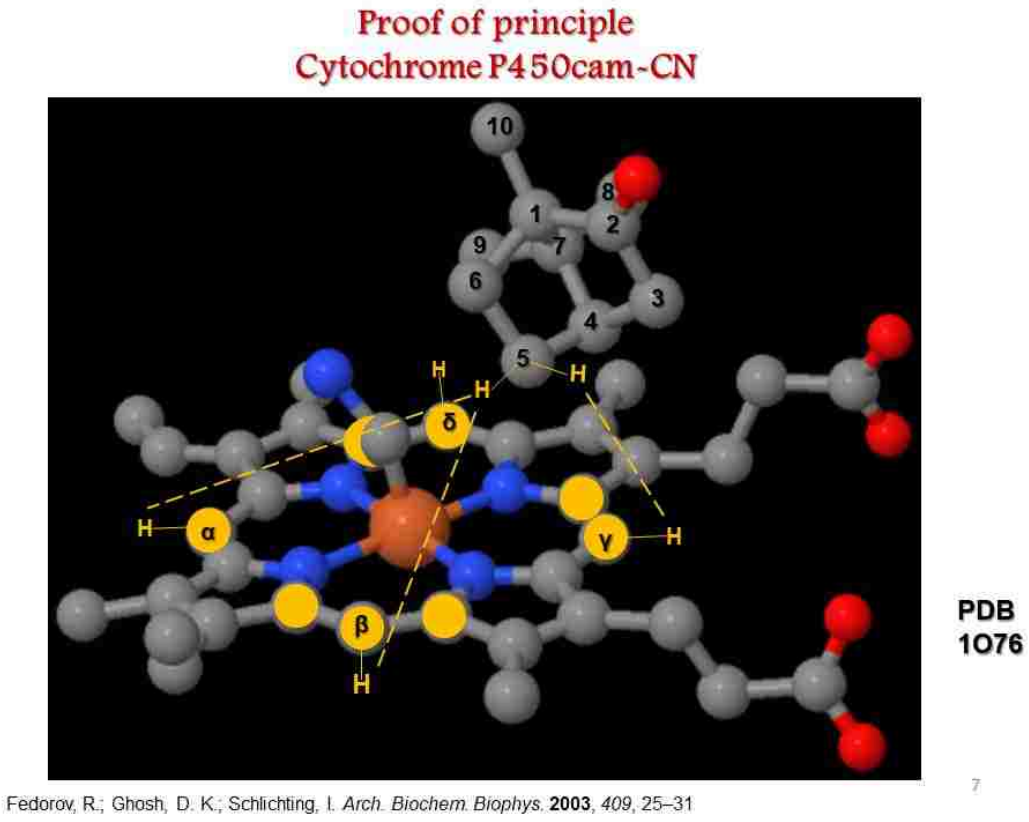

Figure 14 The active site of P450cam with camphor bound showing distances from protons on ^{13}C-labelled positions on heme (yellow) to protons on substrate molecule[66] (Adapted from reference 66)

2.2 Material and Methods

Chemicals were of high quality grade and used as received unless stated otherwise. Most chemicals were purchased from Sigma Aldrich. HU227 strain of *E. coli* was a kind donation from Professor Raner. Unlabeled glycine was purchased from Sigma Aldrich. Phthalic anhydride, Thionyl chloride, Toluene, Zinc/ copper couple, Ethyl 3-bromopropionate, 2-butanone, sodium iodide, Tetrakis (triphenylphosphine) palladium (0), dimethyl acetamide, hexane, diethyl ether, sodium chloride and sodium hydrogen carbonate were all purchased from VWR. Labeled glycine [2-^{13}C glycine] was purchased from Cambridge isotopes. Hexane is further distilled to make it very pure for the chromatographic work. The Cytochrome P450 2D6 plasmid[67] was a kind gift from Dr. E Johnson of Scripps research institute.

Instrumentation

^{1}H NMR and ^{13}C NMR performed using a Varian Model AS 400, 2D HMQC and NOESY experiments were performed using a Model Varian AS 600 MHz, equipped with a triple resonance cryoprobe. Melting points were determined from a Yanaco micro melting point. GC/ MS spectra performed on an Agilent Technologies GC Model G6850A (G2630A) and MS Model G2577A. The software for acquisition and processing is MSD ChemStation G1701DA. GC/MS spectra further processed with MestRenova software. UV-Visible measurements were obtained using a Hewlett-Packard (HP)) Model 8452A Diode Array UV-Vis Spectrophotometer.

2.2.1 Expression and purification of P450cam

2.2.1.1 **Transformation**

A water bath was set up at 42 °C. BL21 cells were thawed on wet ice and 2 falcon tubes were chilled by placing on ice. The cells were mixed gently by flicking the tube using the index finger (finger flicking technique). 50 µL of cells were pipetted into each of the chilled falcon tubes. 2 µL of P450cam DNA was added to tube 1. Unused cells were frozen on ice for 5 minutes and returned to the -80 °C freezer. 2 µL of control DNA was added to tube 2 and mixed gently by using the finger flicking technique. The tubes were incubated in the cold room for 30 minutes. Cells were heat shocked for 30 s in a water bath preset at exactly 42 °C. The tubes were put on ice for 5 minutes without shaking. 250 µL of pre-warmed SOC medium was added to each tube. Tubes were incubated at 37 °C and shaken at 225 rpm for 1 hour to grow the cells. After 1 hour, the cells (50µL) were plated onto an LB agar plate to grow the cells in the appropriate antibiotic, in this case 100 mg/L ampicillin. The plates were inverted and incubated at 37 °C overnight.

2.2.1.1 Preparation of plates

10 g of LB agar was added to 250 mL of water in a 500 mL-plastic conical flask. The solution was heated in a microwave oven for 2 minutes while turning off power (pause) every 15s and gently shaking to avoid formation of bubbles. The solution was cooled for about 10 minutes and ampicillin (100 mg/L) was added with gentle shaking.

The solution was poured onto clearly labeled plates and allowed to cool down for 30 minutes. Plates were sealed with parafilm and stored in 4 °C freezer until needed.

2.21.3 **Preparation of 2YT (Yeast extract and Tryptone) media 4 x 1 L**

1 L of water was added to each flask, followed by16 g tryptone, 10 g yeast and 5 g of NaCl. Water was added first then the solid to prevent micro-fog. To another small 250 mL flask about 80 mL of water was added followed by 2.5 g LB broth (starter culture). All flasks were covered with aluminum foil and autoclaved for 20 minutes. The media was cooled and 100 mg/L ampicillin was added to each flask. The starter culture was inoculated with a single well separated colony from the plates and incubated at 37 °C, 250 rpm overnight.

2.2.1.4 **Inoculation**

The 4 large flasks were incubated for about 45 minutes and 10 mL (1 %) of the starter culture inoculated into each flask. 5ml of this solution was taken and stored in the cold room (blank solution). The cells were incubated at 37 °C and 250 rpm. The growth of the cells was monitored by checking optical density after every 30 minutes until OD600 was 0.6-0.8 (about 3.5 hours). Results obtained in my second trial are shown in Table 3 (below).

Table 3 Typical growth of cells showing ideal time for inoculation

Time/minutes	0	15	30	80	100	160	180	200	210
Absorbance at 600nm	0.0154	0.0136	0.1076	0.1164	0.1198	0.2126	0.3646	0.544	0.621

Glycerol stock Solution

At this stage when cells had maximum growth rate (OD 600 of 0.6), 800 µL of the cells was withdrawn and put in an Eppendorf tube, 200 µL of glycerol was also added to the tube, thoroughly mixed by vortexing and stored in -80 °C freezer.

Induction

I M Isopropyl β-D-1-thiogalactopyranoside (IPTG) was prepared by dissolving 10 g of IPTG in 42 mL water in a large tube and stirred to ensure all the material dissolves. Note IPTG is photosensitive hence the tube was covered with aluminum foil.
IPTG (final concentration 1 mM) was added to each flask and aminolevulinic acid (ALA)[i] (final concentration 30 µM).

The solutions were incubated at room temp (24 °C) and shaken at 190 rpm for 21 hours. 1 hour before harvest after, camphor was added to each flask (to a final concentration of 1 mM) and incubation continued for another hour. Cells were harvested by centrifugation using large centrifuging tubes at 7000 rpm (6300 g) for 15 minutes. Harvested cells were stored in a plastic tube at -80 °C. Average mass of wet cells was about 65 g.

2.2.1.5 **Purification**

Column preparation (DEAE)

DEAE column was prepared by running 6 column volumes of running buffer through the column. DEAE column was cleaned by running 6 column volumes of 1 M KCl. When the column was very dirty, it was cleaned by running 2 column volumes of 0.1 M KOH, then 2 column volumes of 0.1 M HCl then equilibrated with the correct buffer.

Preparation of Buffers

This section shows a detailed way in which one of the buffers for purification of protein was prepared. A more summarized version of this and many other buffers and stock solutions used are shown in the appendix section and this made it easier for more buffers prepared during my research studies. 4 L of 1 mM camphor was prepared. All solutions prepared use the 1 mM camphor solution.

0.25 M Tris-chloride stock solution was prepared by dissolving 39.4 g of Tris-hydrochloride in about 0.5 L of 1 mM camphor solution in a 1 L volumetric flask and made up to the mark using the same solution.

0.25 M Tris-base stock solution was prepared by dissolving 60.57 g of Tris-base in about 0.5 L of 1 mM camphor solution in a 1 L volumetric flask and made up to the mark using the 1 mM camphor solution.

Running buffer (A): 50 mM Tris Chloride pH7.5, 25 mM KCl and 1 mM camphor. This buffer was prepared by adding 400 ml of 0.25 M Tris-Chloride to 2 L volumetric flask. 3.7272 g of KCl was also added to this and made up to 2 L mark using

the 1 mM solution of camphor. The base was prepared in an analogous way, using the stock solution. The pH was adjusted to 7.5.

Cell Lysis

Lysis buffer contains: 50 mM Tris-Cl pH 7.5 at room temperature, 25 mM KCl, and 1 mM camphor. Assuming cells have a density of 1 g/ml the final lysis volume would be 65 g x 3=195 ml≈200 mL. Two thirds of this amount will be the lysis buffer so for this volume it implies 133 ml of DEAE running buffer prepared in previous section was added to a beaker and the cells would make up the difference. All lysis components were added as shown below:

Phenylmethylsulfonylfluoride (PMSF 1 mM), 1 µg/ mL leupeptin, 1 mg/mL pepstatin, 1 mg/mL antipain, 32 Units/mL DNase, 3 Units/mL RNase, 1 mg/mL lysozyme. The cells were physically cracked into smaller pieces and added to the beaker with lysis components and the buffer. The components were sonicated using 50 % duty cycle, power 3, timer on hold. Components were sonicated for 1 minute, 5 times allowing 5 minutes between cycles to cool. Cells were kept on ice for all this period to avoid frothing.

The supernatant was obtained by centrifugation at 14000 rpm (25 200 g) for 20 minutes followed by centrifugation again at 20000 rpm (51 428 g) using smaller centrifuge tubes for 1 hour. The resulting protein was concentrated using a concentration cell to a volume of about 20 ml. Buffer exchange was done 5 times adding the DEAE running buffer prepared. This is important to remove the other components and this enables the protein to bind in the DEAE column.

Column Preparation

500 ml of 0.5 M Tris-acid and 100 mL of 0.5 M tris-base were prepared. 50 g of DE53 pre-swollen anion exchange gel was weighed and placed in 500 ml beaker. 300 mL of Tris-hydrochloride was added and mixed gently using a glass rod. The pH of the solution was adjusted using Tris-base to pH 7.4 and transferred to a 500-ml conical flask, degassed and left to settle for about 30 minutes. The top layer with buffer and fine particles was decanted and carefully poured the gel suspension to a vertical column in 1 continuous pour and was left to settle. The column was already equilibrated by passing through the running buffer to ensure the pH, voltage and conductivity of the buffer is almost equal to that of the eluent. This was checked using a calibrated pH meter and the conductivity meter and typical results for one of my trials is shown in the table below.

Table 4 Column equilibration

	pH	Voltage/mV	Conductivity / s/cm
Buffer	7.52	31.7	2.73
Eluent	7.49	31.3	2.82

The column was well equilibrated and the protein was loaded and washed with several column volumes of running buffer. The absorbance of eluent was checked to be almost the same as that of the buffer to ensure no components were eluting. The protein was eluted using a gradient of 0 % to 100 % with a flow rate of 2-3 ml/ min and fractions of about 2.0 mL each were collected. Elution buffer (buffer B) was 50 mM Tris chloride, 300 mM KCl, 1 mM camphor, pH 7.5. All fractions with a significant brown color were

pooled and fractions with Rz values (A_{392}/ A_{280}) > 0.5 were loaded to the Phenyl sepharose column. Typical results are shown in Table 5 below.

Table 5 Typical Rz values for fractions of P450cam during purification on a DEAE column

Fraction #	A_{392}	A_{280}	Rz value
1	0.7265	2.2623	0.321
2	1.117	2.3369	0.476
3	1.6597	2.541	0.653
4	_	_	_
5	_	_	_
6	_	_	_
7	_	_	_
8	_	_	_
9	_	_	_
10	1.8308	2.126	0.861
11	_	_	_
12	_	_	_
13	_	_	_
14	_	_	_
15	1.1653	1.6415	0.7099
16	_	_	_
17	_	_	_
18	_	_	_
19			
20	0.8482	1.5253	0.556
21	0.8099	1.5965	0.507
22	0.9847	1.9928	0.494
23	0.636	1.3949	0.456
24	_	_	_
25	0.8087	1.9887	0.407

Note that to save time not all fractions were checked and fractions 3-21 with Rz values > 0.5 were pooled and mixed. The other fractions were also mixed and purified again using DEAE as before. However, it is advisable to reject fractions with very low Rz

values and those without a significant brown color. Protein was concentrated and stored in the -80 °C freezer for further purification.

Phenyl Sepharose (Hi-Res) column

Running buffer (buffer A): 50 mM Tris-Cl pH 7.5, 50 mM KCl (needed for substrate binding, 25 % $(NH_4)_2SO_4$, 1 mM camphor

Elution buffer (buffer B): 50 mM Tris-Cl pH 7.5, 50 mM KCl, 1mM camphor.

The column was equilibrated with several column volumes of the buffer checking the pH and conductivity of the solution. The concentrated protein fractions with Rz values > 0.5 were placed in small centrifuge tubes and buffer exchange done 5 times adding fresh running buffer. When buffer exchange was complete, 75 mg/ml ammonium sulfate was added to the protein slowly and immediately loaded the protein to the equilibrated column. Note that, if the protein precipitated, it was diluted with a minimum amount of buffer (running buffer for sepharose) and load protein immediately. When protein was fully loaded, the buffer was added gently using a dropper and washed the protein with several column volumes of buffer. About 48 hours is an ideal wash to get pure protein. The protein was eluted using gradient elution as before collecting several fractions of about 2 mL each. Protein purity was checked and fractions with Rz $\geq$ 1.4 were pooled and are suitable for assays.

The protein was concentrated as before and buffer exchanged with Phosphate buffer (100 mM PB, 100 mM KCl, 1 mM camphor, pH 7.4) to remove ammonium sulfate. The concentration of protein was determined using Beer's law and extinction coefficient 102 $mM^{-1}cm^{-1}$ at 394 nm. The protein was stored in a plastic tube in -80 °C freezer.

2.2.1.6 Preparation of substrate free substrate free CYP101

The substrate free form of CYP101 was prepared by passing CYP101 samples, isolated in the presence of camphor, through a G25 column slowly with 50 mM MOPS (morpholino-propane sulfonic acid) pH 7.4. The purity of substrate free form was checked using UV-visible spectroscopy. The MOPS buffer was removed by buffer exchange (5 x 1 mL 100 mM PB pH 7.4, 100 mM KCl) through centrifugation at about 4000 rpm. The purified substrate free samples were used the same day, as it converts to P420 easily during the experiment or when stored.

2.2.2 Synthesis of ALA

Summary

Aminolevulinic acid (ALA) was synthesized in four steps by the condensation of glycine and phthalic anhydride, followed by the conversion to the chloride, coupling reaction with a three-carbon unit and hydrolysis. For practice synthesis was done with unlabeled glycine as shown in scheme 2 below

Abbreviations, Aminolevulinic acid (ALA), Phthalimido acetic acid (PAA), Phthalimido acetyl chloride (PACl), Ethyl 3-iodopropionate (EIP), & Ethyl phthalimido levulinate (EPL)

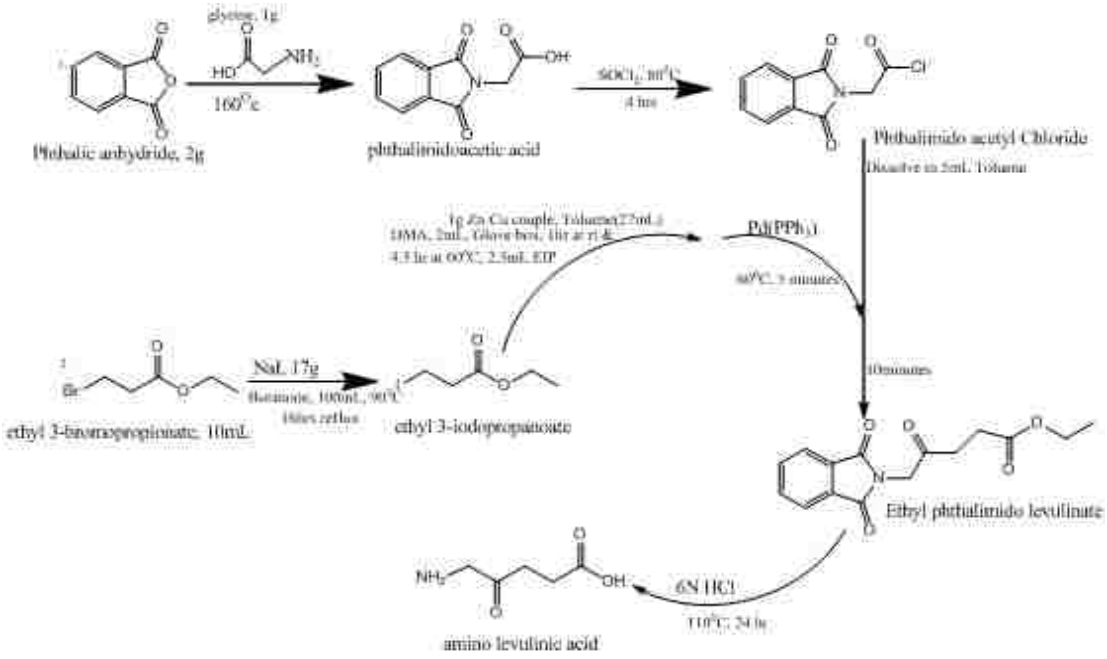

Scheme 2 Aminolevulinic acid synthesis

Phthalimido acetic acid (PAA)

Glycine (1.0 g, 13.0 mmol) and phthalic anhydride (2.0 g, 13.5 mmol) were thoroughly ground using a mortar and pestle to increase surface area of reactants & heated using a heating mantle at 160 ˚C under nitrogen, until all of it was melted. Heating was continued for a further 2 minutes to ensure complete reaction. After cooling, the residue was recrystallized from 100 mL of hot water to give phthalimido acetic acid as white needles (2.3 g, 90 % yield). The solid was filtered and allowed to dry under vacuum for a couple of hours and further dried by heating in an oven at 100 °C for a few more hours to yield about 2.3 g of dried product which was stored in a desiccator under vacuum at room temperature. Melting point was 192-194 °C implying that this product was pure.^{1}H NMR ($CDCl_3$) δ: 4.49 (dd, J=143.3Hz, ^{2}J=1.1Hz), 7.75-7.92 (m, 4H); ^{13}C NMR ($CDCl_3$) δ=38.4 (d, J=13.3 Hz).

Ethyl 3-iodopropionate (EIP)

A suspension of ethyl 3-bromopropionate (10 mL, 78.0 mmol) and NaI (17 g, 113.4 mmol) in 2-butanone (100 ml) was refluxed at 90 °C for 3 hours under nitrogen. After cooling, the crystals were removed by filtration. The filtrate was evaporated, diluted with ether 80 mL, and washed with 50 mL of saturated brine 4 times. Distillation of the crude product gave ethyl 3-iodopropionate (13 g). This is illustrated in Scheme 2 above. ^{1}H NMR ($CDCl_3$) δ: 1.29 (t, 3H, J=7.1Hz), 2.97 (t, 2H, J=7.1 Hz), 3.34 (t, 2H, J=7.1 Hz)), 4.19 (q, 2H, J=7.1 Hz)

Ethyl phthalimido levulinate (EPL)

Note that for the following moisture sensitive reactions all liquids were transferred using syringes to flame dried flasks which were immediately stoppered. The reaction is moisture sensitive and reversible hence all water is eliminated to force reaction forward according to Le Chatelier's principle. A mixture of phthalimido acetic acid (2.3 g, 11.1 mmol) and thionyl chloride (10 mL) was refluxed at 80 °C for 3 hours. The excess thionyl chloride was removed using the rotor vapor and further removed by washing with about 6 mL of hexane 3 times. The residue was dissolved in dry toluene (5 ml) under nitrogen. 2.5 ml of ethyl 3-iodopropionate was put into a 10-mL flask and nitrogen was bubbled through for about 5 minutes. 1 g of zinc/copper couple was placed in a two-neck flask and nitrogen was also bubbled through. This was repeated for two other small flasks with 2 mL of Dimethylacetamide (DMA) and 27 mL of toluene. Using a female- female delivery tube the 2 mL of DMA was transferred to the two-neck flask with zinc/copper couple. The same process was repeated to transfer the 27 mL of toluene and ethyl 3-iodopropionate under nitrogen.

The flasks were transferred into the glove box together with a weighing paper, a dropper. The two-neck flask was stirred for one hour. After 1 hour, the temperature was increased to 60 °C and stirring was continued for 4.5 hours. After 4.5 hours the catalyst, 418 mg of $Pd(PPh_3)_4$ and 5 minutes later the solution of phthalimido acetic acid was added using a dropper and reaction was complete after 10 minutes. The solution was taken out of the glove box and diluted with 200 mL of ethyl acetate and washed 3 times with 50 mL of 1N HCl, followed by 50 mL of saturated $NaHCO_3$ and then lastly washed 3 times with 50 mL of saturated brine. The product was dried with 20 g of $MgSO_4$ and

evaporated. Silica gel chromatography of the crude product on silica gel using 50% Hexane: 50 % ethyl acetate, then 30 % hexane: 70 % ethyl acetate gave 1.1 g of ethyl phthalimido levulinate. About 24 fractions were collected every 20 minutes and fractions checked using thin layer chromatography. Clean fractions containing the product were pooled and evaporated. ^{1}H NMR also confirmed the product. The other fractions were also mixed and purified again by thin layer chromatography. Typical results are shown in the results section. Melting point of product was 70-71 °C, slightly lower than the theoretical value of 75-77 °C. This means that the product is not very pure and the impurities could be removed by recrystallization in ethanol. For trial 4 the ^{1}H NMR showed that the product is clean hence no silica gel chromatography was carried out. The product is recrystallized in about 3 mL of hot ethanol to aid dissolution and heated using the blower and leave flask standing for some hours to ensure crystals form.

Aminolevulinic acid (ALA)

A solution of ethyl- phthalimido levulinate (1.1 g) in 6 N HCl was refluxed at 110 °C for 24 hours to remove the protecting group. The reaction mixture was cooled to room temperature and filtered. The filtrate was washed with ether (10 mL) using a small separating funnel. Note that the product is in the aqueous layer therefore after separation of the organic layer from the aqueous layer the product bottom layer was taken out into a 50-mL beaker, the ether layer then taken out into another beaker then the product is put back into the separating funnel and 10 mL of ether added until 4 washes were done.

The product was evaporated using the rotor vapor to drive off the water and HCl. Note this was done at 80 °C and took a long time. When it had completely dried, the solid

product was recrystallized using 3 mL of hot ethanol to dissolve the product and a few drops of warm ether was added using a dropper. The ether was warmed to about 30 °C. The 50-mL flask with product ALA, ethanol and ether was left standing overnight to allow crystallization of the product. The product was filtered and stored in vials in the desiccator.

2.2.3 Biosynthesis of ^{13}C-labeled hemes

To label the hemes, the approach outlined by Rivera and coworkers was used as shown in Figure 15. In the studies done so far in our lab we are interested in labeling methine carbons hence see resonances from protons on these as reference points thus [5-^{13}C]-ALA was used. The ALA itself was synthesized in our lab starting with ^{13}C labeled glycine to form [5-^{13}C]-ALA.

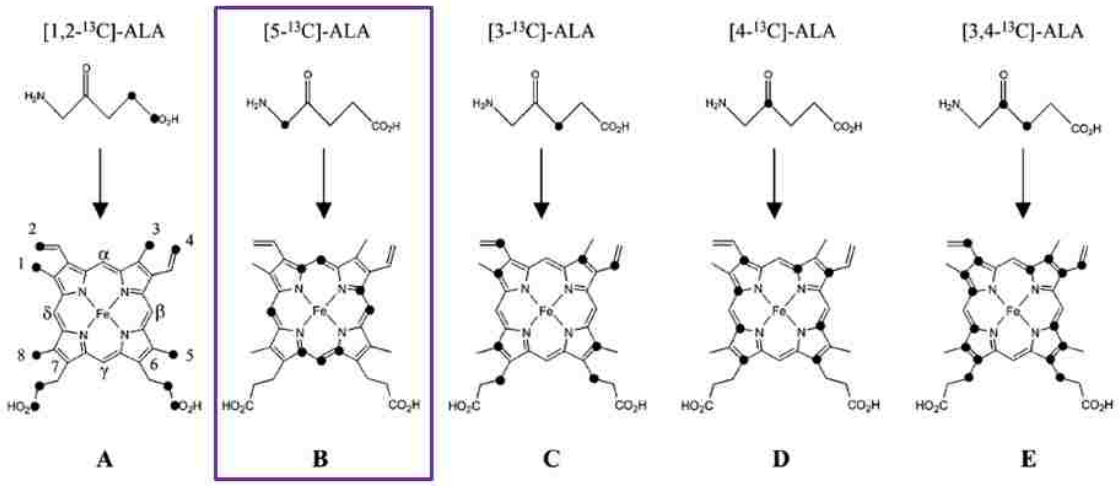

Figure 15 Expected labeling scheme starting with labeled ALA[58]

The protons labeled in this work are symmetrically arranged around the heme, hence allows to look at all positions around the heme. The labeled positions using [5-^{13}C]-ALA are also not floppy unlike labeling the vinyls or propionates which are likely to give varying distances from the substrate.

The biosynthesis of labeled heme is highlighted in more detail in the scheme below**:**

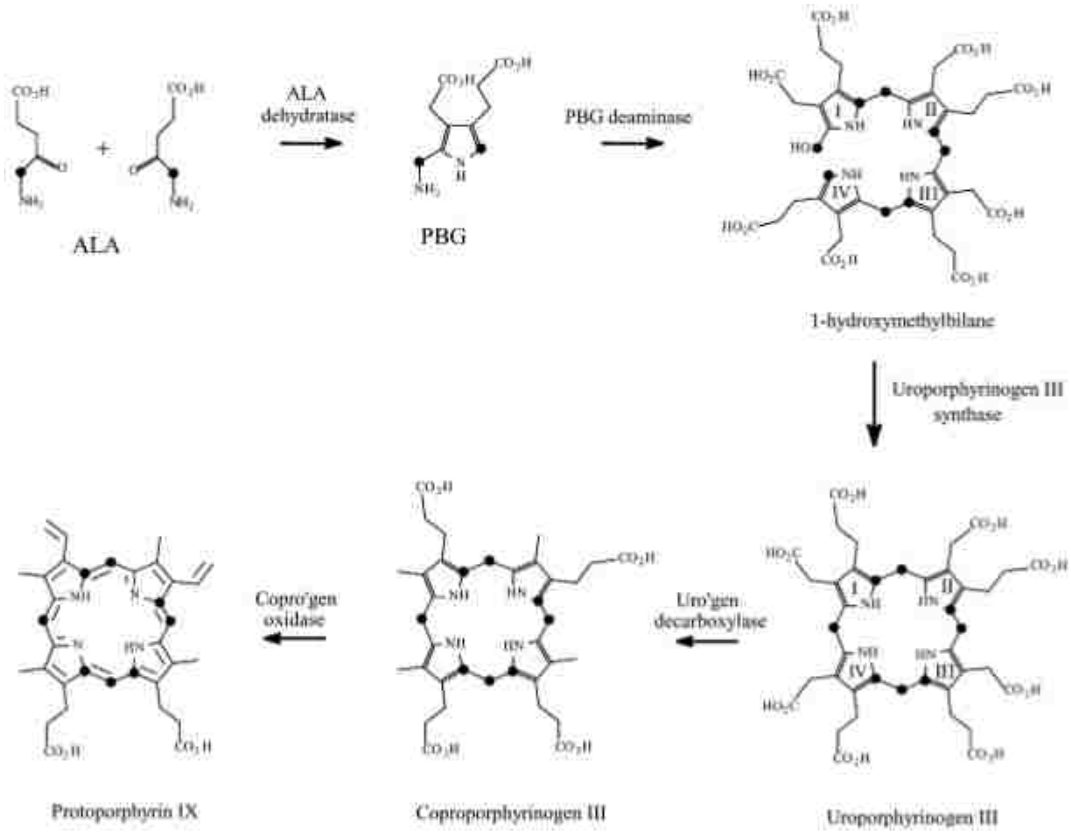

Figure 16 Heme biosynthesis from labeled [5-^{13}C]-ALA[58]

HU227 strain of E. coli was used and this strain lacks the gene to synthesize ALA therefore the medium was supplemented with ALA as the sole source of ALA which was taken up to label the heme at positions indicated. The detailed biosynthesis of the labeled heme is outlined on Figure 16. This will not be discussed further but was included to illustrate the biosynthesis of heme.

2.2.4 Expression of 5-^{13}C ALA P450cam

The same procedure for expressing P450cam above was repeated using HU227 cells instead, the *E. coli* strain lacking the gene for ALA synthase instead of the normal

BL21 cells. For this expression, the 2YT medium was supplemented with 20 mg/L [5-^{13}C] labeled ALA and all other expression steps are the same.

2.2.5 CYP 2D6 transformation and expression

CYP 2D6 transformation

The original plan to explore the utility of using [5-^{13}C]-ALA generated ^{13}C-labeled P450s was to begin with an actual drug-metabolizing enzyme, specifically, CYP2D6. A lot of work was done in our lab by other graduate students to try to express this enzyme, but it was eventually determined that the plasmid that had been obtained from another lab was defective, so the efforts were abandoned and a decision was made to focus efforts on CYP101. At some later point, a new plasmid containing the CYP2D6 gene was obtained from Dr. Eric Johnson of The Scripps Research Institute and I began new efforts to express CYP2D6, as described below.

This work was done at Concordia University of Wisconsin and started in Fall of 2013. A 20 µL aliquot of BL21 cells were pipetted into a pre-cooled Eppendorf tube and 2 µL of DNA added to the cells. The cells were mixed gently by flicking with an index finger to ensure DNA collects at the bottom of the tube. The tube was placed on ice for about 5 minutes. The cells were heat shocked by placing tube in a water bath preset at exactly 42 °C ensuring the solution is fully submerged in the water. Tubes were placed back in ice for 2 minutes and 80 µL of pre-warmed SOC medium was added to the mixture and incubated at 37 °C and 250 rpm for 1 hour to grow the cells prior to plating on LB ampicillin plates. The cells were plated onto 2 plates adding 5 µL and 10 µL into each plate. The plates were inverted and incubated in an oven at 37 °C overnight. There was no growth from all the plates.

The transformation was repeated using 50 µL of DH5α cells added to a falcon tube, 1 µL of DNA 2D6 plasmid added and put on ice for 30 minutes. After exactly 30

minutes the falcon tube was placed in a 42 °C water bath tightly controlled. The tube was placed back on ice for 2 minutes. 250 µL of clear and pre-warmed SOC medium was added and tube incubated at 37 °C, 250 rpm for 1 hour. These cells were plated in three labeled plates 10 µL, 100 µL and 200 µL. Cells were delivered with micropipettes using sterile tips and spread throughout the plates using a sterile glass rod. The three plates were incubated overnight at 37 °C and good colonies were obtained from these plates. A colony well separated was selected and grown again to ensure a colony with the 2D6 plasmid was used. This was achieved by taking a well separated colony and inoculating it on a new plate using a sterile wooden splint. A sterile metal loop was used to spread the cells evenly so that we get good colonies. Two plates were prepared and incubated at 37 °C overnight.

LB broth supplemented with 100 mg/ mL ampicillin was inoculated with a single colony from the plates and incubated for 3 hours at 37 °C. OD_{600} was checked at and mid-log phase these cells had one plasmid, the 2D6 plasmid. After 3 hours, cells were put on ice for about 10 minutes and centrifuged for 8 minutes at 4500 rpm to obtain a good pellet. The pellet was resuspended in 100 µL of water and transferred to an Eppendorf tube and centrifuged at 13 000 rpm for 1 minute. 1 µL of 10 ng/µL of chaperone pGro7 was pipetted into the Eppendorf tube and mixed gently with the pipette tip. This solution containing cells with 2D6 plasmid and the chaperone pGro7 was transferred to a disposable electroporation cell shown in **Figure 19** below. To introduce the chaperone, pGro7 electroporation was used which is using an electrical pulse to increase the permeability of the lipid bilayer and once the pulse is stopped the chaperone is incorporated and the lipid bilayer heals with the chaperone inside.

Electroporation

Electroporation was used to incorporate a second plasmid called pGro 7 which contains the chaperones groES and groEL which are important in folding of the protein. The promoter for this plasmid is araB and the inducer for this promoter is L-arabinose[68].

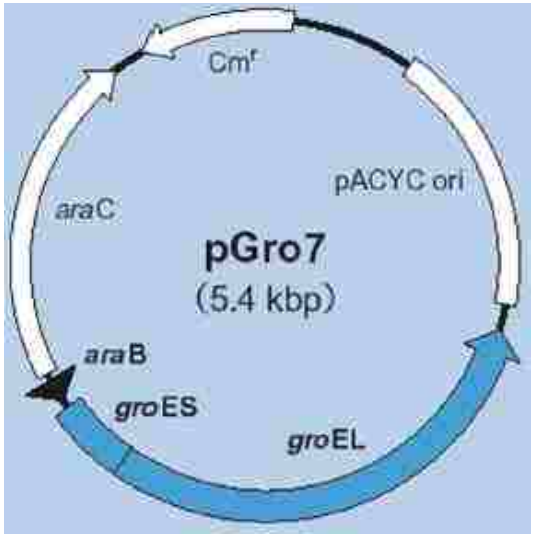

Figure 17 Plasmid pGro7,[69,70] containing chaperones groES and groEL

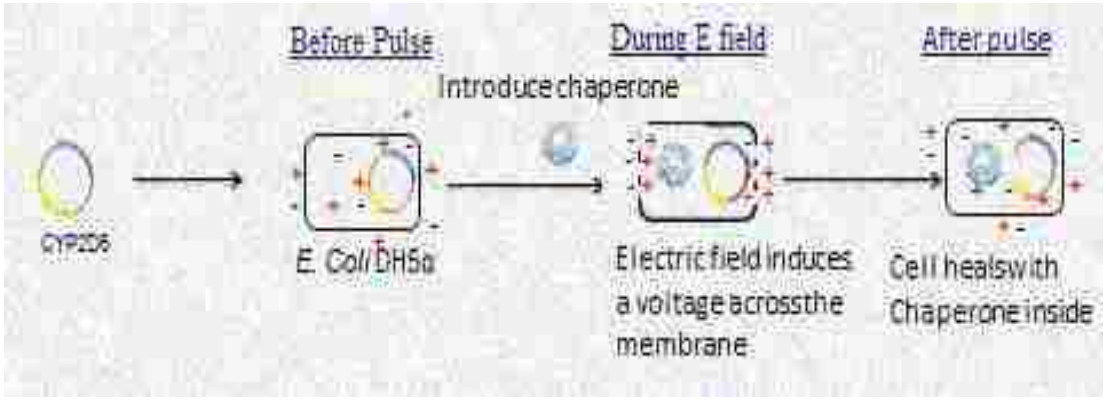

Figure 18 showing electroporation to incorporate the chaperone into the E. coli DH5α cells. The first step involves normal transformation of 2D6 plasmid in DH5α cells, whereas the second step is the electroporation step to incorporate the chaperone plasmid.

The pGro 7 chaperone is as shown in **Figure 17** above. It contains the chaperones groES and groEL. These chaperones help in the proper folding of the 2D6 protein,[71,72]. Induction of 2D6 is by IPTG whereas pGro7 is induced by arabinose. For successful expression of 2D6, transformation of the 2D6 plasmid was carried out in a normal way as already discussed. To incorporate the second plasmid, pGro7 electroporation was used which uses a high voltage and a short pulse to create a voltage across the lipid bilayer thus facilitating entry of the chaperone as pores are formed on the lipid bilayer.

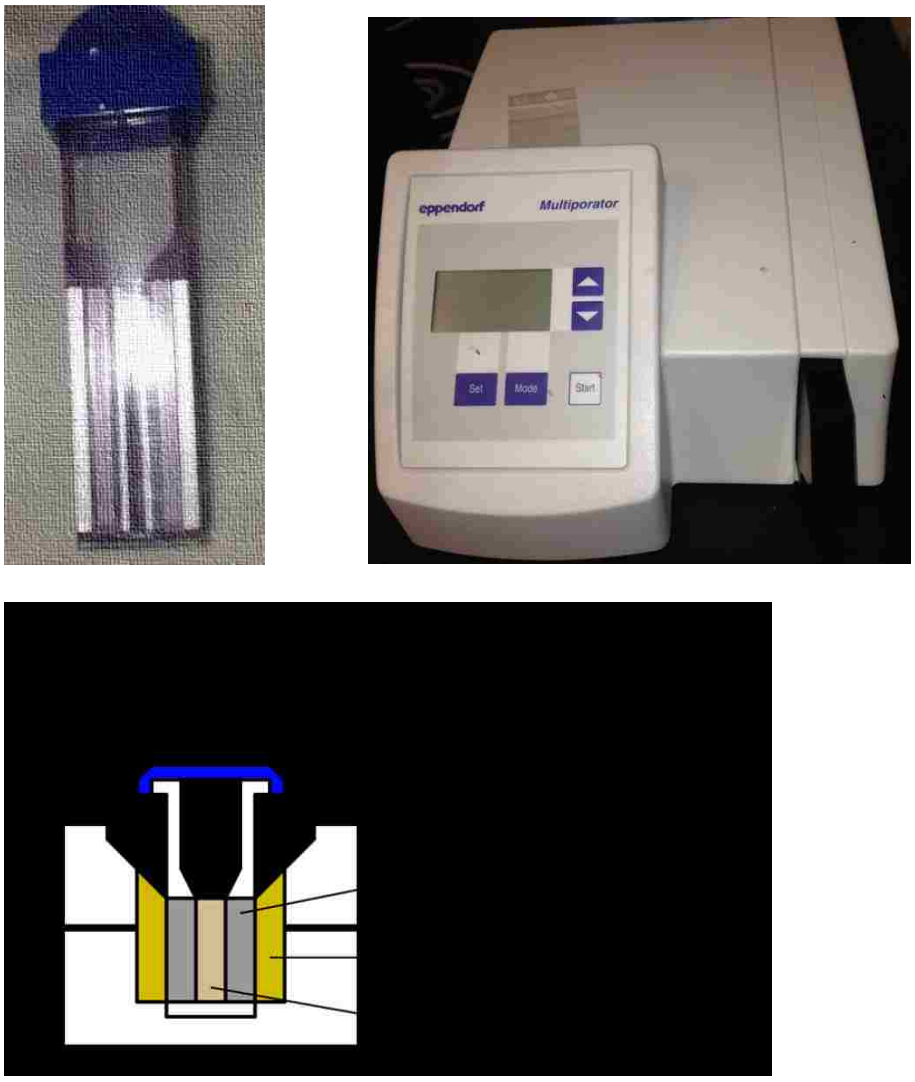

Figure 19 Electroporation cell (left), multiporator (right) for incorporation of second plasmid and details about the electroporation process (bottom)

For this electroporation process cells in suspension were placed in the electroporation cell shown in **Figure 19** above. The electroporation cell was placed in the multiporator shown in **Figure 19** (right) above and the mode for electroporation of bacteria and yeast was selected and charge set to U 2500 V and τ of 5 ms, where U is the voltage set and τ is the time constant. Electroporation was triggered by pressing the start key and charge appeared on the display U 2000 V, τ 5 ms and o. After charging procedure had ended discharging occurred and it was indicated by a flash and a double acoustic signal. After the experiment ended a double acoustic signal is emitted and the initial information and the set parameters appeared on the display. The actual parameters U_a (actual measured voltage, in volts) and τ_a (actual time constant, in ms) also appear on the display. For this experiment U_a 2260 V, τ_a 3.0 ms, o appeared. That marked the end of the experiment and cell were recovered from the electroporation cell by adding 250 µL of SOC medium and a micropipette used to suck and release cells from the electroporation cell. The micropipette was used to draw the solution from the cell and placed in a 50-mL tube and incubated for 1 hour at 37 °C to allow growth of the cells with both 2D6 plasmid and the chaperone pGro7.

After I hour, the cells were inoculated onto plates containing 100 mg/mL of both ampicillin and chloramphenicol. Three plates were prepared, 10 µL, 100 µL and all recovered cells. Plates were incubated at 37 °C overnight. There was successful growth in plates as expected and a new plate was grown from a few selected colonies. This is important to ensure only cells with both plasmids grow.

Checking if Electroporation was successful

From the plate grown with both plasmids 2D6 and pGro7, a single well separated colony was grown in 10 mL of LB broth and incubated overnight at 37 °C. Glycerol stocks were prepared from this overnight culture. Only 1.5 mL of this culture was digested to get pure DNA using the QIAprep spin miniprep kit.

Plasmid Purification

1.5 mL of bacterial overnight culture was centrifuged at 4500 rpm for 10 minutes at 15 °C. The pelleted bacterial cells were resuspended in 250 µL of buffer P1 and transferred to a microcentrifuge tube. 250 µL of buffer P2 was added and mixed by inverting the tube six times. 350 µL of buffer N3 was added and mixed immediately and thoroughly by inverting the tube six times. The cells were centrifuged at 13000 rpm in a small table top microcentrifuge for 10 minutes. The supernatant was applied to a QIAprep spin column by decanting and centrifuged for 60 s. The column was washed with 0.5 mL of buffer PB and centrifuged for 60 s. The column was also washed with 0.75 mL of buffer PE and centrifuged for 60 s and centrifuged again for 60 s to remove any residual wash buffer. The column was placed in a clean microcentrifuge tube and the DNA eluted by adding 50 µL of buffer EB (10 mM tris-CL, pH 8.5) to the center of the spin column. It was left to stand for 1 minute on ice then centrifuged for 1 min.

Agarose gel Electrophoresis

The buffer 50X Tris-acetate-EDTA (TAE) was available and 1X TAE was prepared by dissolving 20 mL of the 50X TAE stock with 980 mL of highly polished water. Agarose gel (1 %) was prepared by adding 1 g of agarose to 100 mL of 20X TAE

buffer and heating in a microwave for about 2 minutes until all the agarose had dissolved. The solution was cooled for 5 minutes and poured into a gel tray and the well comb was placed. The gel was left to cool down for about 20 minutes at room temperature.

Preparations of samples: Two vials were used and 8 µL of the pure DNA eluted was added to the first vial. 12 µL of deionized water and 2.2 µL of loading buffer was added. The marker was prepared by adding 1.5 µL of standard, 18.5 µL of deionized water and 2.2 µL of loading buffer. The cell was set up as shown below:

Figure 20 Agarose gel electrophoresis (left) and Foto/UV 26 where the gel is exposed to UV radiation and picture obtained.

The sample was loaded onto the gel, marker placed in lane 1 and the digested DNA in lane 2 and lanes 3 and 4 left out as negative blank. The voltage was 100 mV and

60 s and the cell was run for 1 Hour. After I hour, the cell was stopped and the gel removed and immersed in Ethidium bromide (EtBr) for 10 minutes. The gel was exposed to UV radiation in a Foto/UV 26 as shown below and focused to get a better picture. The picture obtained is shown in the results section.

CYP2D6 expression

20 mL of LB broth solution supplemented with 100 mg/L ampicillin and 100 mg/L chloramphenicol was inoculated with a single validated transformant and incubated overnight at 37 °C and 200 rpm. IL, 100 mL and 100 mL of Terrific broth (TB) were prepared and the recipe for this preparation is shown in the appendix section. TB was also supplemented with 100 mg/L ampicillin and chloramphenicol. 10mL solution of LB broth was inoculated into the 1 L flask 1 mL of LB broth solution with cells grown overnight was inoculated into each of the 100 mL of TB. The three flasks were incubated at 37 °C, 220 rpm and OD was checked after about 3 hours. When OD600 was 0.7, 5 mL of 1 M aminolevulinic acid (ALA, 5 mM), 1 mL of 1 M isopropyl β-D-thiogalactopyranoside (IPTG, 1 mM) and 4 g of arabinose (4 g/L) were added. To the first 100 mL culture ALA (5 mM) and IPTG (1 mM) were added. To the second 100 mL flask (clearly labeled), ALA (5 mM) and arabinose were added. ALA is the heme precursor, IPTG induces 2D6 and arabinose induces the chaperone pGro7. The cells were incubated at 30 °C and 190 rpm for 24 hours. After 24 hours, the cells were harvested by centrifugation at 4000 rpm for 20 minutes. 10 g/L obtained from the 1 L culture and 2 g/L obtained from each of the 100 mL cultures.

Cell Lysis

1 g of cells was taken from the three tubes and placed in small beakers labeled both IPTG & arabinose (B), IPTG only (I) and Arabinose only (A). 5 mL of 2D6 running buffer was added to each tube and mixed for 20 minutes. The cells were broken down by sonication 1 minute each tube allowing 5 minutes to cool. The protein was collected by centrifugation at 20000 rpm for 25 minutes.

Purification of 2D6

A very quick method (His-spin protein miniprep) to purify Histidine tagged proteins from cell-free extracts was followed to get protein for analysis by SDS PAGE. This is an easy and fast way to prepare pure protein for small scale studies. This method can be used to form purified high-quality protein in about 20 minutes. 250 µL of His-affinity gel was pipetted to each of the three Zymo-spin P1 columns (labeled both IPTG & arabinose, IPTG only and arabinose only) and resin fully resuspended by vortexing and the columns were placed in a collecting tube. The gel was centrifuged at 13 000 rpm for 10 s. 300 µL of protein sample was added to each spin column and the gel was resuspended by shaking. The protein interacted with the gel by incubating and shaking for 2 minutes. The mixture was centrifuged for 10 s and the flow through were discarded and the spin column was placed back into the collection tube. 250 µL of 2D6 running buffer prepared as shown in the appendix was added and the gel was resuspended then centrifuged for 10 s. The washing was repeated one more time to purify the protein. The spin column was placed in a standard microcentrifuge tube and 150 µL of elution buffer added and the gel was resuspended. The mixture was centrifuged for 10s at 13 000 rpm to collect the protein.

SDS-PAGE for 2D6

Samples for analysis by SDS-PAGE were prepared by adding 5 µL of the whole cells and adding 10 µL of sample buffer. The sample buffer (Laemmli Buffer- 1X) was prepared by adding 950 µL of sample buffer to 50 µL of β-mercaptoethanol. For the pure protein purified obtained using His-spin protein miniprep to purify Histidine tagged proteins, 10 µL of protein was pipetted into an Eppendorf tube and 10µL of 1X Laemmli buffer was added. 10µL of marker protein was added to a labeled Eppendorf tube. All tubes were heated at 85 °C for 8 minutes to denature the proteins. The tubes were centrifuged at 13 000 rpm for 30 s and tubes placed on ice ready to load.

The samples were loaded onto ready SDS-PAGE gel. The gel was run at 60 V for 2 hours. After 2 hours, the cell was disassembled and stained with about 100 mL of Coomassie blue for 2 hours. The gel was washed 5 times with highly polished water and 100 mL of distaining solution, and 2 kimwipes (to absorb the Coomassie blue) were added and mixture was mixed by gentle shaking at 90 rpm overnight. The gel was washed with highly polished water five times and a photo of the gel was taken.

2.2.6 Resonance Raman spectroscopy of [5-^{13}C] δ-ALA P450cam

RR measurements of ferric forms of the natural abundance and ^{13}C enriched P450cam were acquired using 406 nm laser excitation line from the Kr^{+} laser (Coherent Innova Sabre Ion Laser) at the sample at 4 °C. All spectra were measured using a Spex 1269 spectrometer equipped with a Spec-10 LN liquid nitrogen-cooled detector (Princeton Instruments, NJ). The slit width was 150 μm and the laser power incident on ferric samples was 10 mW. Rayleigh scattering was removed from the Raman signal by using an appropriate notch filter (Kaiser Optical). The samples were placed in a N_2-driven spinning NMR tube and the spectra were collected using a 180°backscattering geometry with a cylindrical lens to achieve a line focus on the tube. Spectra were calibrated with data acquired for fenchone and processed with Grams/32 AI software (Galactic Industries, Salem, NH)

2.2.7 NMR spectroscopy of [5-^{13}C] δ-ALA P450cam

NMR samples contained ~0.4-1 mM P450cam (both for the natural isotopic abundance and ^{13}C enriched camphor bound P450cam), 30 mM PB, pD 7.4, 100 mM KCl, 1 mM camphor. Substrate free samples were prepared as described on page 47 above followed by equilibration with 30 mM PB, pD 7.4, 100 mM KCl. The substrates camphor and norcamphor were added by buffer exchange with 30 mM PB, pD 7.4, 100 mM KCl, 1 mM camphor/ norcamphor. Substrate binding was confirmed by UV-visible spectroscopy and finally10 mM CN^- was formed by incubating with the same buffer in D_2O containing CN^- to form the low spin complex.

One dimensional ^{1}H NMR experiments were performed using 0.1 s acquisition time, 20 ms relaxation delay with a total of 256 scans at 25 ℃ and were collected before and after ^{13}C and 2 D NMR measurements to verify sample integrity. A total of 400 000 scans were collected for the ^{13}C NMR experiment at 20 ℃ for both the natural abundance and ^{13}C enriched substrate bound P450cam. The 1 D version of ^{1}H-^{13}C HSQC measurements for the natural abundance and ^{13}C enriched substrate bound and free P450cam were performed at 20 ℃ using 23 ms acquisition time, 0.2 s relaxation delay and J_{CH} = 200 Hz; a total of 240 000 scans were collected. ^{1}H-^{13}C HMQC experiments, with the decoupler turned off, were performed using 50 ms acquisition time, 10 ms relaxation delay and J_{CH} = 300. ^{1}H-^{1}H NOESY was obtained with pre-saturation delay of 100 ms, acquisition time of 43 ms, 10 ms mixing time, J_{CH} = 600 and 7200 number of scans. All 1D NMR data were processed with the Spinworks NMR processing software or MestRenova.

2.2.8 Synthesis of D_2 camphor

Ketocamphor synthesis

10 g (1R) -(+)-camphor, 150 mL glacial acetic acid were added to three-neck flask. 20.7 g chromium trioxide was carefully added in three portions over 30 minutes (CAUTION: CHROMIUM TRIOXIDE MAY EXPLODE, ENSURE ENOUGH ANTI-BUMPING STONES ADDED TO REACTION MIXTURE) and refluxed for 1 hour. The solution was quenched with 150 mL of water and cooled to room temperature. The organic layer was extracted using 100 mL ether. The extraction was repeated 3 times and the combined organic layer was washed with saturated sodium bicarbonate solution 3 times, followed by washing with 100 ml of saturated brine. The product was dried with 20 g of $MgSO_4$, filtered and the solvent dried out under vacuum.

The product was purified by passing through a silica gel [prepared by heating at 150 ºC until no water is lost, then added 10 % of water][73] using a hexane/ acetate mixture (95:5), followed by alumina gel [activated the same way as silica gel above] using the same solvent mixture. Fractions containing relatively pure ketocamphor were pooled and analyzed by ^{1}H NMR, ^{13}C NMR and most importantly GC/MS.

Synthesis of D_2 Camphor

Initial attempts

0.05 g of ketocamphor, 0.0432 g d_4-hydrazine and 0.134 g potassium tert-butoxide were dissolved in 10 mL of DMSO-d_6 and refluxed for 18 hours at 175 °C. After 18 hours, the mixture was cooled to room temperature and quenched by addition of

10 mL D_2O and 1 mL of 30 % DCl (to neutralize excess potassium tert-butoxide) and stirred at room temperature for 30 minutes[74]. The method outlined was extracted from Perera paper but did not get the product after several trials. The method was also not detailed and we later abandoned the method and we tried modified Wolff Kishner reduction from literature. The product was obtained by removal of DMSO using extraction with 10 mL of ice-cold water and 10 mL ethylacetate. The DMSO is miscible in water hence is in the aqueous layer, whereas the product D_2 camphor is soluble in ethylacetate hence collected in the organic layer. The extraction was repeated at least 3 times followed by extraction with 10 mL of saturated sodium bicarbonate to get rid of excess acid, and lastly 10 mL of saturated NaCl, dried with 20 g of $MgSO_4$, filtered and solvent evaporated under nitrogen. The product was purified by silica gel chromatography and analyzed by GC/ MS.

Refined Procedure

Freshly sublimed potassium-tert butoxide or potassium tert-butoxide dried at 110 ºC under vacuum prior to use and cooled in a vacuum desiccator. DMSO-d6 was freshly distilled prior to use to drive out any water. 10.8 mg d_4-hydrazine and 33.5 mg potassium tert-butoxide were added to 2.5 mL of DMSO-d_6. 12.5 mg of ketocamphor and refluxed for 18 hours at 175 ºC. The formation of products was monitored by withdrawing a small sample using a long needle and checking using TLC and GCMS. The reaction was quenched by slow or dropwise addition of 2.5 mL D_2O and 250 µL of 30 % DCl and stirred at room temperature for 30 minutes.

Removal of DMSO achieved using extraction with 25 mL of ice-cold water and 10 mL ethylacetate. The DMSO is miscible in water hence is in the aqueous layer,

whereas the product D_2 camphor is soluble in ethylacetate hence collected in the organic layer. The extraction was repeated at least 3 times followed by extraction with 10 mL of saturated sodium bicarbonate to get rid of excess acid, and lastly 10 mL of saturated NaCl, dried with 10 g of $MgSO_4$, filtered and solvent evaporated under nitrogen. The product was purified by silica gel chromatography and analyzed by TLC and GC/ MS.

The method for hydrazine reduction was unsuccessful after several attempts, hence decided to use Cram modification of Wolff Kishner method. Adamantanone was initially used for practice since the ketone is not sterically hindered and initially thought to be a good model to study reduction of ketocamphor. This method involves isolation of hydrazone then adding the hydrazone slowly to refluxing DMSO and potassium tert-butoxide. However it is well documented in literature that isolation of hydrazone can be complicated by formation of corresponding azine which can be formed during the initial formation of hydrazone or after isolation.[75] Added to this is formation of the hydrazone as a very minor product for adamantanone and azine as the major product.

This led to the reasoning that we need a better choice of model ketone for the reduction. Norcamphor was used and promising and giving more percentage hydrazone as we would expect in 5-ketocamphor.[76] Formation of hydrazone generally was performed by stirring a solution of the ketone in anhydrous ethanol and under a nitrogen flow overnight. After the reaction was quenched with water and extracted with chloroform, dried with $MgSO_4$ and analysis done using NMR, GC/MS and FTIR.

Benzophenone hydrazone was also studied and was the best in terms of stability of hydrazone which is stable for several months. However, this was dismissed as it was not a good model for aliphatic hydrazone like ketocamphor hydrazone.

2.3 Results and Discussion

2.3.1 Expression and Purification of P450cam

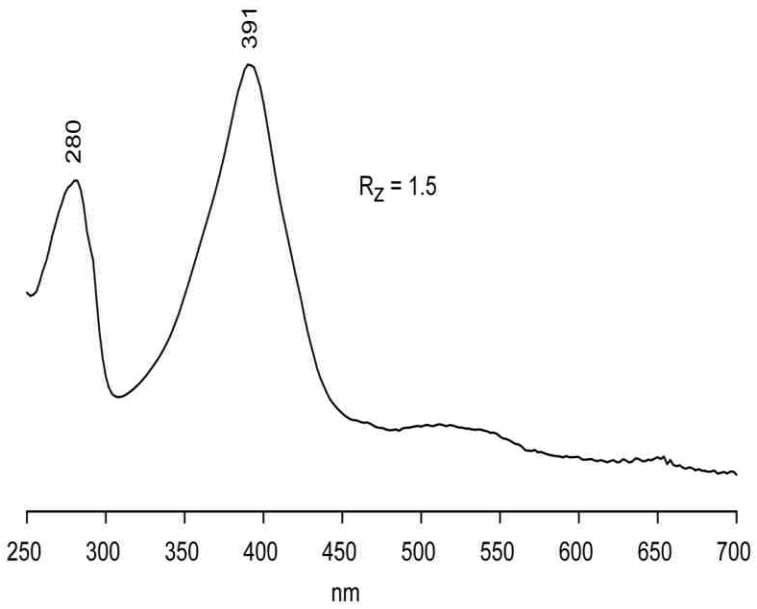

Figure 21 Absorption spectrum for pure substrate bound (high spin) P450cam after expression and purification

The P450cam was expressed and high purity protein obtained. Typical yields are 0.5 mL of 0.8 mM P450. The protein was stored at -80 °C.

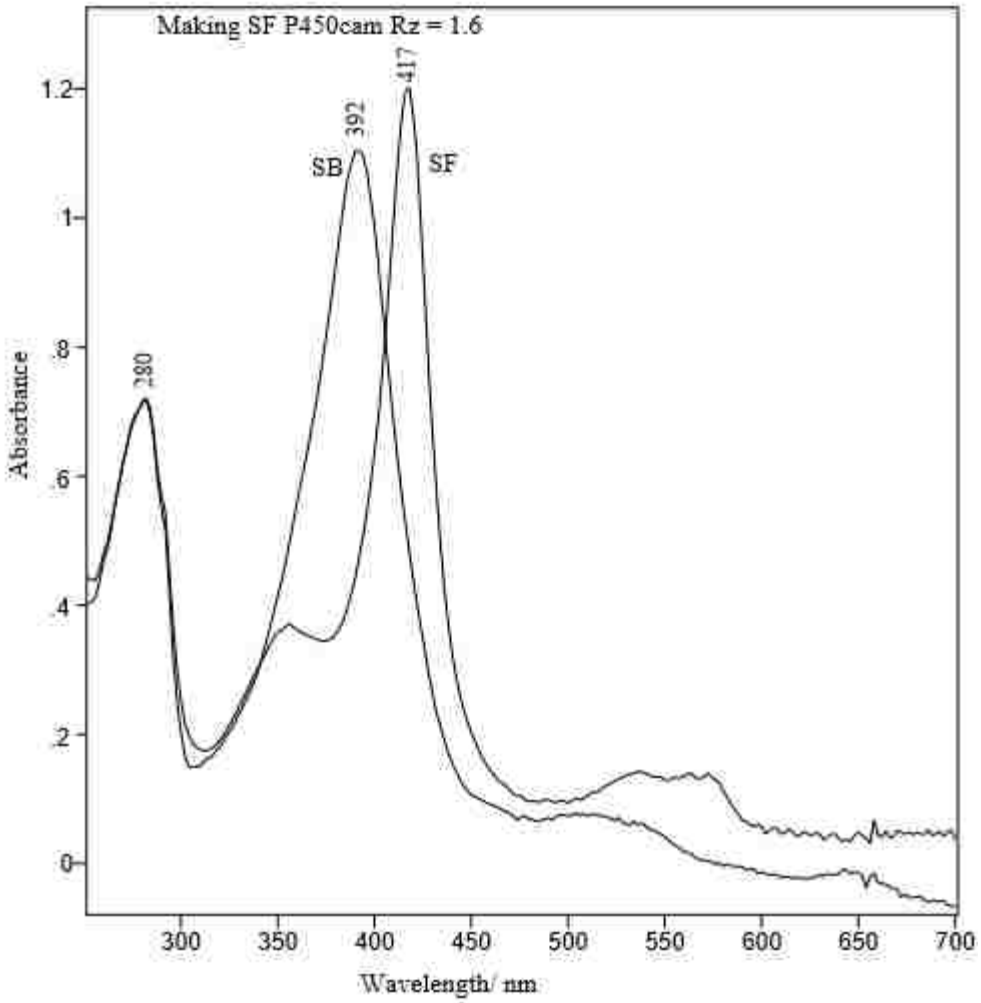

Figure 22 Absorption spectrum of SF natural abundance CYP101 using the MOPS column. Initially had about 95 % high spin (SB) after purification of CYP101. After passing the SB protein through a MOPS column ≈96 % low spin (SF) was formed.

Conversion from low to high spin state in P450s is correlated to the loss of the distal water ligand and this can be directly measured by monitoring the shift in the absorbance maximum from 415 nm to 390 nm. The extent of spin state conversion depends on temperature, pH, and ionic strength. For the idealized case, as in CYP101, shown in Figure 22 above we observed clean shift from HS to LS upon removal of the substrate.

2.3.2 Synthesis of ALA

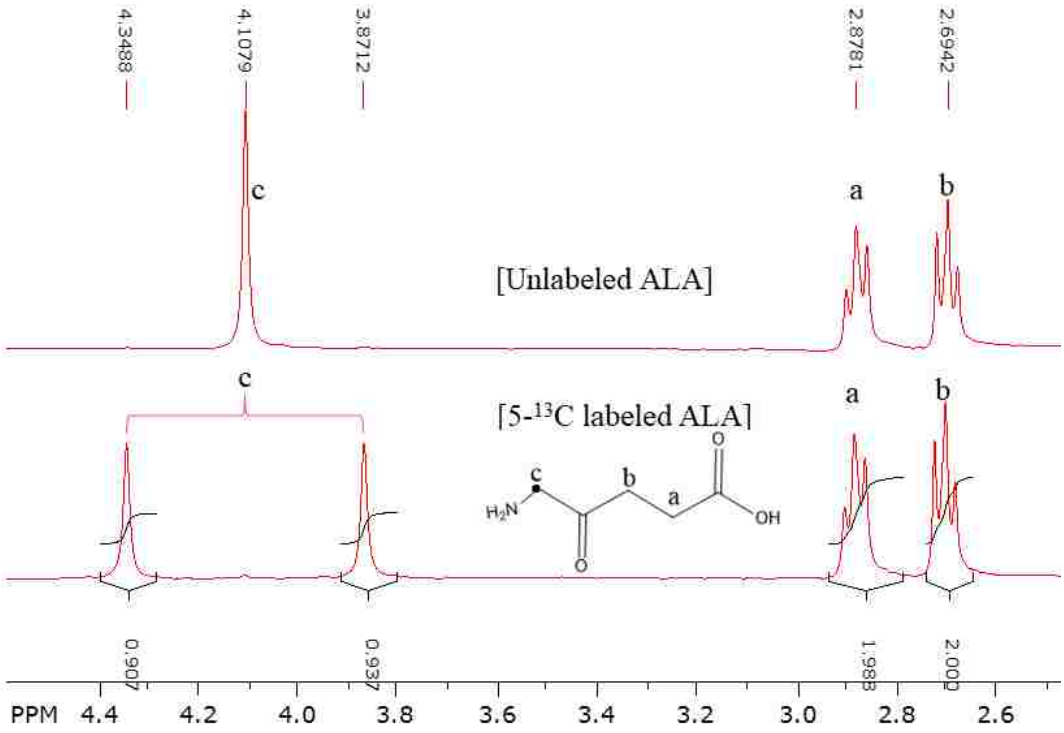

Figure 23 ^{1}H NMR Comparing labeled to unlabeled ALA

The spectra above compare the unlabeled relative to the ^{13}C labeled ALA showing a doublet at 4.10 ppm in the labeled ALA and a singlet in the unlabeled case. This is one unique case of one proton signal (for two equivalent protons) coupled with ^{13}C or where coupling is observed between two equivalent protons (on carbon labeled c) split by one ^{13}C to give rise to a doublet (^{13}C-^{1}H coupling)[77, 59]. In the unlabeled case, no coupling between those two equivalent protons and the ^{12}C hence it's a singlet. The spectra clearly demonstrate successful synthesis of pure labeled aminolevulinic acid. The yield of ALA is 57 % based on the amount of the amount of ethyl phthalimido levulinate used.

2.3.3 Expression of [5-^{13}C]-ALA P450cam

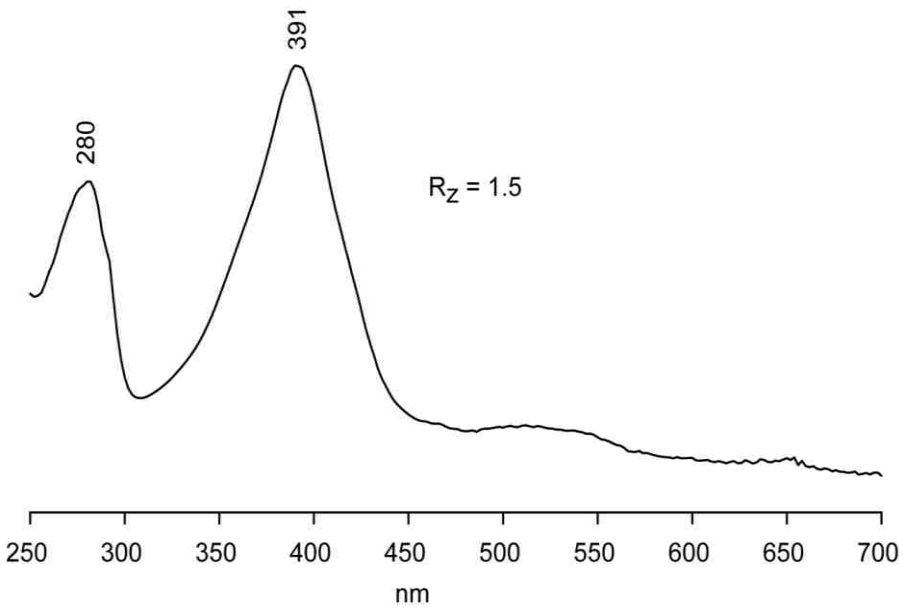

Figure 24 Absorption spectrum for pure substrate bound [5-^{13}C]-ALA P450cam

The UV-visible spectrophotometry was used to check purity of the protein. As shown in **Figure 24** above, CYP101 was successfully transformed and expressed in HU227 cells to form [5-^{13}C]-ALA P450cam. The yield was 0.5 mL of 0.6 mM protein.

2.3.4 CYP 2D6 Transformation and expression

Transformation of 2D6 was very successful and good growth of cells was observed when 2D6 plasmid was transformed in DH5α cells. Electroporation was also a success to incorporate the second plasmid for the chaperone proteins into the DH5α cells. This was confirmed using agarose gel electrophoresis and the results clearly showed both plasmids in the cell (see **Figure 25** below)

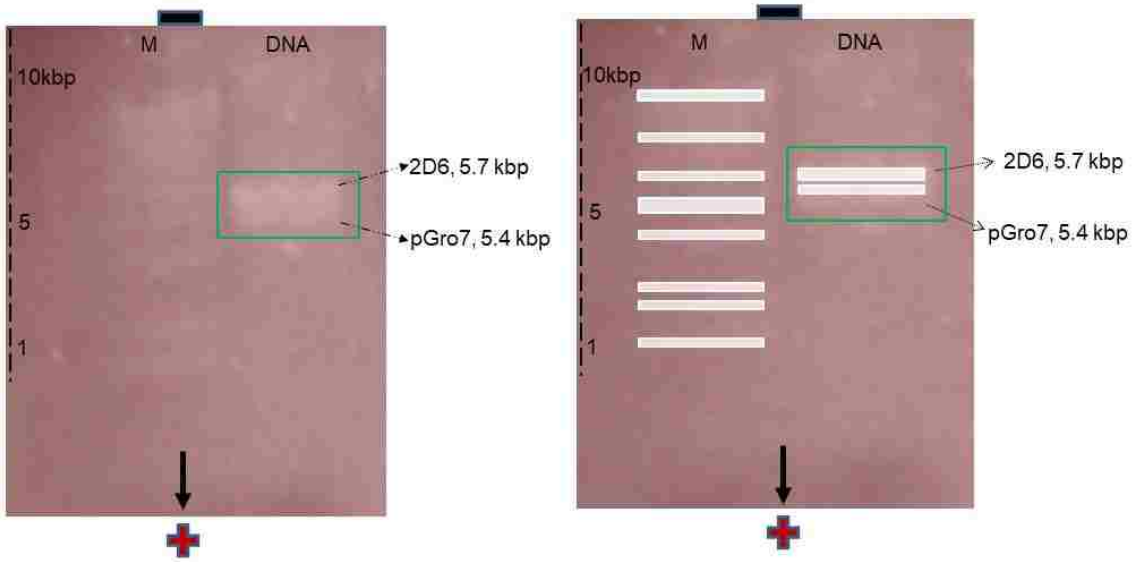

Figure 25 Agarose gel electrophoresis for 2D6 DNA, showing two bands in right lane from the 2D6 DNA and chaperone pGro7 DNA and their mass relative to marker bands (M) in left lane. The left picture shows a scanned copy of the original picture which was very faint and to the right same picture highlighted to show the bands clearly

The transformed cells were used to express 2D6 and this was also a success. This was checked as SDS PAGE showed formation of CYP2D6 protein

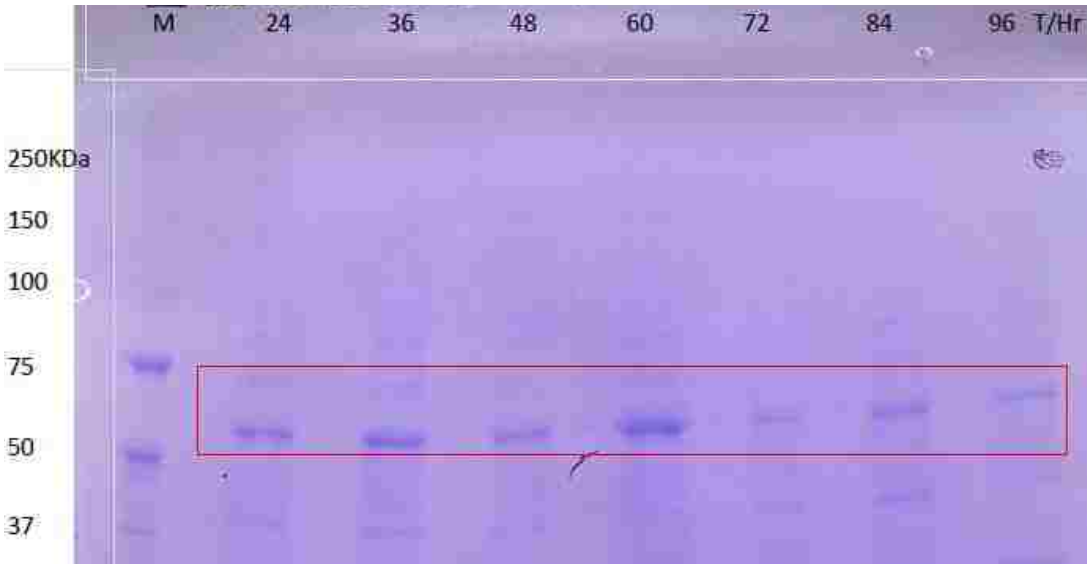

Figure 26 SDS PAGE showing optimization for the expression of 2D6 with time (T in hours) and the mass of 2D6 protein (≈52 kDa) relative to the markers (M).

As shown in **Figure 26** above the 2D6 band could be traced during expression checked during the 96-hour period. From this experiment, it can be concluded that 2D6 was formed (≈52 KDa) and maximized at 60 hours shown by the relative intensity of that band. This project was however stopped because even though there was evidence of forming the protein, it was hard to purify and get the protein from the Ni NTA column probably due to the high instability of this *truncated* mammalian protein.

2.3.5 Resonance Raman Spectroscopy of [5-^{13}C] δ-ALA P450cam

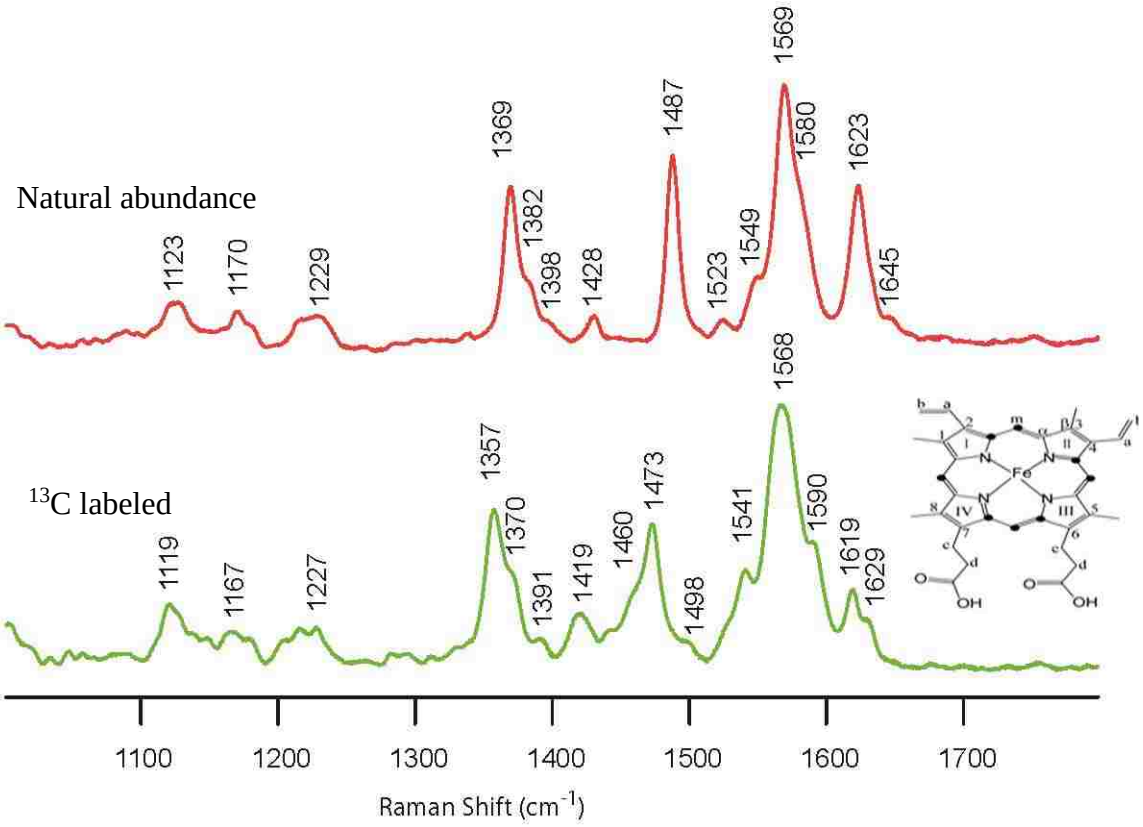

Figure 27 High frequency RR spectrum of CYP101 ^{13}C labeled relative to the natural abundance CYP101

The high frequency resonance Raman spectra, **Figure 27** above shows the [5-^{13}C]-ALA P450cam relative to the natural abundance P450cam. The oxidation state marker band, ν_4 for natural abundance P450cam occurs at 1369 cm^{-1}as expected for the ferric form but shifts by 12 cm^{-1} to 1357 cm^{-1} for the ^{13}C labeled protein. This is expected since A1g porphyrin breathing mode contains significant contributions from the C-N stretches[78, 79], as well as C-C stretching modes, i.e. it is a breathing mode of the whole macrocycle. Another mode of interest is the ν_3, which shifts significantly from 1487 to 1473 cm^{-1}. This is also as expected as the mode arises mainly from Cα-Cm symmetrical stretches.[78]

2.3.6 NMR spectroscopy of [5-^{13}C] δ-ALA P450cam

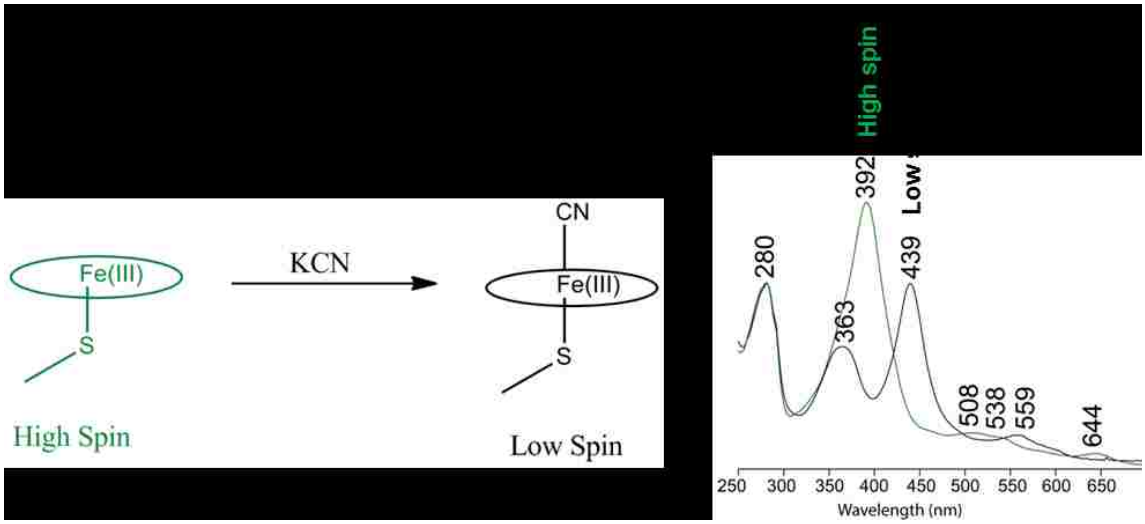

Figure 28 UV-visible absorption spectra for the high spin and low spin complexes of P450cam[80]

This experiment was important in generation of low spin ferric complex by use of a strong field ligand CN[6]. The spectra show the spectrum obtained for the high spin (HS) form, without cyanide and the low spin (LS) for the cyanide complex of CYP101, the latter was used in all subsequent NMR experiments for the [5-^{13}C] δ-ALA P450cam. Full spin state conversion was observed upon cyanide binding.

1D ^{1}H NMR

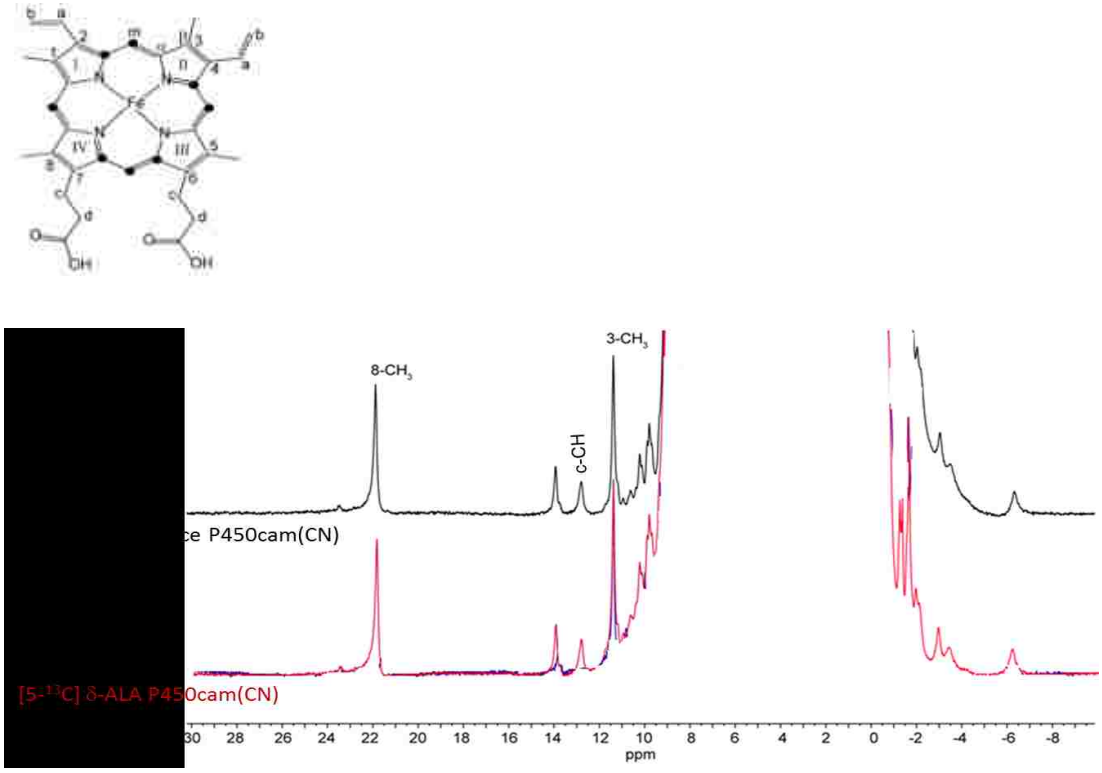

Figure 29 ^{1}H NMR of the cyanide complex of natural abundance and [5-^{13}C] δ-ALA P450cam measured at room temperature[80]

^{1}H NMR is used to investigate the electronic environment and physical structure of the heme and its protein environment for several oxidation/ spin states. Proton NMR is particularly useful as the proton resonances are often shifted outside the bulk of the diamagnetic resonances (0-10 ppm) by the strong ring current shift of the porphyrin ring and by isotropic shifts for the paramagnetic proteins. The peaks experiencing this hyperfine shift arise from the heme itself, amino acids coordinated to the heme or amino acids <7 Å from the heme, but not coordinated. Assignments of the paramagnetically shifted signals at 11.5 ppm, and 22.1 ppm was done previously for the 3- and 8- methyl

peripheral groups respectively. The signal at 13 ppm was assigned to the proximal C-CH on propionate.[81] The signal at 14.1 ppm was not assigned. The proton NMR was checked before and after the HMQC and NOE experiments to check protein integrity.

^{13}C NMR [5-^{13}C] δ-ALA P450cam

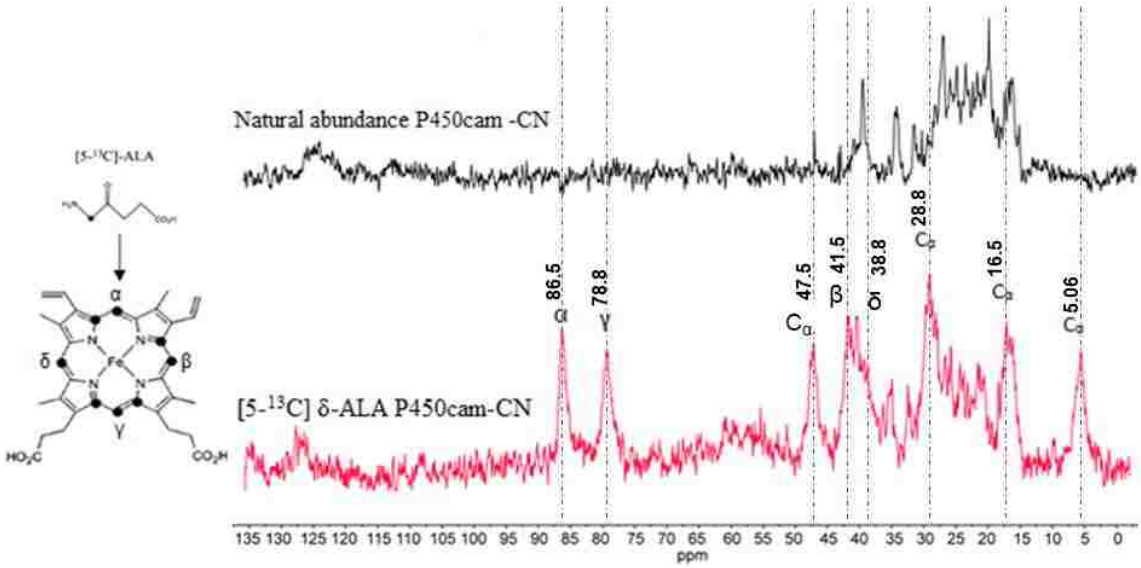

Figure 30 ^{13}C NMR for natural abundance and [5-^{13}C]δ-ALA P450cam[80] acquired at 25 °C

It must be noted that signals in ^{13}C-labeled protein α, β, γ, δ and four-C_α are clearly absent in the natural abundance spectrum (black trace) and the signals are due to the exclusive enrichment of methine and C_α positions. Assignment of these methine protons was based on previous assignments of [5-^{13}C] δ-ALA outer mitochondrial cytochrome B5 by Rivera and co-workers,[82] who unambiguously assigned protonated carbons and pyrrole α and β carbons using various NMR techniques and specifically labeled hemes. This assignment was further refined using HMQC results shown in Figure 31 below. However, assignments of C_α protons is not possible at this point. It was observed that natural abundance P450cam-CN complex showed very low sensitivity due

to the low natural abundance of ^{13}C. This challenge is overcome by labeling of hemes as illustrated in Figure 30 above

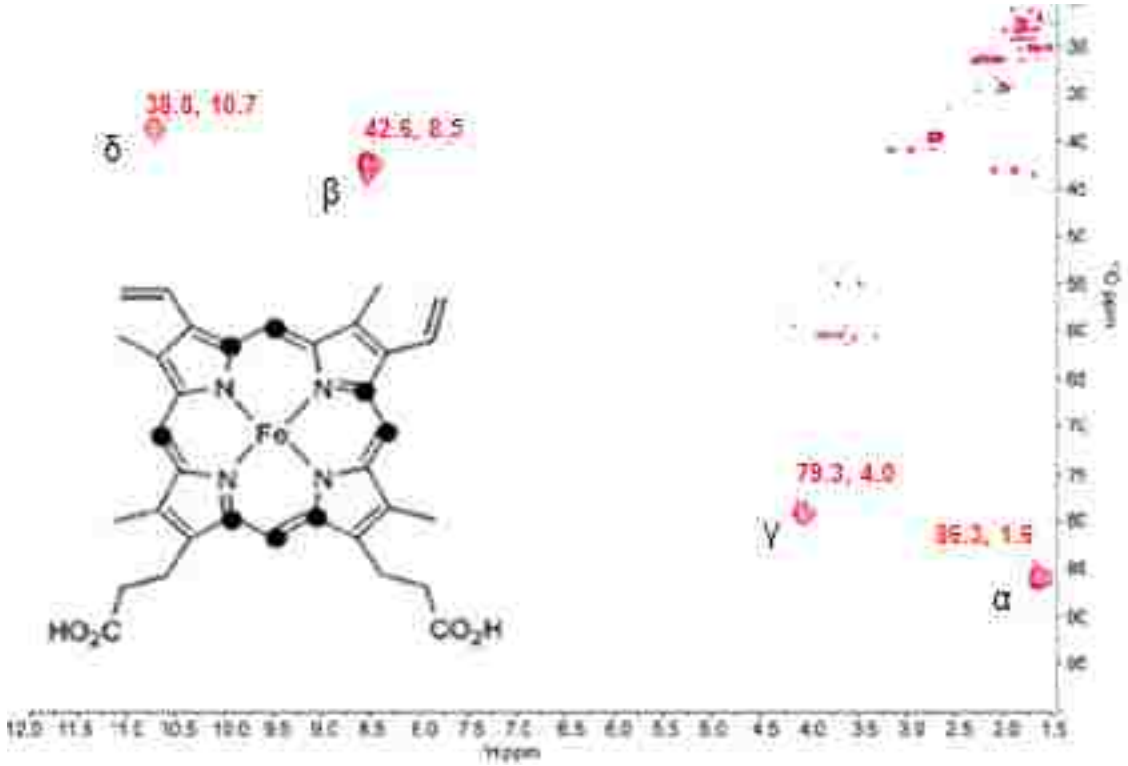

Figure 31 HMQC for [5-^{13}C] δ-ALA P450cam at 25 °C[80]

Heteronuclear Multiple-Quantum Correlation (HMQC) is a 2D experiment used to correlate directly bonded carbon (^{13}C)-proton (^{1}H) nuclei of heme substituents. This technique utilizes proton detection and has high sensitivity due to the high natural abundance of hydrogen (^{1}H). These correlations can be used to map known carbon assignments (Figure 30 above) onto their directly attached protons. A control experiment, with natural abundance ^{13}C (1.1 %) was also acquired and compared to the spectrum above and clearly showed resonances labeled α, β, γ and δ are due to the enrichment of the hemes with ^{13}C. Therefore, we can identify which protons are directly attached to the

methine carbons α, γ, β and δ. This was accomplished and assignments are shown in the HMQC spectrum above.

Nuclear Overhauser effect (^{1}H-^{1}H NOESY): Correlation through Space

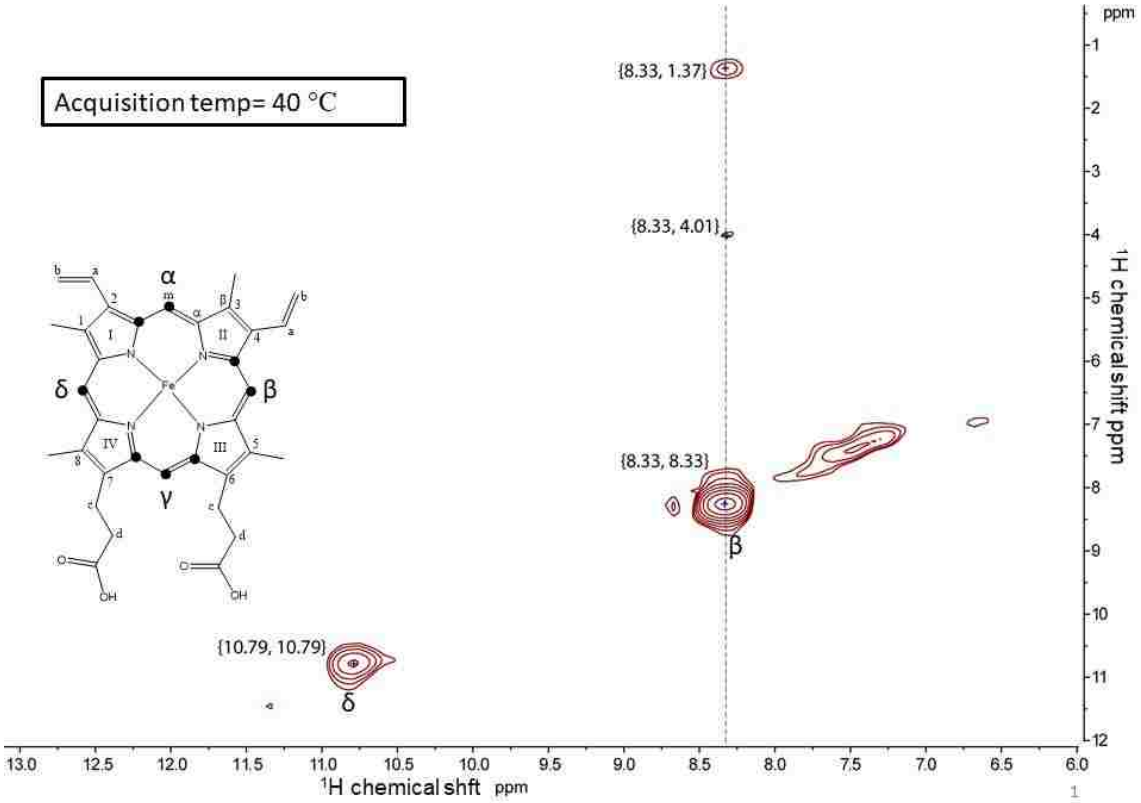

Figure 32 ^{1}H-^{1}H NOESY-HMQC spectrum of ^{13}C-enriched cyanide complex of substrate bound P450cam at 40 °C[80]

The experiment gives information on distances between protons nearby in space (<5 Å), even though the amino acid residues may be far away in primary sequence. The results showed that two meso protons were detected, a signal at 8.33 ppm (β proton) exhibiting 2 cross-peaks at 4.01 and 1.37 ppm. The resonance at 4.01 ppm is probably from a nearby protein residue. Note that NOE intensity is strongest if spins are close in space < 5 Å and NOE drops off quickly with distance, proportional to $1/r^6$. Therefore, we can conclude that the signal at 4.01 ppm is weak (≈ 5 Å from the β proton) whereas the

signal at 1.37 ppm is strong (≈ 2 Å from the same β proton). These values are merely estimates based on intensities of NOE crosspeaks obtained. Calculations to determine the exact distances are not possible since we do not have any known proton-proton distance to use as a reference pair as outlined in the introduction. However, the results clearly demonstrate that NOE is a useful probe of spatial proximity distances, information which could be useful for docking studies.[83, 84]

Using the software (SPDBV 4.1.0) we used the crystal structure to estimate which amino acid residues are in active site within < 6Å from the β-proton (refer to **Figure 33** below).

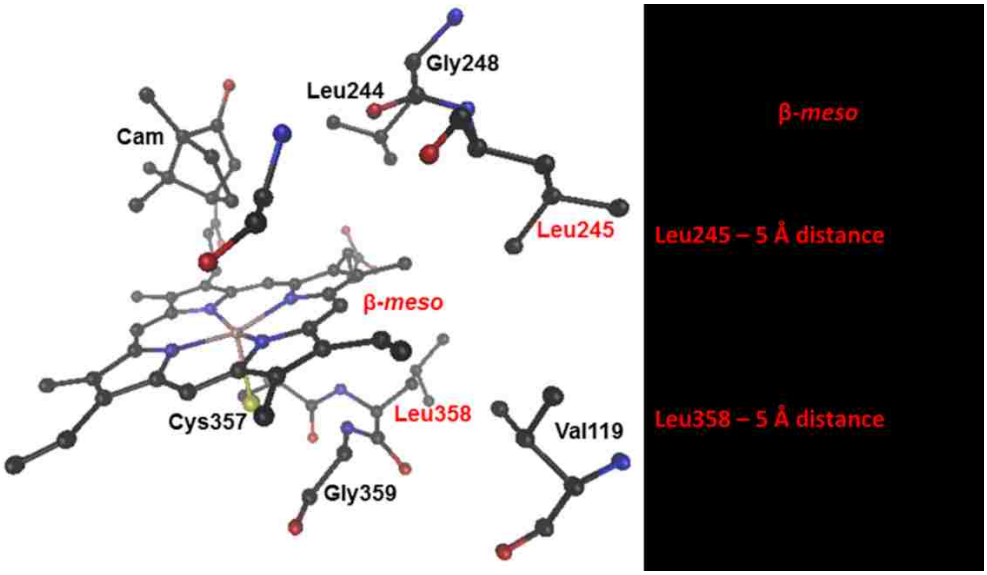

Figure 33 Amino acid residues within 6 Å from the β-meso proton. The most likely candidates are Leu358 or Leu245 which are closest to the β-meso proton.

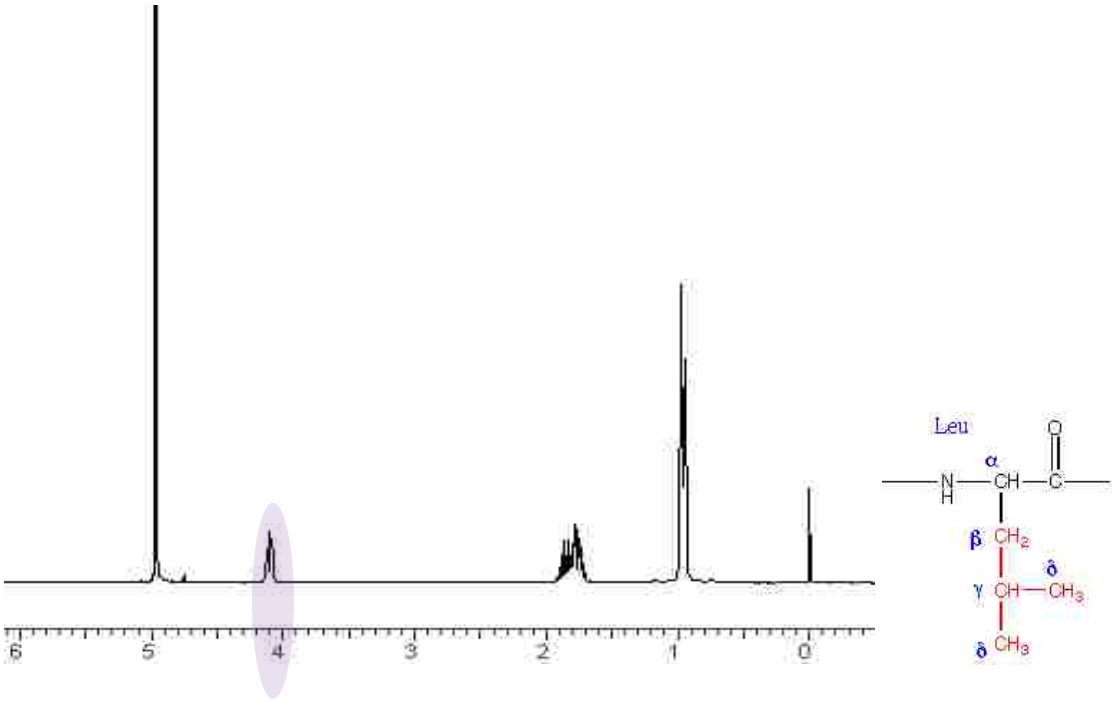

Figure 34 ^{1}H NMR of Leucine showing a resonance around 4.0 ppm highlighted. We tentatively assign the NOE resonance from the β-proton on ^{13}C labeled heme to this leucine proton.

The assignment is reasonable since the signals observed at 4.01 ppm cannot be from a camphor molecule; i.e. the camphor protons are all upfield (between 0-2.6 ppm) relative to this signal (Figure 35 below).

Where does the signal at 1.37 ppm come from?

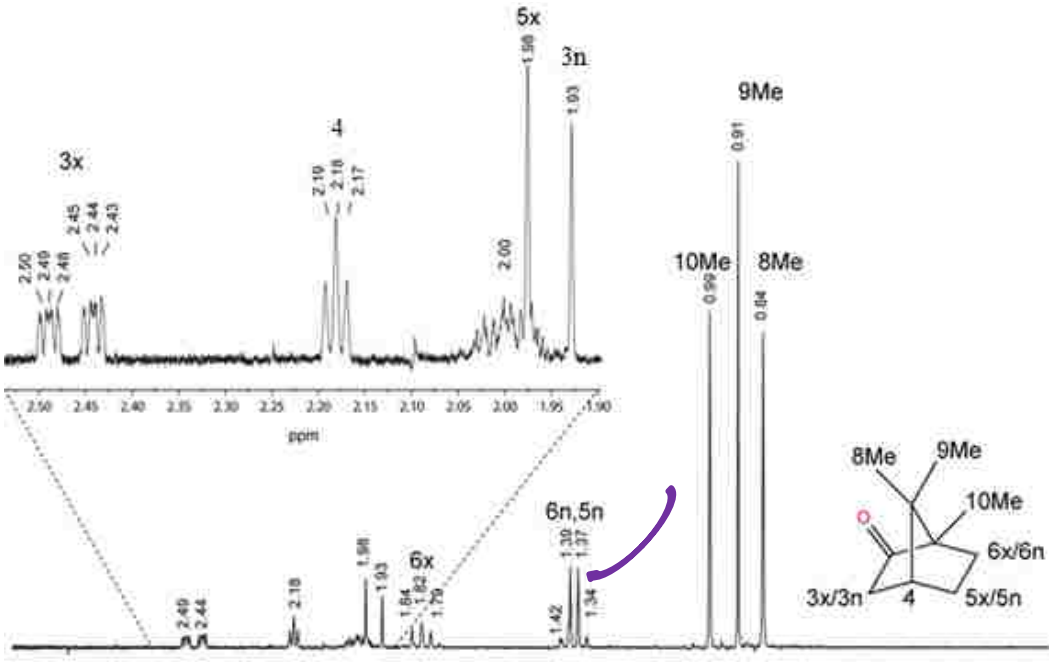

Figure 35 ^{1}H NMR of camphor showing the resonance we observed at 1.37 ppm could be coming from a 5n proton from camphor (highlighted)

It was reasoned that if we can get deuterated camphor and repeat the NOE with D_2-camphor as the substrate, the disappearance of the signal at 1.37 ppm should confirm that assignment. The work described below involves our efforts to get D_2 camphor. Our first attempt was to request a small amount of D_2 camphor from Perera's group after they published a paper[74] using this compound in their studies. They agreed to collaborate and sent us a sample which was a brown oil. We checked the ^{1}H NMR spectrum, which is shown in Figure 36 below.

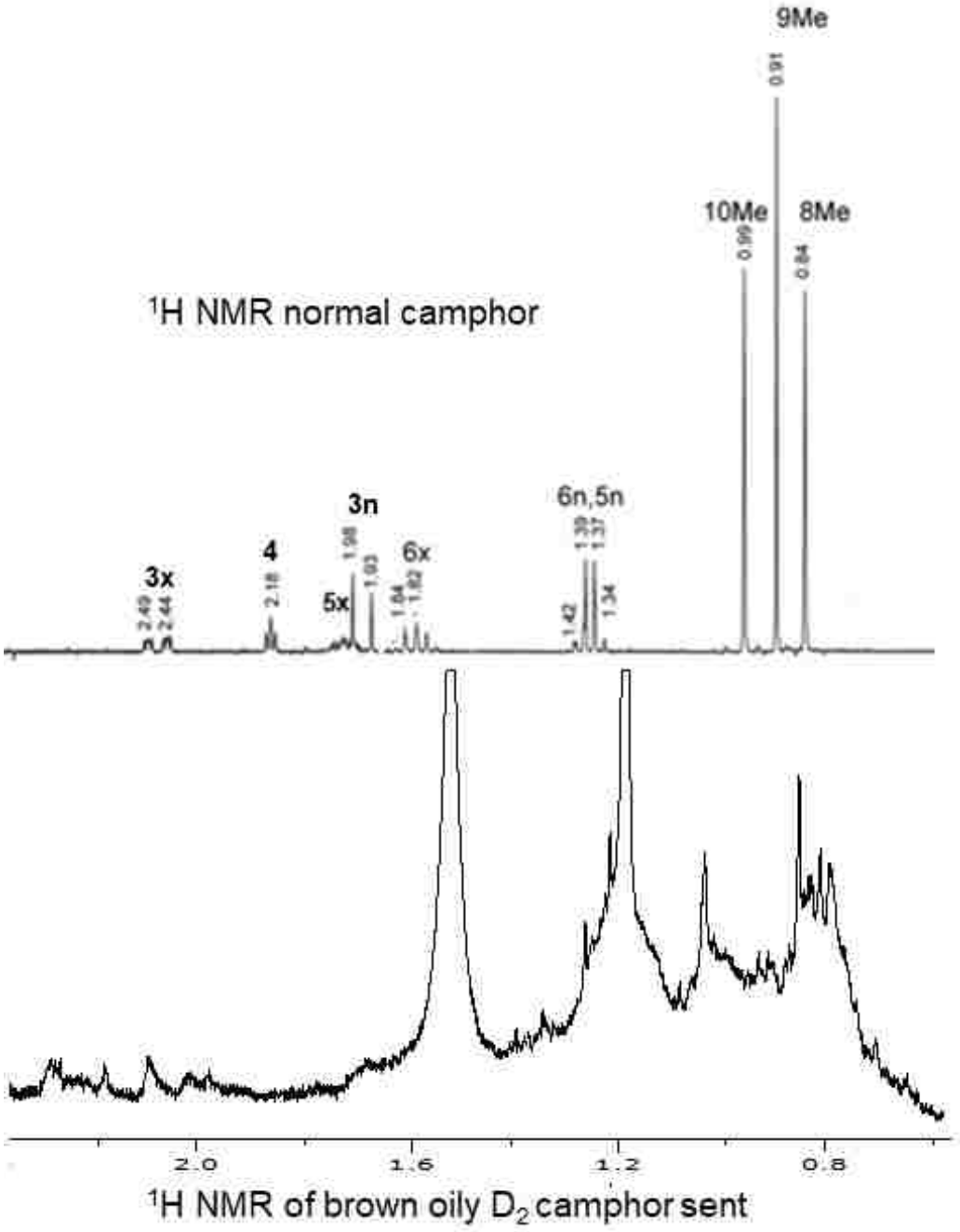

Figure 36 ^{1}H NMR of 5-D_2-camphor (bottom) relative to commercial normal camphor, assignments of normal camphor from previously published data[85, 86, 87–89].

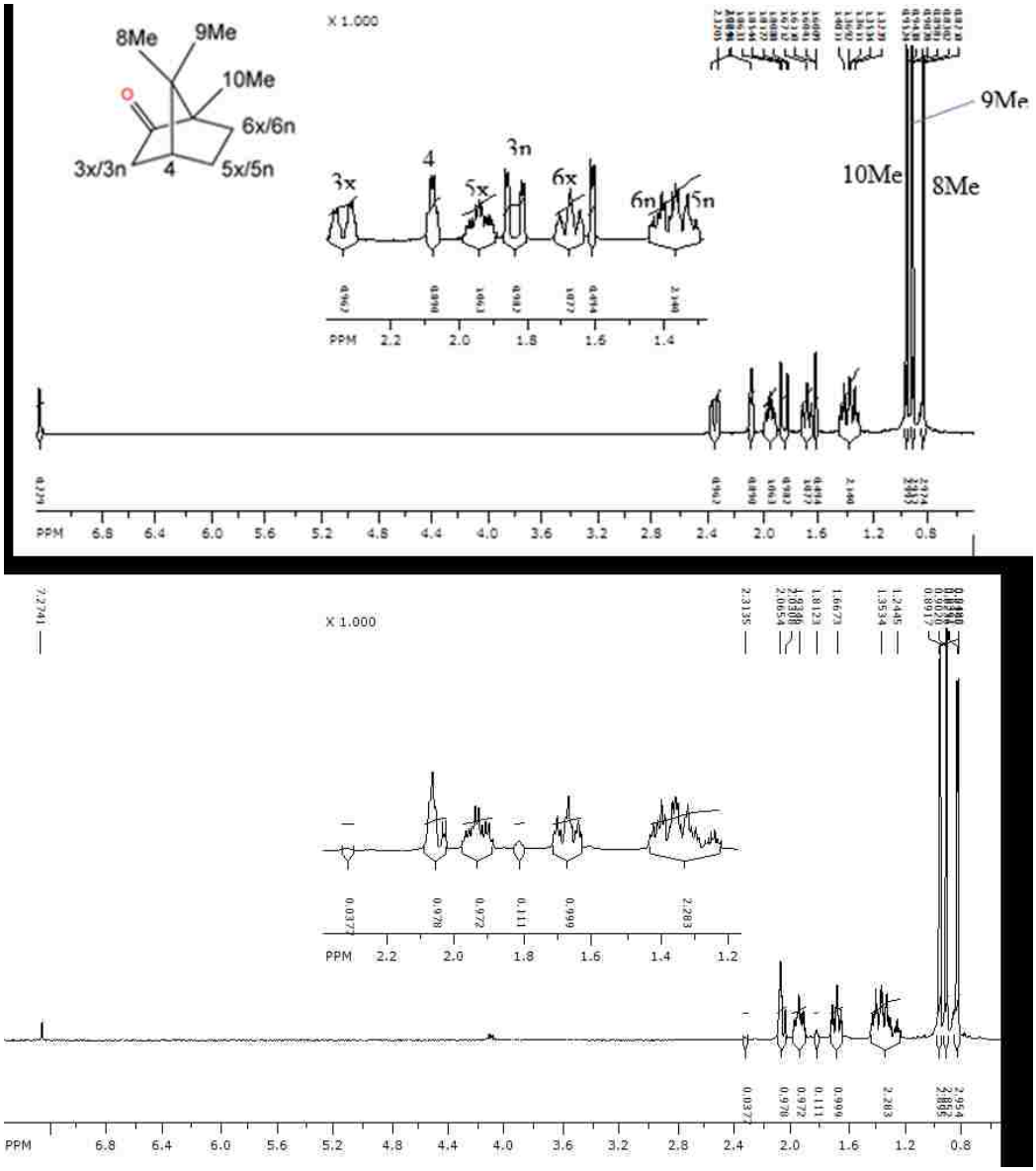

Figure 37 3-D_2-camphor synthesized clearly showing the two protons 3x and completely deuterated and absent from the ^{1}H NMR (bottom spectrum). The insert shows the non-methyl proton enlarged.

For clarity also compare to another form of D_2-camphor synthesized during this work shown in **Figure 37** above. It was clear that the sample sent wasn't pure and we contacted Dr. Perera, confirming the sample sent was not d_2 camphor. While he agreed to cooperate, further requests to get a pure sample were not successful, eventually the

communication stopped altogether. We then faced the task of synthesizing it in our lab using their rather poorly described synthetic method.

2.3.7 Synthesis of D_2 Camphor

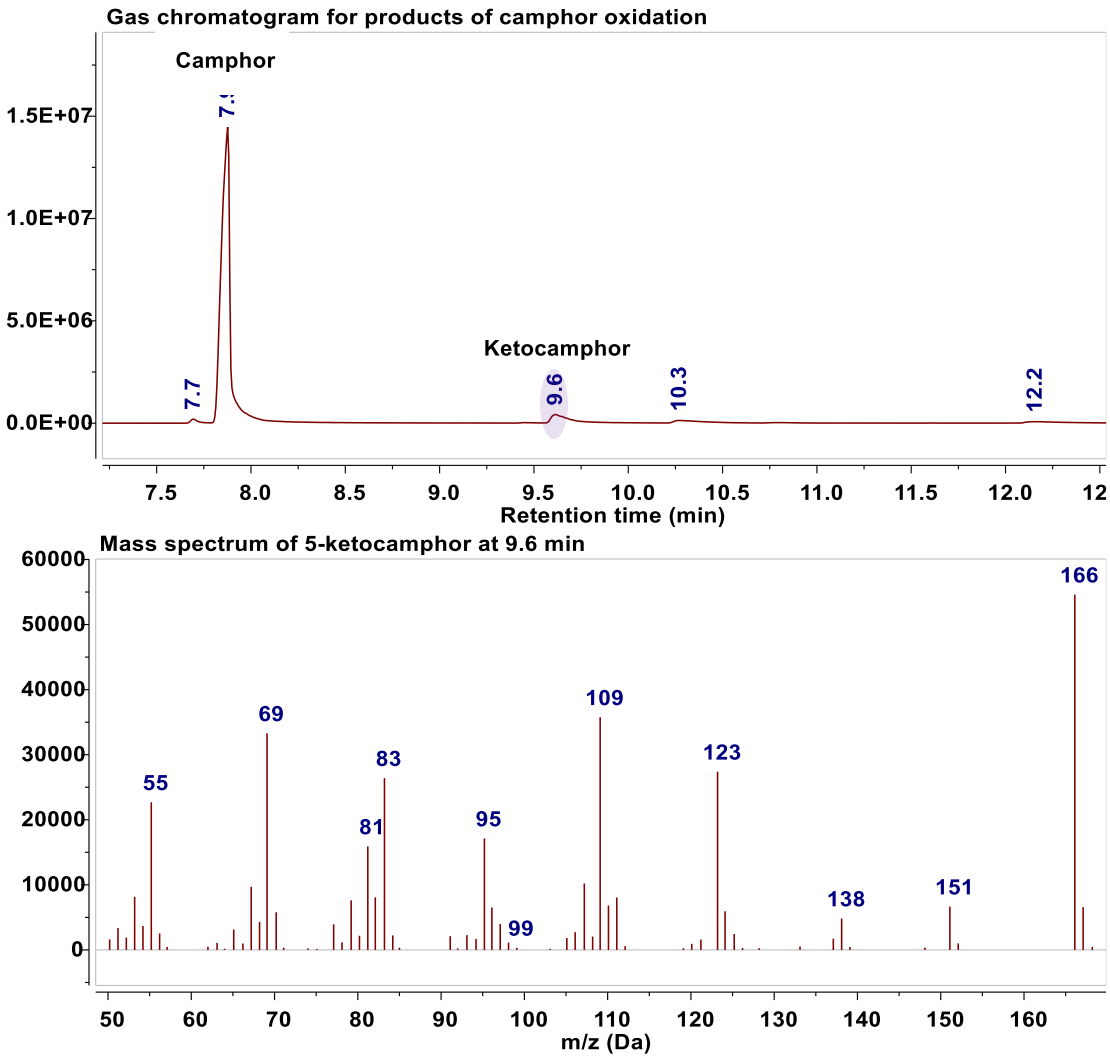

Figure 38 GC/MS spectrum of crude ketocamphor after extractions. The top spectrum shows GC spectrum of product (5-ketocamphor (highlighted)) after extractions, which is only about 5 % and with a retention time (RT) of 9.6 minutes. The largest component in the mixture is the starting material camphor (RT = 7.9 minutes). The bottom spectrum shows the mass spectrum of the product 5-ketocamphor.

Proceeding with the synthesis of 5-ketocamphor described on page 68, 5.43 g of a white solid was recovered which contained mostly unreacted camphor starting material, as shown in Figure 38 above. The mass spectrum shows a peak corresponding to 5-ketocamphor confirmed by fragmentation pattern and matching with previously

published data (see Figure 40 below) The percentage yield of 5-ketocaphor is ≈5 % based on the % area of the peaks obtained by integration of the GC/MS peaks. It proved possible by chromatographic methods described earlier to isolate 5-ketocaphor from unreacted camphor. This was achieved by a better selection of solvents and type of gels separation. In these studies, 5 % ethylacetate and 95 % hexane was used on silica gel then the same solvent was used for the alumina column.

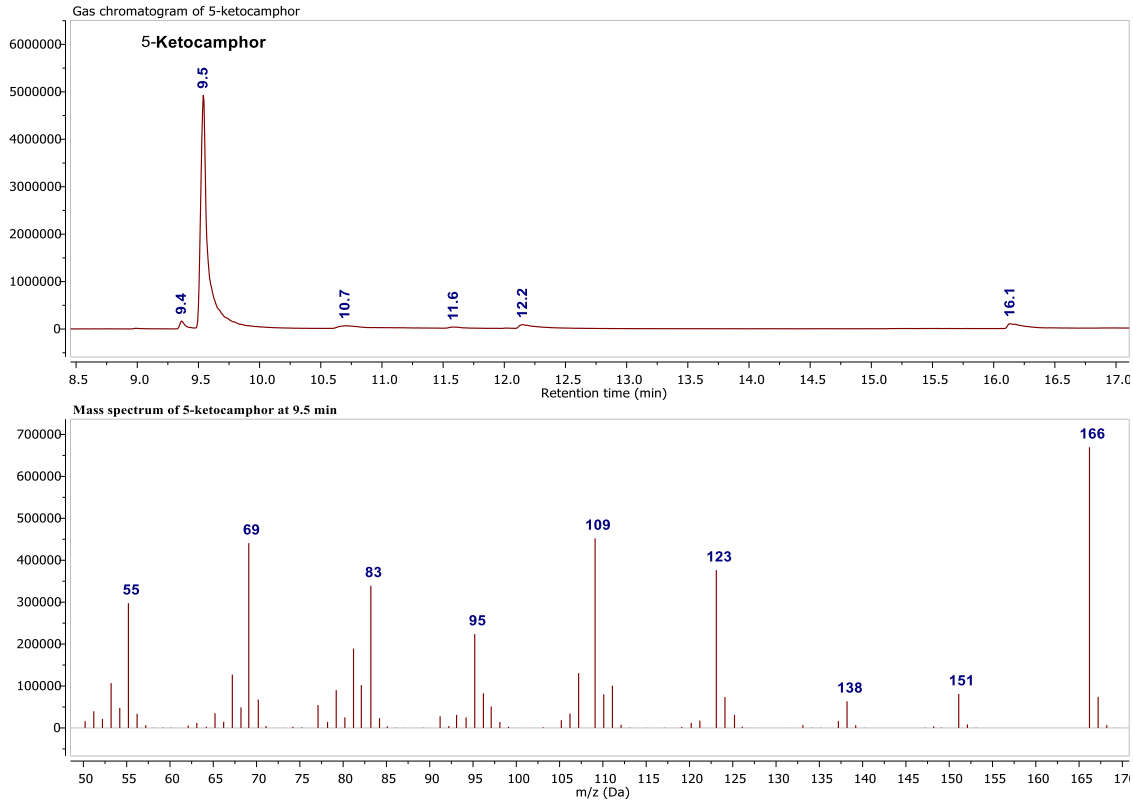

Figure 39 The top spectrum shows the GC spectrum of 5-ketocamphor purified by a couple of columns from a mixture shown in **Figure 38** above. The bottom spectrum shows the mass spectrum of the pure 5-ketocamphor obtained after the purification

Typical yield of 5-ketocamphor (Figure 39 above) was 230 mg and its % purity ≈90 % from integration of GC/MS peaks. We report the isolated 5-ketocamphor (most abundant peak at 9.7 minutes). The white solid was stored in the desiccator until required.

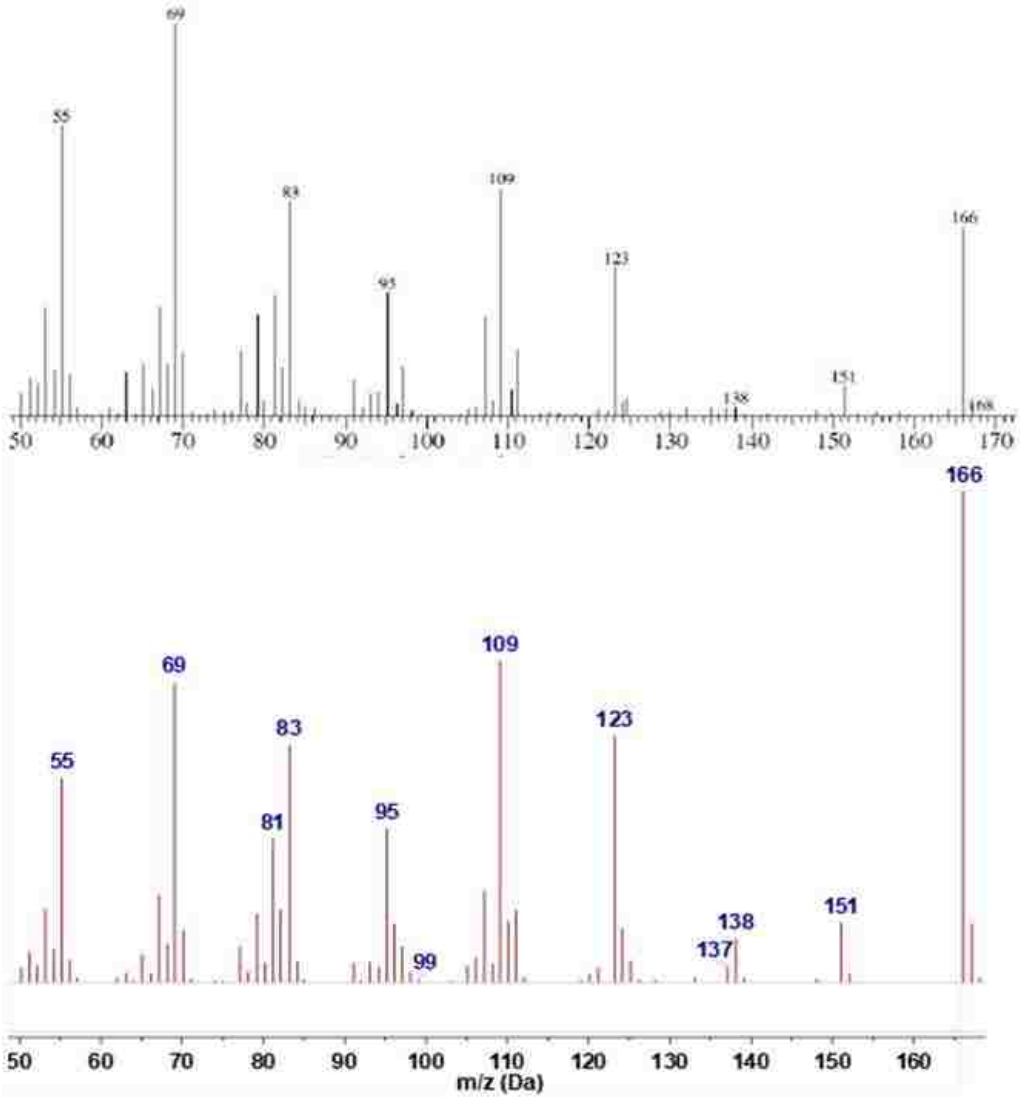

Figure 40 Mass spectrum of 5-ketocamphor published[74] (top spectrum) relative to the experimental spectrum (bottom spectrum)

Evidence to support isolation of 5-ketocamphor is obtained by comparing the experimental data to the published. The two fragmentation patterns show an exact match between published and experimental data with only slight differences in the ratios of peaks, which we attribute to different conditions in equipment.

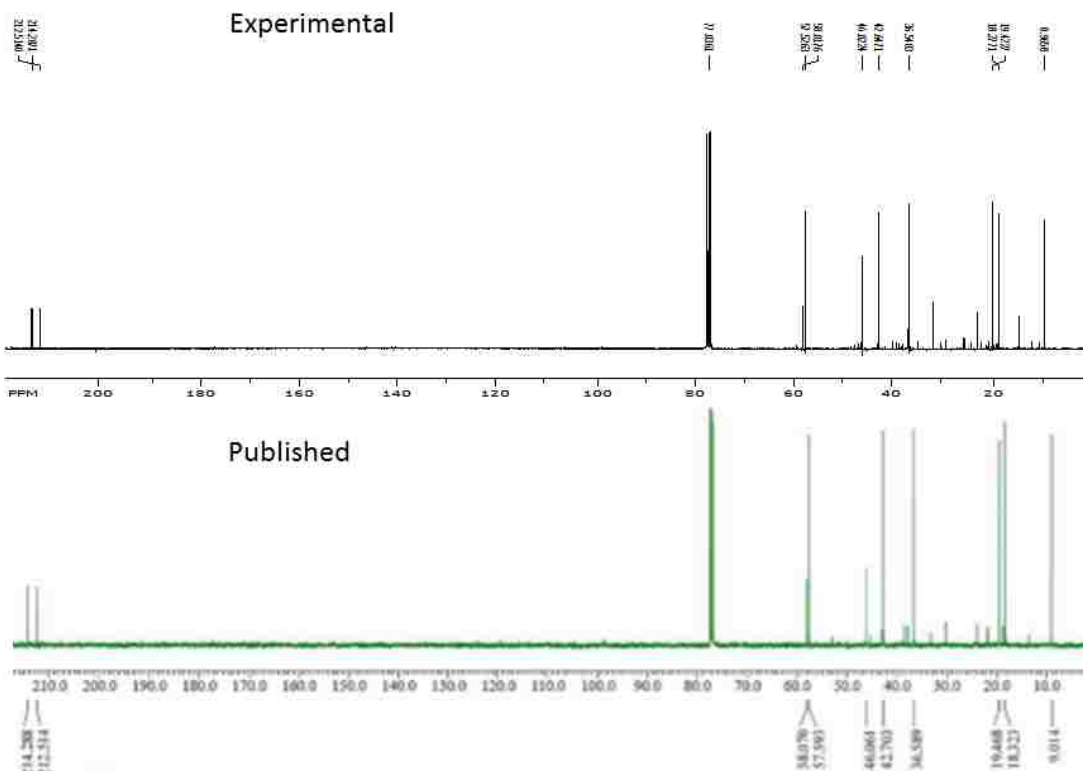

Figure 41 Comparison of ^{13}C NMR spectrum of ketocamphor synthesized relative to the published[74].

The ^{13}C NMR spectra provides further evidence for the success in the synthesis of 5-ketocamphor, though the yield was very low (≈5 % relative to unreacted camphor starting material). We present here the ^{13}C NMR, which clearly shows we have 10 different carbon atoms (labeled with the corresponding chemical shifts) with the two carbon atoms bearing the oxygen atoms downfield around 212-214 ppm, also matching with published spectra.[74] Note that the most intense peak (around 77 ppm) is solvent peak $CDCl_3$. To generate D_2 camphor, the next step involves hydrazine reduction, using deuterated hydrazine.

Step 2 Synthesis of D_2 camphor

It is well documented that the hydrazine reduction can be complicated by the transformation of the hydrazone to the corresponding azine.[75, 90, 91] This challenge may be overcome by using absolute ethanol and anhydrous hydrazine for the Wolff-Kishner reduction. Other methods to suppress azine formation include use of aprotic solvents and inclusion of molecular sieves in the reaction. These methods are only effective to some degree and upon work up, concentration, standing and during purification, hydrazones undergo rapid transformation to azines. Some of the observations in our studies will be discussed in the examples below.

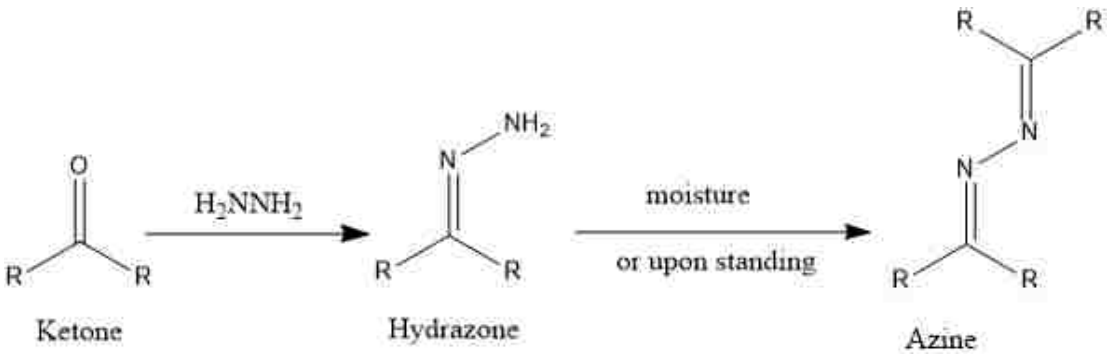

Figure 42 Synthesis of hydrazone scheme showing how the reaction is complicated by formation of azine a stable side product.

Synthesis of norcamphor hydrazone for practice

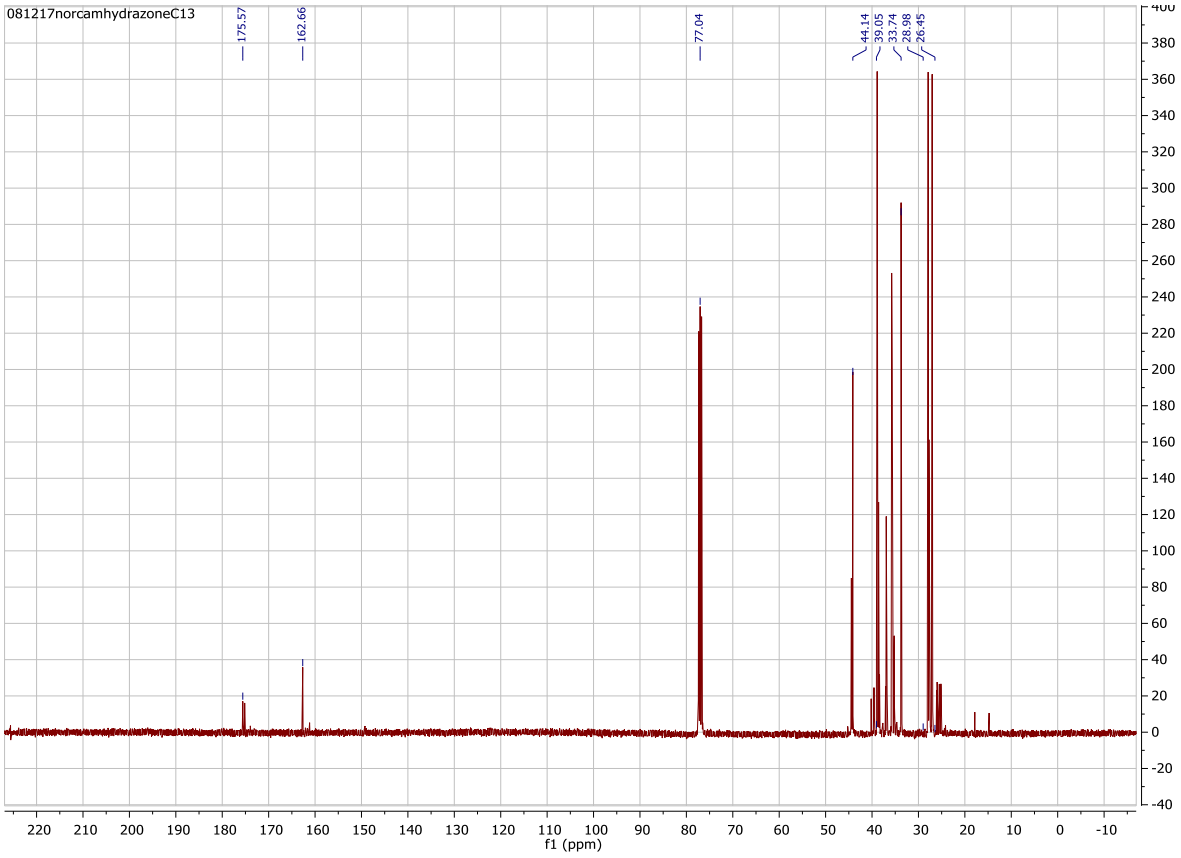

Figure 43 Shows ^{13}C spectrum of norcamphor hydrazone after overnight acquisition. The spectrum clearly shows this is a mixture of norcamphor hydrazone (peak 162 ppm) and the azine (peak at 175 ppm). This was also confirmed by GC/MS spectrum where the hydrazone is formed in appreciable amounts during the reaction but surprisingly turns to azine during work up or upon standing. No starting material (norcamphor remaining)

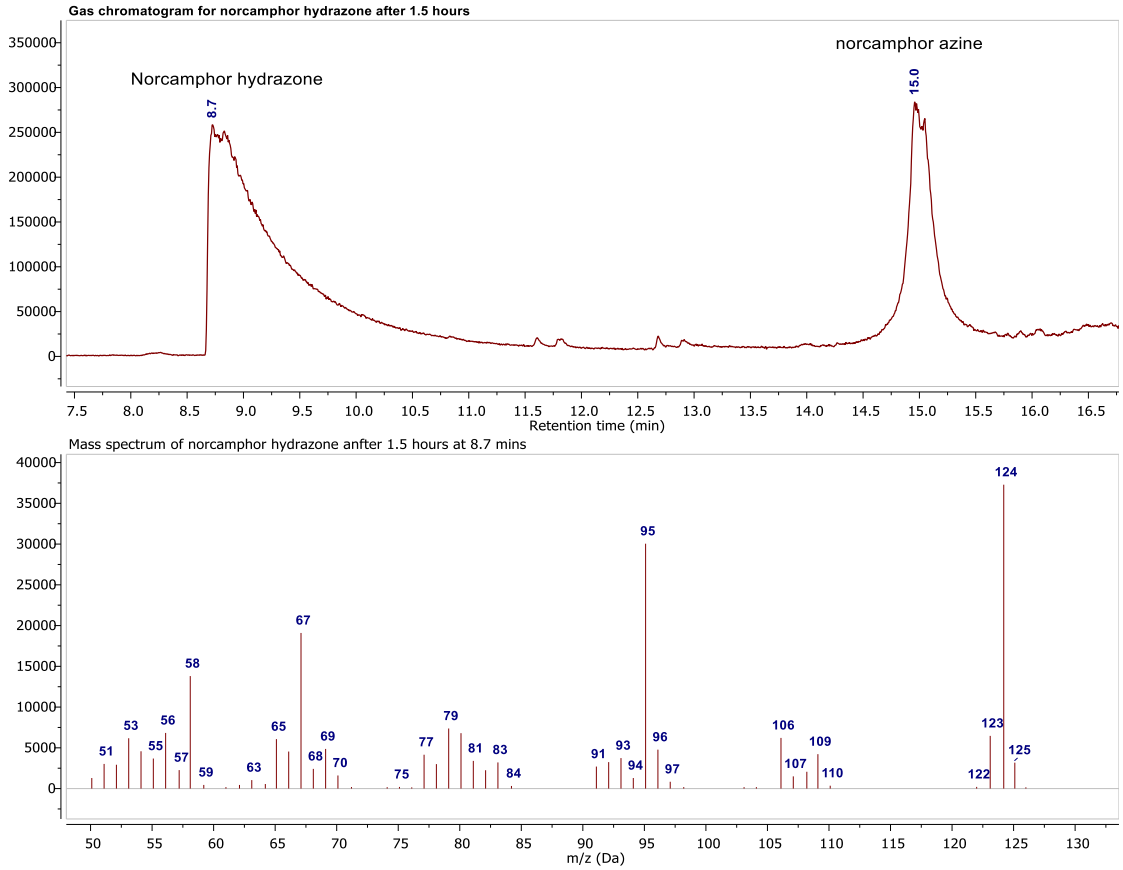

Figure 44 GC/MS spectra for norcamphor hydrazone showing and confirming the existence of the hydrazone (Retention time 8.7 mins, 71 %) and azine (Retention time 15.0 mins, 29 %).

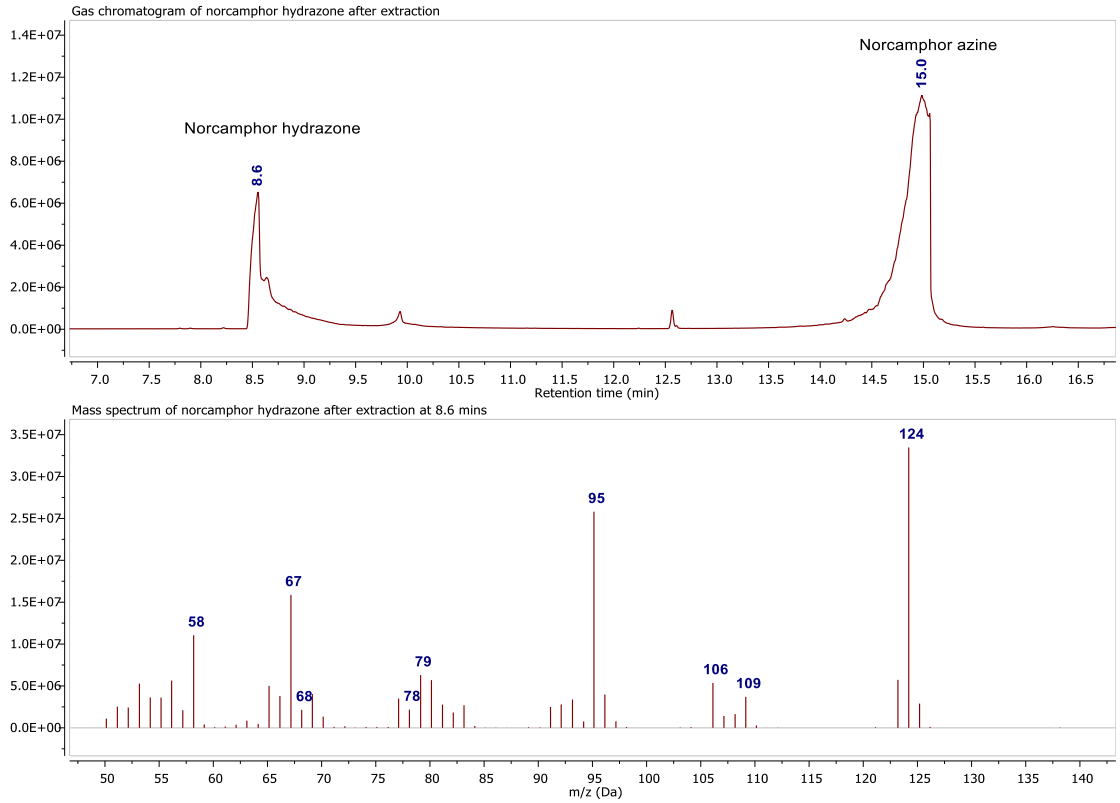

Figure 45 GC/MS spectra of norcamphor hydrazone (26 %) and azine (74 %) after extraction. This demonstrates how hard it is to isolate a hydrazone as it transforms to azine during work-up, or on standing.

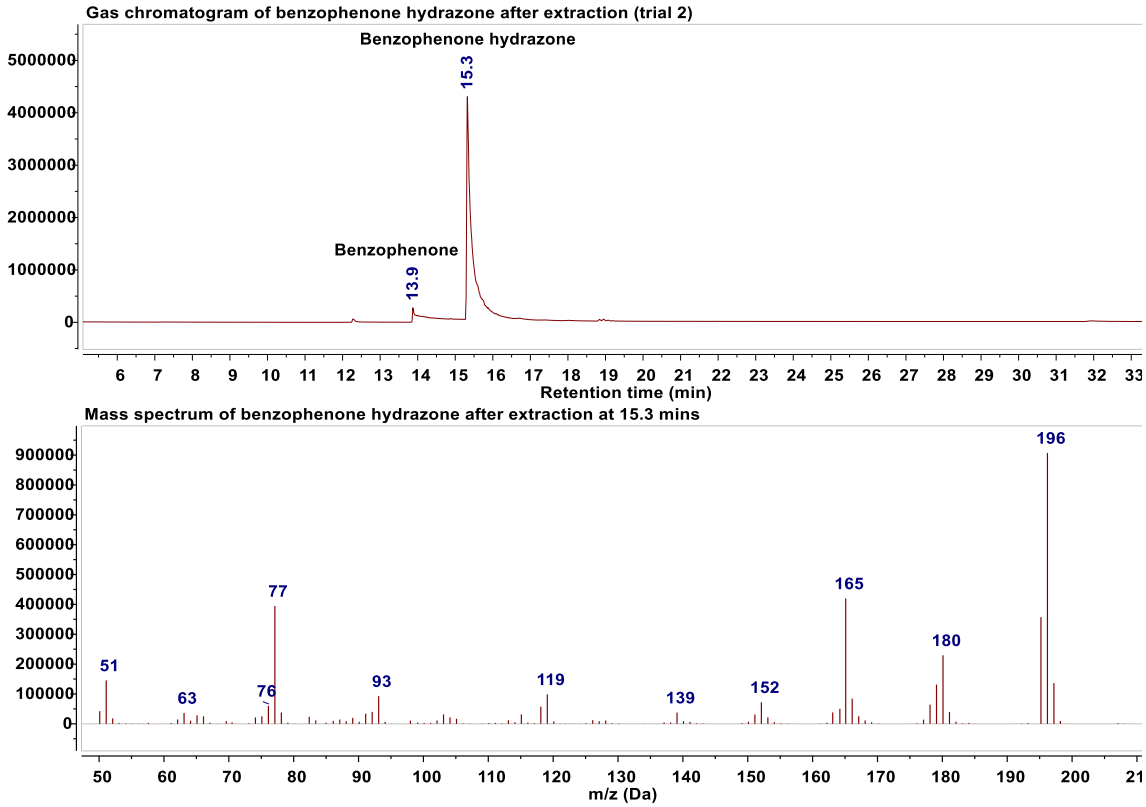

Figure 46 GC/ MS spectra of benzophenone hydrazone. The hydrazone of benzophenone is stable and will be used to practice, then use the method to get ketocamphor hydrazone.

In this work, we report some lessons gained in synthesis of hydrazones. In the first, case camphor due to steric hindrance of the ketone by methyl group 10 (see Figure 47 below), does not form hydrazone or appreciable amounts of azine if reduction is carried out at room temperature or without a catalyst (HCl). This was also reported earlier by Kolb and co-workers.[76] We also know that the unhindered ketone of 3-ketocamphor (camphorquinone) can be reduced at room temperature forming the hydrazone. This was also reported by Kolb and co-workers. Adamantanone was used as the first model for hydrazone synthesis as it contains an unhindered ketone. This turned out to be a bad choice since adamantanone forms azine almost immediately as the major product (≈96 %) and hydrazone minor product (≈4 %). The hydrazone also converts to the azine upon

standing, or catalyzed by acid. Norcamphor was a better choice in the sense that hydrazone was the abundant product but also converts to azine during work up and upon standing (see Figure 44 and Figure 45 above). It also formed an oil after extraction which could not dry and likely to convert to azine faster than if a solid hydrazone was isolated[76]. The conclusions that can be made from the studies include strictly eliminating water and to avoid use of acid catalyst as the acid catalyzes formation of azine.

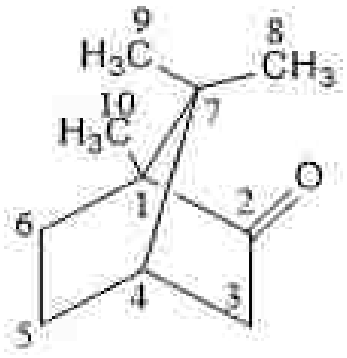

Figure 47 Camphor structure and labeling

A. Synthesis of hydrazones

During synthesis of hydrazones by treatment of ketones with an excess of hydrazine hydrate, we made the following observations. Some ketones gave quantitative yields of hydrazones like benzophenone while others gave very low yields of hydrazones and high yield of azines like adamantanone and norcamphor. Sterically hindered ketones gave low yields of hydrazones with great difficulty including reflux overnight and use of acid catalyst[76]. Also, the hydrazones once formed easily transformed into azines during work up and upon standing. Norcamphor hydrazone (see Figure 48 below) forms substantial amounts during the reaction but transforms into the azine during work up and

on standing. This could be formed by coupling of the initially formed hydrazone with excess norcamphor.

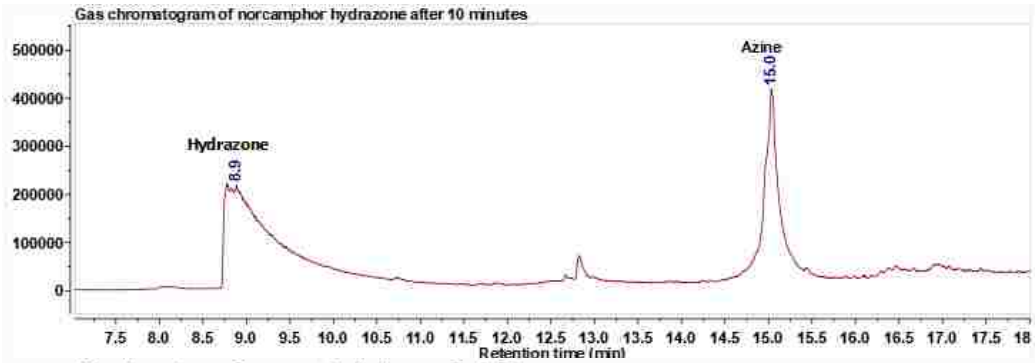

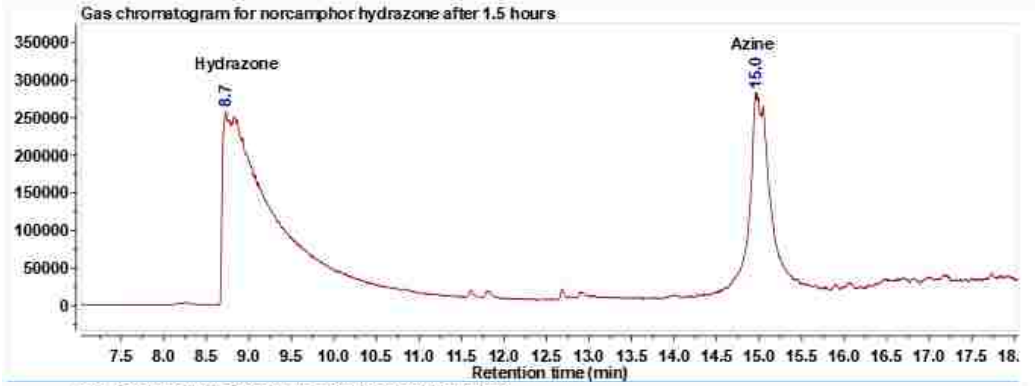

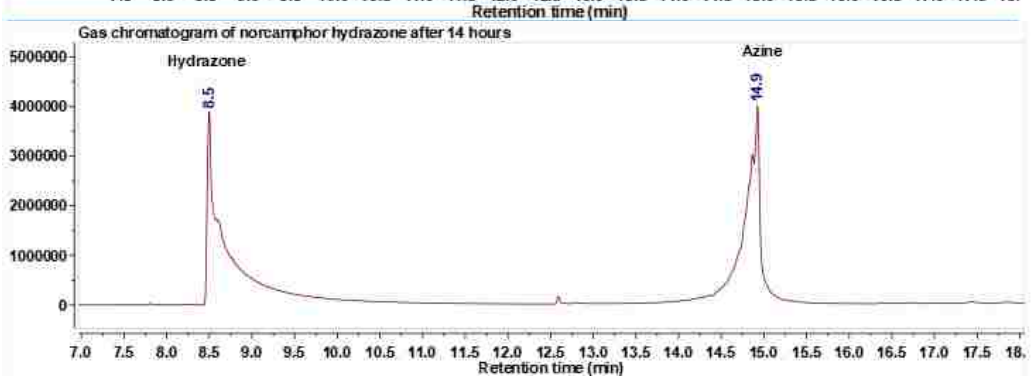

0

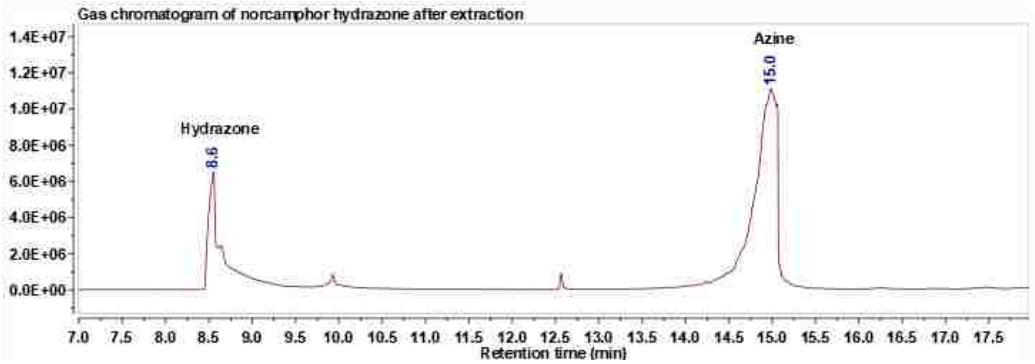

Figure 48 Gas chromatograms showing monitoring the formation of Norcamphor with time. Initially small amount of norcamphor hydrazone was formed and accumulated with time maximum around 1.5 hours. Most of the hydrazone transformed to azine during work up remaining with negligible amount of hydrazone. This shows that it is difficult to isolate the norcamphor hydrazone but it forms in substantial amounts close to 80 % during the reaction.

In conclusion, we know formation of hydrazone is sensitive to steric hindrance, illustrated by camphor hydrazone which only forms after prolonged reflux and use of acid catalyst. In contrast, unhindered ketones either form hydrazone easily at room temperature yet quickly converts to azine during work up or upon standing or forms quantitative yields of hydrazone which is stable for several hours, days or even months depending on the ketone being investigated. This is illustrated by adamantanone forming hydrazone almost immediately and azine major product (95 %) and norcamphor hydrazone forming maximum amount of hydrazone (80 %) in a couple of hours and transforms on further incubation, work up or standing to the azine. On the other hand, benzophenone hydrazone forms in about 72 hours but is stable for several days or months. In the cases were azines formed, their amount increases on standing, faster if hydrazone is liquid and slower when it is solid. In summary, the few ketones studied here the mechanism of formation of hydrazones is neither simple nor straightforward as illustrated by the examples above. The knowledge gained though will possibly allow formation of the hydrocarbon using the Cram modification of the Wolff Kishner reduction.

Alternate Approach

Use of norcamphor as the substrate instead of camphor was attempted to help confirm the effectiveness of the approach that had been indicated by observation of a probable camphor proton resonance in our earlier studies using camphor as substrate. This idea came after a discussion during the annual review meeting that instead of using D_2 camphor a camphor analogue could be used and adamantanone was initially suggested. However, on careful analysis of the free adamantanone ^{1}H NMR spectrum we observed that the resonances for all protons are not well resolved. However molecular volume, hydrogen bonding, high spin percentage in CYP101 for adamantanone and binding mode of strongly mimics that of camphor.[92]

Norcamphor has well resolved proton resonances but has its drawbacks. It lacks 3, 7 and 10 methyl groups as in camphor, which are important for hydrophobic interactions hence holding camphor in a defined position in the active site, hence it is floppy and undergoes multiple hydroxylations by CYP101, approximately 50 % at the 5-exo and 6-exo positions. To effectively do this assignment, two samples were prepared under the same exact conditions and using same batch of protein, one sample with camphor bound as done previously and the other with norcamphor bound as shown in figure 49 below

2.3.8 Use of Norcamphor to confirm the assignment

2.3.8.1 Preparation of samples for NMR

The Figure 49 below shows the spectra obtained during synthesis of CYP101-CN complex with ^{13}C labeled hemes. The sample had been stored as camphor bound sample

to avoid degradation. This sample was passed through G-25 equilibrated with MOPS buffer as described above. Greater than 95 % high spin complex was formed as illustrated in Figure 49 below. The sample was split into two and exchange with the appropriate buffer to allow substrate binding (left camphor containing buffer and on the right shows spectra for the other sample with norcamphor containing buffer). The exchange was a success with greater than 90 % low spin substrate bound sample obtained in each case. The last step was incubation with CN- to a total concentration of 10 mM and this was also a success confirmed by the UV-visible spectra below and agrees with previously published data of cyanide complex of microsomal P450.

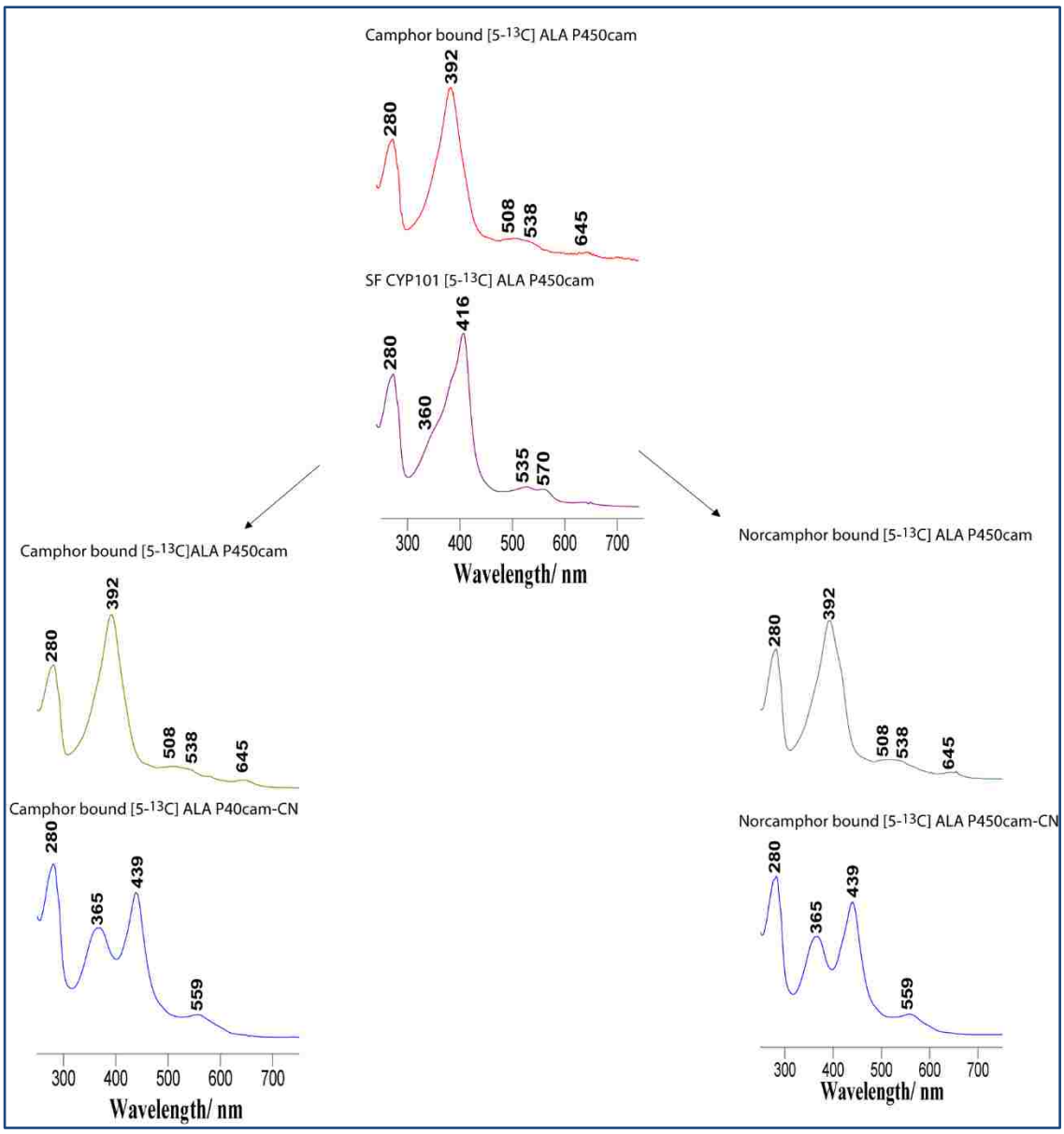

Figure 49 UV-visible absorption spectra showing preparation of [5-^{13}C] ALA CYP101-CN ligated samples for NOE measurements.

^{1}H-^{13}HMQC for CYP101-CN complex camphor bound

Figure 50 below shows the 2D HMQC spectra of the cyanide complex of camphor bound ^{13}C enriched P450cam collected at 25 °C with a recycle delay of 10 ms and decoupling turned off. Protons giving rise to the signals labeled α through to δ are reasonably assigned to the methine positions in as much as the corresponding ^{13}C chemical shifts are consistent with those observed in the 1D ^{13}C NMR experiment for the cyanide complex of camphor bound ^{13}C-labeled P450cam (Figure 31 above). In the current work a similar pattern was observed in the HMQC experiment (Figure 31 above) performed at 25 °C with resonances reproducing what was observed earlier (see Figure 31 above). The experiment was repeated with norcamphor bound in the active site, all other conditions kept the same.

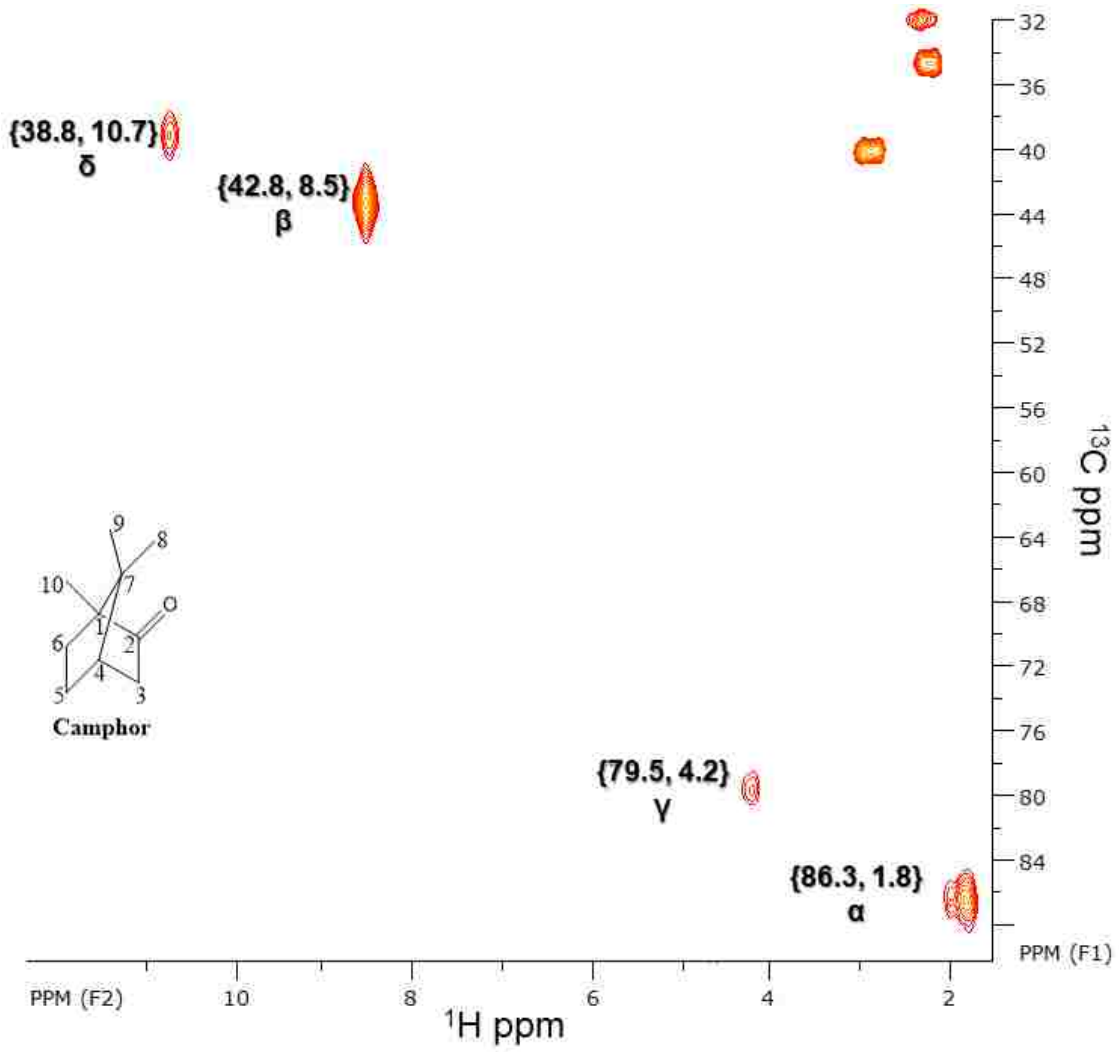

Figure 50 ^{1}H-^{13}C HMQC spectrum of CYP101-CN complex with camphor bound acquired at 25 °C

Nuclear Overhauser effect (^{1}H-^{1}H NOESY): Correlation through Space

The spectrum in Figure 51 below shows the ^{13}C-edited NOESY spectrum of CYP101-CN complex with camphor bound collected at 25 °C and total collection time 69 hours. A single diagonal peak at 8.35 ppm (β) was observed. Earlier studies (see Figure 32 above) showed two methine protons β and δ. The δ proton was not observed this time due to a different, smaller spectral acquisition window (ending at about 9.4 ppm) which

cut out the delta peak which was observed previously in NOE. Two crosspeaks were observed with this diagonal peak as previously reported by Daniel Kaluka[80]. There was a slight shift in these chemical shifts, the more intense peak previously 1.37 ppm now 1.72 ppm and a weaker peak previously 4.01 ppm now 3.32 ppm. These changes are attributed to different temperatures at which the data was acquired (current spectra (Figure 51 below) was acquired at 25 °C while the previous data (Figure 32 above) was acquired at 40 °C. A new crosspeak was observed after careful analysis of the spectra and this comes around 1.98 ppm.

The most intense crosspeak (8.35, 1.72 ppm) was arbitrarily assigned an intensity of 1, hence the three crosspeaks at 1.72 ppm, 1.98 ppm and 3.32 ppm have intensities 1: 0.221: 0.196 respectively based on peak volumes obtained by integration of the peaks. Also, assuming the weakest or less intense peak at 3.32 A is 5 Å away, then the distances of the other crosspeaks were calculated using the equation below (adapted from reference 60):

$$\eta_A\{B\}/\eta_X\{Y\}=r^{-6}_{AB}/r^{-6}_{XY}$$

$\eta_{A\{B\}}$ is the intensity of crosspeak A, whereas r_{AB} is the distance between the protons giving rise to the crosspeak. Three of the parameters are known; hence it is possible to calculate the relative distances between the protons. The results are summarized in the Table 6 below. The calculated distances are within acceptable range from the X-ray data considering that the distances in solution are likely to be slightly different from X-ray due to free movement in solution. Molecules undergo significant motion, including vibrational motion and transitions between states.[93] NMR data is a model of the physical reality to describe the solution distances. Crystal structures can be affected by

intermolecular packing or crystal lattice packing which may lock the structure into a particular position, whereas in solution, the molecule can adopt many possible conformations.[93] A combination of both methods is however ideal in problem solving as the methods complement each other and gaining better understanding of the problem. We have developed a method allowing accurate determination of distances between protons on labeled positions using NMR.

Table 6 Proton-proton distances from NOE experiment

Diagonal ^{1}H chemical shift/ ppm	Crosspeak ^{1}H chemical shift/ ppm	NOE integral	Interproton distance/ Å		Possible assignment
			NMR	X-ray[64]	
	1.72	1	3.81	5.03	5-exo of camphor
β 8.35 ppm	1.98	0.221	4.90	5.51	5-endo of camphor
	3.32	0.196	5.00	6	α-proton of L358

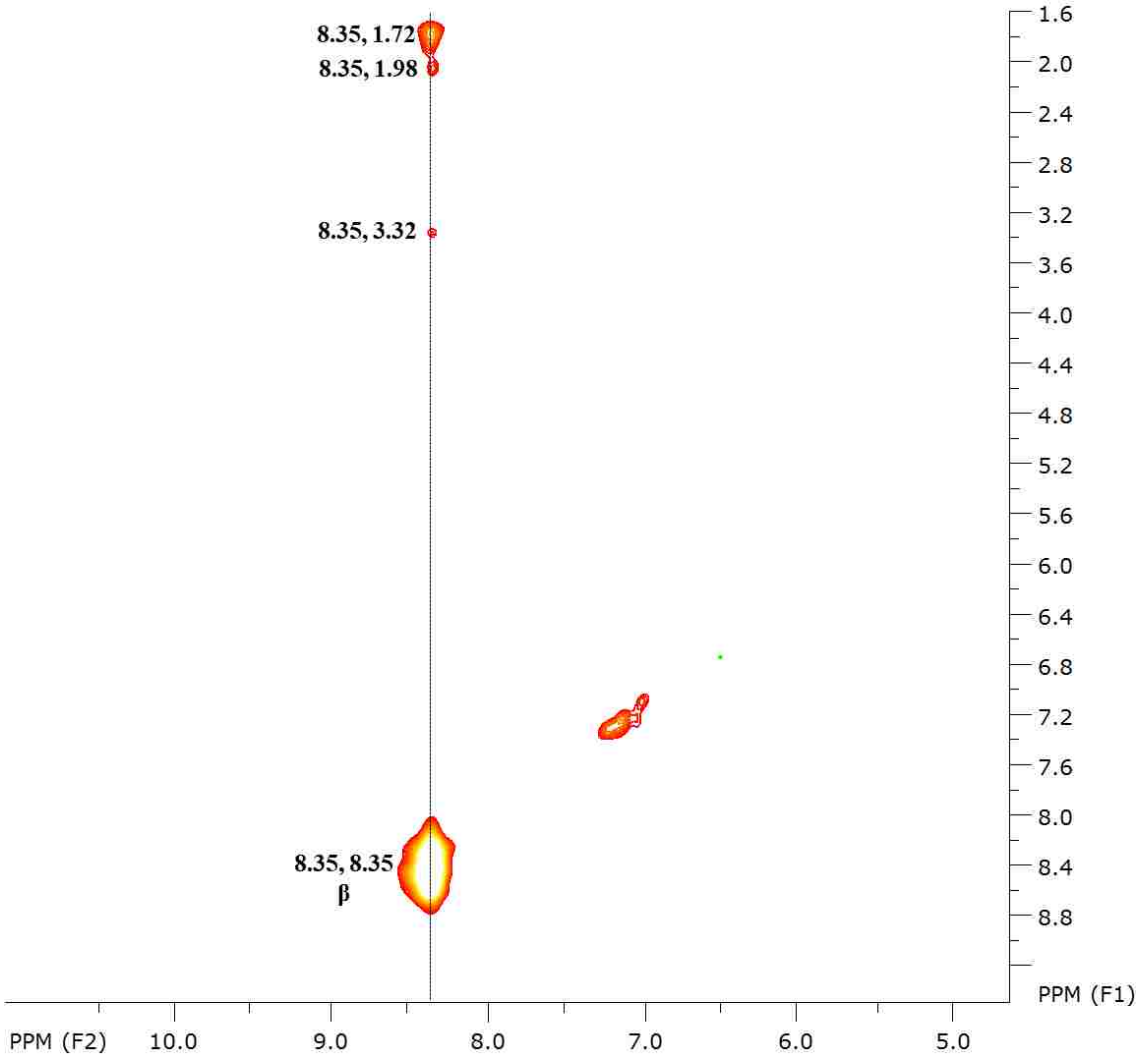

Figure 51 ^{1}H-^{1}H NOESY-HMQC spectrum of ^{13}C-enriched cyanide complex of substrate bound P450cam at 25 °C

^{1}H-^{13}HMQC for CYP101-CN complex norcamphor bound

Figure 52 below shows the HMQC spectrum of CYP101-CN with norcamphor bound. The spectrum was disappointing in two ways. Firstly, the signals were very weak even though the collection time was 18 hours relative to the 1-hour spectrum of camphor bound CYP101 shown in Figure 50 above.

Secondly, the signals drifted relative to the camphor bound spectrum. This was surprising since the UV absorption spectra showed very similar spectra for the low spin complex described in Figure 49 above. We attribute this to the slow decomposition of the sample with norcamphor as it is apparently loosely bound in the pocket.

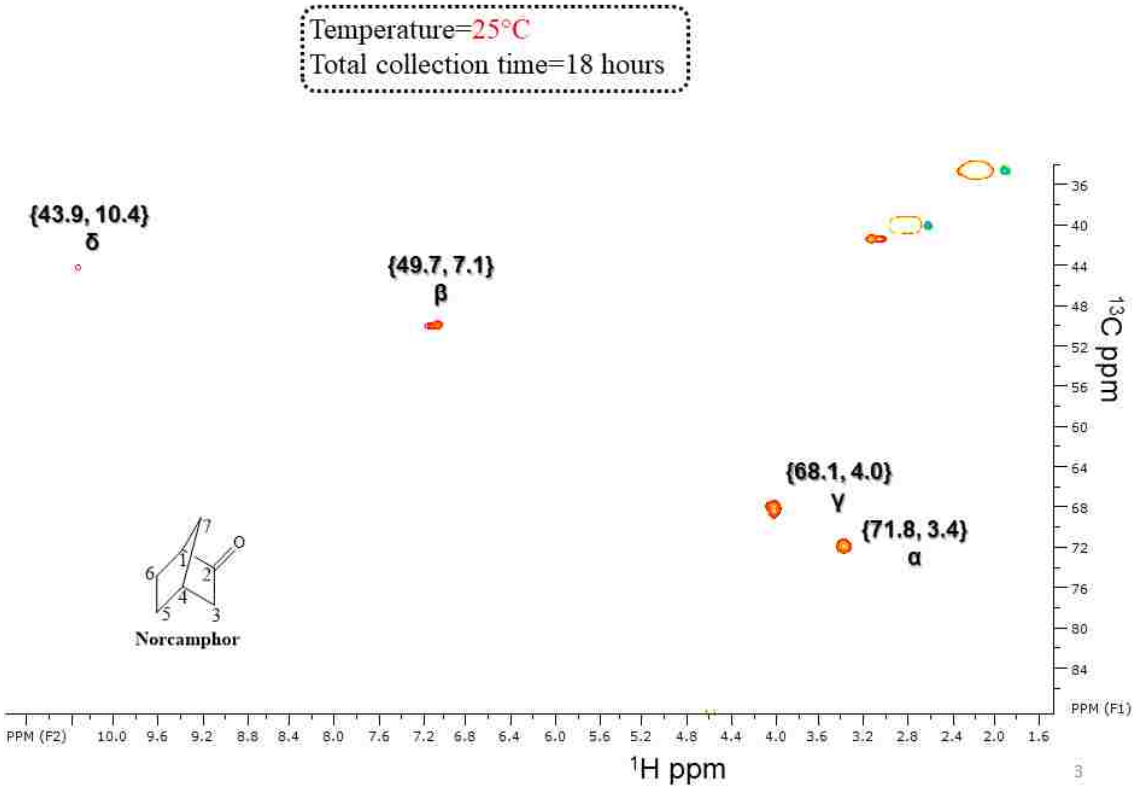

Figure 52 ^{1}H-^{13}C HMQC spectrum of CYP101-CN complex with norcamphor bound

Figure 53 below compares HMQC for CYP101-CN complexes with camphor and norcamphor bound. All other conditions were the same except the acquisition time for the camphor spectrum was 1 hour, whereas for norcamphor it was 18 hours. The α resonance was 86,3. 1.8 for camphor and shifted to 71.8, 3.4 ppm for norcamphor, while the γ resonance was 79.5. 4.2 for camphor and shifted to 68.1, 4.0 ppm for norcamphor. The β resonance was 42.8. 8.5 for camphor and shifted to 49.7, 7.1 ppm for norcamphor. The δ

resonance was 38.8, 10.7 for camphor and shifted to 43.9, 10.4 ppm for norcamphor. There was a drift in chemical shifts observed, but it is emphasized that the sample with norcamphor bound is apparently unstable, leading to weak signals and drift in chemical shifts.

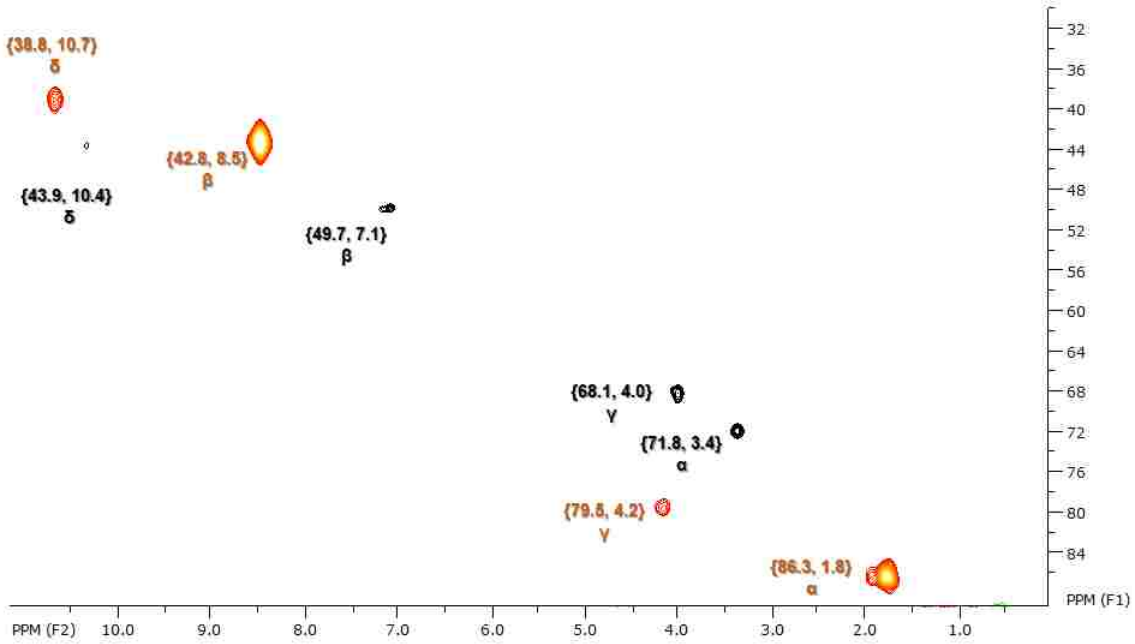

Figure 53 Overlay of ^{1}H-^{13}C HMQC spectra of CYP101-CN complex with camphor bound (red) and norcamphor bound (black)

Figure 54 below shows the ^{13}C-edited NOESY experiment for the norcamphor bound sample of CYP101-CN. Unfortunately, no useful signals were obtained in this experiment. This is attributed to the instability of the sample during the long acquisition hours.

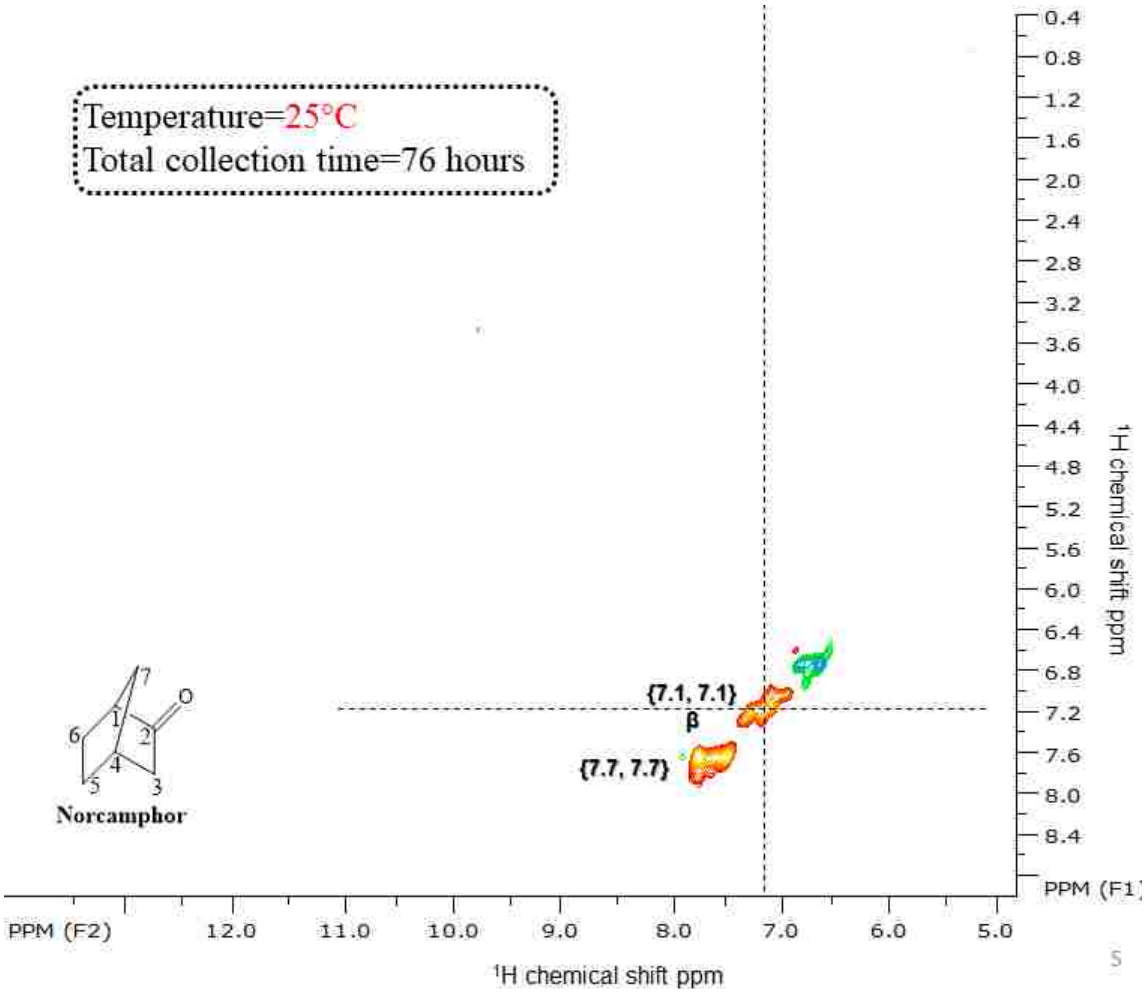

Figure 54 ^{1}H-^{1}H NOESY-HMQC spectrum of ^{13}C-enriched cyanide complex of CYP101 norcamphor bound at 25 °C

2.4 SUMMARY

Owing to severe difficulties encountered in the purification of 2D6, it was decided to abandon that project and the revised plan was to complete studies on CYP101 as proof of principle. A sample of 5-^{13}C ALA was successfully synthesized and used in an expression procedure to yield P450cam labeled with ^{13}C at the four methine carbons (as well as four positions which don't bear hydrogen atoms). Previous experiments in our lab showed that NOE signals can be obtained from protons on labeled ^{13}C positions and protons on nearby protein residues or substrate. Thus, distances can be obtained experimentally from heme to substrate protons for use in restricting docking parameters, with data generated in this work leading to estimated distances based on arbitrary assignment of 5 Angstroms to the longest distance (weakest crosspeak intensity). Attempts to definitely assign the 1.37 ppm signal, suspected to be the 5 position proton of camphor were planned employing D_2 camphor. It proved possible to successfully synthesize and isolate a key intermediate in D_2 camphor synthesis (i.e., 5-ketocamphor) from unreacted camphor, other keto-camphor isomers and additional derivatives bearing hydroxyl groups. However, several attempts to synthesize D_2-camphor from this intermediate were unsuccessful, leading us to undertake an alternate approach involving the use of a camphor analogue that would potentially give rise to a new crosspeak; i.e., norcamphor was selected. While all the necessary NMR measurements were performed for samples containing norcamphor, owing to an apparent instability of this complex, no useful NMR data were obtained.

CHAPTER 3

UTILIZATION OF FLOURINATED SUBSTRATES TO STABILIZE COMPOUND 1 INTERMEDIATES OF CYTOCHROMEs P450 (CYP119)

3.1 Introduction

CYP 119 is a bacterial cytochrome P450 from the thermophilic archaea *Sulfolobus acidocaldaricus*. It has been shown that CYP119 is an effective model system for the study of the intermediate states in cytochromes P450.[94,95] This is an orphan cytochrome, which means that there are no known natural substrates for this enzyme, however, it was shown that CYP119 can hydroxylate fatty acids; e.g., it binds lauric acid with high binding affinity and hydroxylates it in ω the position.[96] Furthermore, it was also shown that CYP119 has relatively stable compound I as compared to other P450s.[97]

CYP119 has an optimum growth temperature of 85 °C and denaturation midpoint (T_m) of 91 ± 1°C[96], which is about 40 °C high than mesophilic P450s like cytochrome P450cam.[98] It has been suggested that the extended 39 Å-long aromatic clusters unique to CYP119 structure (**Figure 55** below) contribute to the temperature and pressure stability; e.g., a single or double mutation of these residues were shown to lower the T_m by as much as 10 °C.[96] In addition to CYP119's unique stability at high temperature, the enzyme displays also very high pressure stability.[99] It is noted that the absorption spectra of reduced and oxidized states, as well as the carbonyl adduct of this protein, exhibit virtually identical characteristics to those of other cytochromes P450.[99]

This enzyme is of great biotechnological interest because its unique thermal properties can be utilized for practical industrial purposes e.g. synthesis of organic intermediates requiring hostile environments like extremes of pH, temperature or organic solvents. Furthermore, the structural features that are responsible for CYP119 heat stability could be introduced into other less stable proteins that are of industrial and medical interest, allowing their more efficient exploitation.[8]

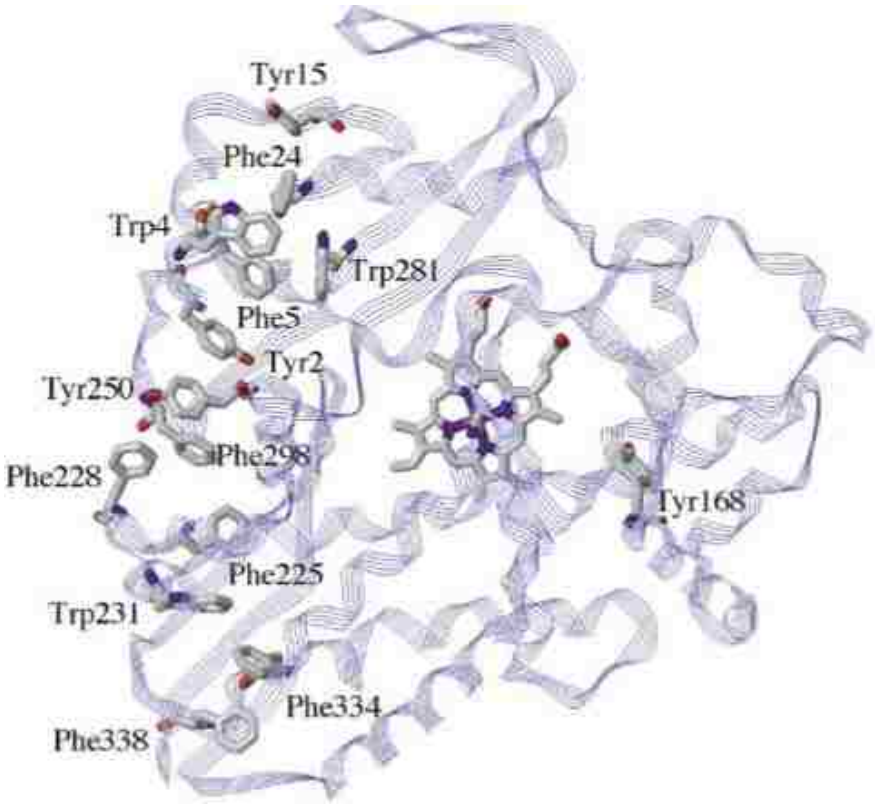

Figure 55 Crystal structure of CYP119 showing the extended aromatic cluster postulated to contribute to the thermal stability[96]

The goal of this project is to use CYP119 and generate, stabilize and characterize the Compound I intermediate using RR technique. As was mentioned in general introduction, the structural characterization of this intermediate is of great ongoing interest for better understanding the chemistry of cytochromes P450.

A wide variety of experimental techniques have been employed to attempt to trap and characterize P450 compound I. These include stopped flow methods with rapid UV-visible detection[35], rapid-mixing freeze-quench methods (RFQ)[95] and photolysis[97]. Also, a wide variety of spectroscopic methods have been employed to detect and structurally characterize this species; e.g.; UV-visible electronic absorption (UV-vis)[35], electron paramagnetic resonance spectroscopy (EPR)[31], Mossbauer spectroscopy[31], vibrational spectroscopy (resonance Raman (rR)[100] and infrared (IR)). A few of these have proved to be effective and efforts have been made to stabilize the highly reactive compound I. Earlier reported studies were carried out for chloroperoxidase (CPO) and horseradish peroxidase (HRP) compound I.[100] The reaction of CPO with oxidants like meta-chloroperoxybenzoic acid (mCPBA) is the model for the peroxide shunt pathway in P450s, since it follows a direct pathway from mCPBA binding to formation of compound I (a green hydroxylating species) in stopped flow experiments.[101] This way of generating compound I was useful in capture and characterization of compound I of CYP119 as described by Green *et al* using stopped flow approach with rapid UV-visible detection (**Figure 56**).[35]

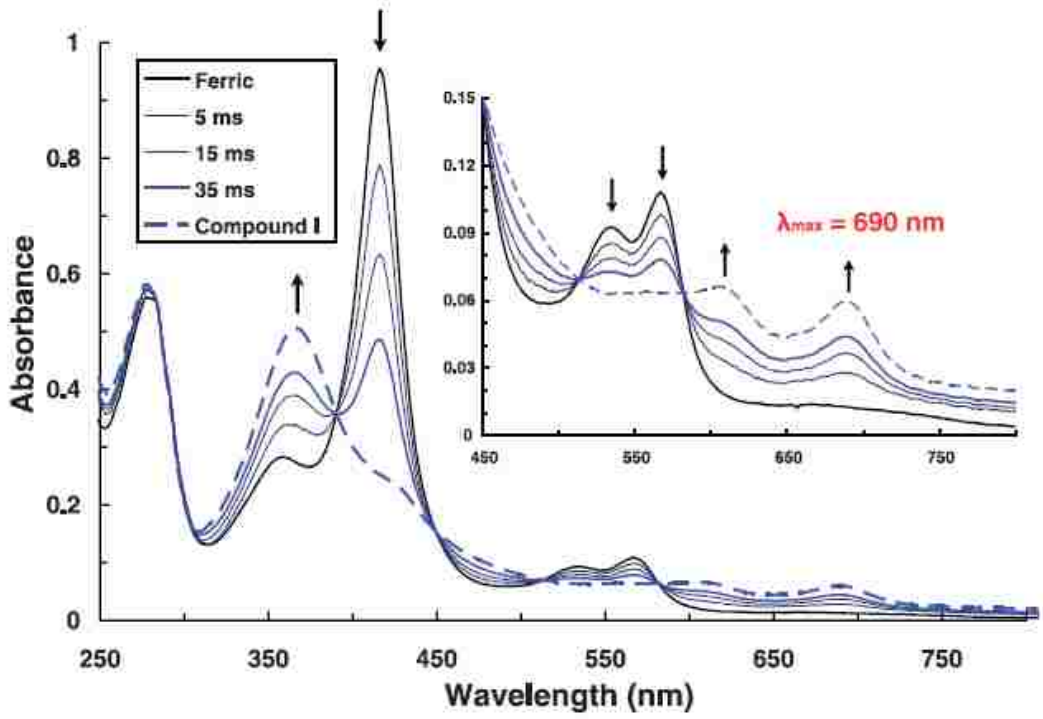

Figure 56 UV/visible obtained from stopped flow mixing (1:1) of 20 µM ferric CYP119 with 40 µM m-CPBA at 4 °C.

Terner and coworkers also reported the rR spectrum of Fe^{IV}=O (oxyferryl) myoglobin at 797 cm^{-1}, confirmed by isotopic shift to 771 cm^{-1} upon reaction with $H_2{}^{18}O_2$.[102] For clarity, compound I is Fe^{IV}=O porphyrin π-radical cation (two oxidation equivalents more than ferric resting state-formally an Fe^{V} heme), whereas compound II is Fe^{IV}=O. Early studies on HRP[103] used Soret excitation (near 400 nm). While HRP-I is stable in the dark, laser irradiation caused conversion to HRP-II-like photoproduct. There was no success using frozen solutions, pulsed lasers or rapid flow. The studies by Terner and coworkers[104] using excitation near 360 nm minimized photolytic conversion and has better enhancement of compound I (Soret near 350 mm). These studies by Terner obtained good rR spectrum showing the ν_4 but no evidence for ν(Fe-O) (due to fast exchange of Fe=^{18}O in water). The Kincaid group used 356 nm excitation, but with very

short (≈1 μs) laser beam exposure to the droplets.[100] This minimized photolytic conversion and also has the better enhancement of compound I (Soret near 350 nm). In this work, a good rR spectrum was obtained showing the same ν_4 as Terner, but now it was also possible to observe the ν(Fe=O) mode appearing at 790 cm^{-1} (based on $H_2{}^{16}O_2/H_2{}^{18}O_2$ studies).

3.1.1 Generation of Compound I, using the peroxide shunt

As shown in the catalytic cycle (Scheme 1) of the majority of cytochromes P450, the Compound I intermediate is generated from ferric hydroperoxo intermediate after a second proton delivery to the terminal oxygen atom of the Fe-O-O-H fragment and cleavage of the O-O bond. However, some other cytochromes P450, called peroxygenases, do not follow this oxygen based cycle, instead, utilize so called "peroxide shunt", in which a hydrogen peroxide, or other peroxy compounds, act as an alternate oxygen donor. As was shown above, the *m*-chloroperoxybenzoic acid (also called *m*-chloroperbenzoic acid; *m*CPBA) was successfully used as a H_2O_2 mimic in generation and trapping Compound I intermediate in several cytochromes P450 (**Figure 56**).[35]

As described in detail above, maximum yield of CYP119-I generated using stopped flow approach was ~ 35~ ms for substrate-free CYP119.[35] It is noted that the commercial *m*CPBA has a purity of about 80 %, as can be determined using iodometric titrations, and a further purification of commercial material is required (vide infra).[105] Furthermore, since the oxygen sensitive modes in the RR spectra of heme proteins are sometimes weak or in crowded regions, the isotopic substitution of the oxidizers are

needed; e.g., the ^{18}O substituted *m*CPBA had to be synthesized (see Experimental Part below).

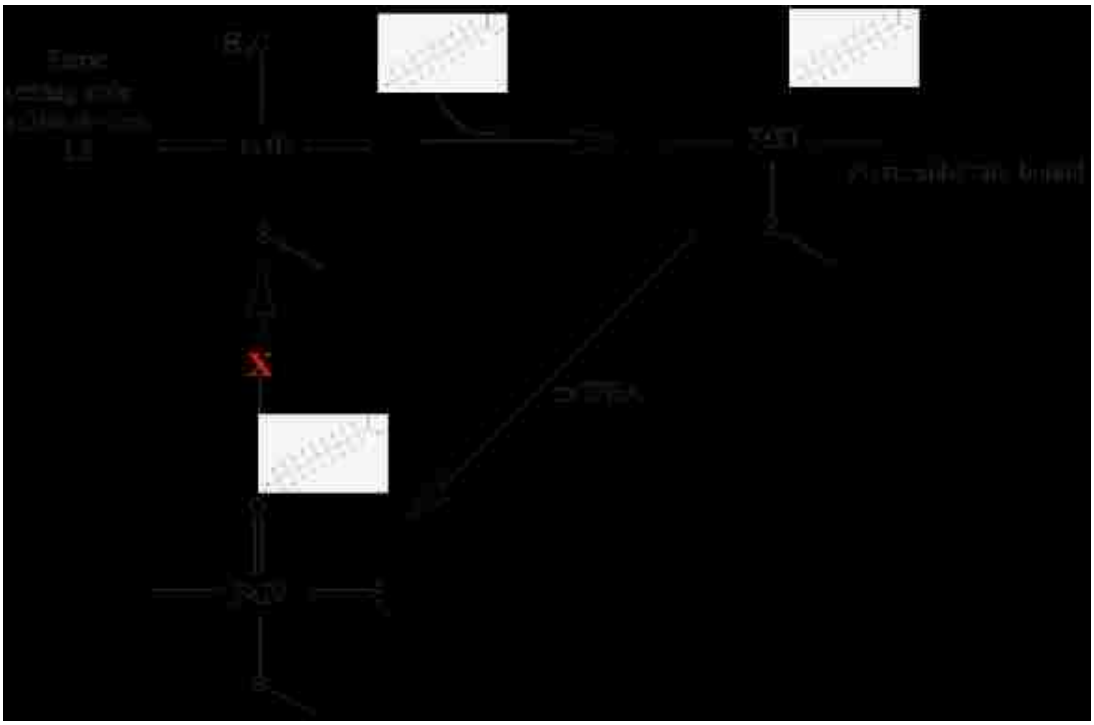

Figure 57 The formation of compound I through the peroxide shunt pathway, oxidizing ferric PFDA bound protein with 3-chloroperoxybenzoic acid (mCPBA)

In the approach presented here, the perfluorinated substrates will be used which are presumed to act as a Teflon cap that will be more difficult to oxidize by Compound I intermediate; e.g., the C-F bonds are less reactive than the C-H bonds leading possibly to prolonged lifetime of Compound I and its accumulation, allowing the characterization of this intermediate using resonance Raman spectroscopy.[106] Naturally, the perfluorinated substrates might exhibit smaller solubility in aqueous condition or bind to CYPs with lower affinity, therefore comprehensive studies of substrate binding were performed as described below.

Such studies of the protein-substrate binding and the determination of stoichiometry of protein complexes constitute an essential element of routine biochemical practice. The concentration of the complex is usually assessed from the changes in absorbance spectra of the protein so that a series of spectra recorded at a constant protein concentration (E_O) and increasing concentration of substrate (S_O) are used to judge the stoichiometry of the complex[107].

In this work, we are interested only in use of dissociation constant (Ks), sometime referred to as binding constant K_d and is defined as **Equation 3** below

Equation 3 The dissociation constant of an ES complex

$$K_d = K_r/K_f = [E][S]/[ES]$$

The reported K_d values for one of the fatty acid of interest to this study, lauric acid (LA), was reported as 1.2 ± 0.2 µM. The K_d value for LA was determined using the method described in previous reports.[108, 109] K_d value of 1.2 µM means that 50% exists as the ES complex at 1.2 µM.

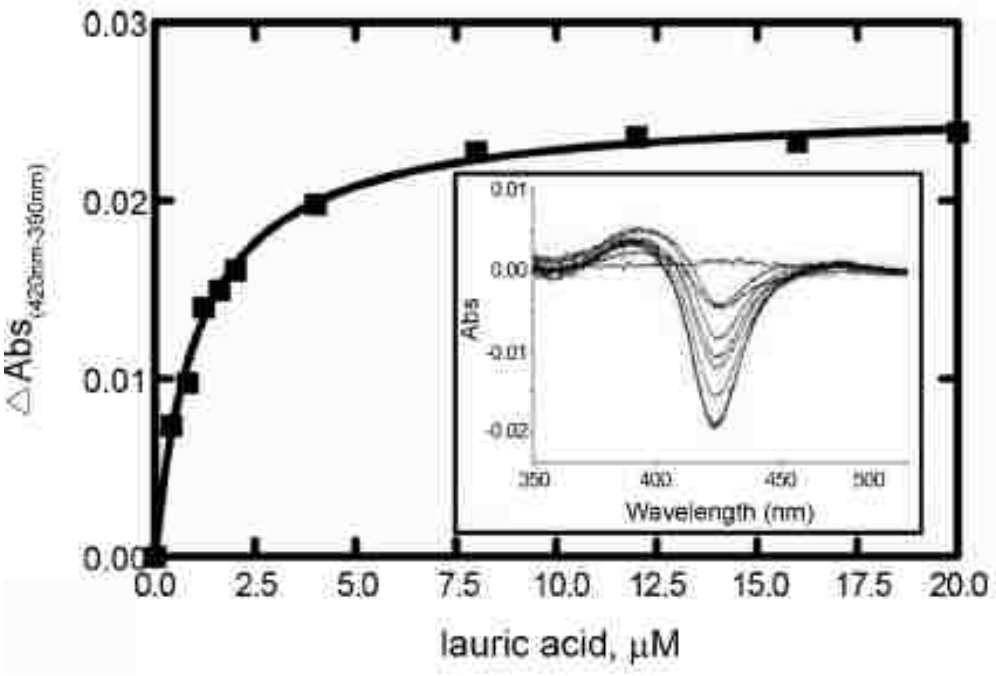

Figure 58 Binding titration of CYP119 with lauric acid: a plot of ΔAbs (390-420) against [LA]. Insert shows titration with increasing [LA]

Finally, it is noted that previous UV-visible absorption and resonance Raman spectra of CYP119 with styrene as substrate, show that at room temperature the enzyme is in low spin state (Figure 59).[25] The absence of spin state change upon substrate binding can be caused by poor displacement of the distal water ligand from the heme iron or indicate that the substrate doesn't bind in the active site. In the above-mentioned studies, the authors showed however, that the same sample does exhibit some spin state changes when warmed to higher temperature. Furthermore, T1 NMR studies in which the distances from the heme to the substrate were calculated, confirmed that even at low temperatures the substrate is bound in the active site;[25] e.g., the distances from each of the styrene protons to the heme are approximately 6.4 Å (Table 7 below)[25]. If the protein is

assumed completely low spin, then calculations showed that the distances will be 4.4-4.5 Å.

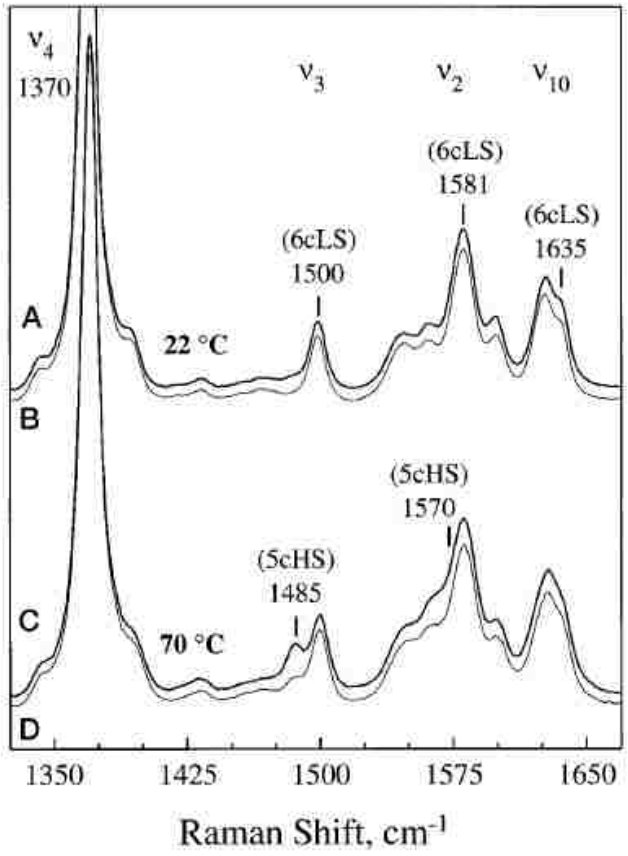

Figure 59 High frequency region of the RR spectra for ferric CYP119 with excess styrene[25] (A) or SF (B) at 22C, and with excess styrene (C) or SF (D) at 70C.

Table 7 [25] Maximum distances of styrene protons from the heme iron atom determined from ^{1}H NMR T1 relaxation data assuming a completely high spin protein

Styrene proton	Distance
	Å
Para	6.2 ± 0.1
Meta	6.5 ± 0.1
Ortho	6.3 ± 0.1
α	6.6 ± 0.2
β	6.4 ± 0.4

3.1.2 Generation of Compound I, using cryoradiolysis

Another way to generate and stabilize the fleeting intermediates in the P450 catalytic cycle is using cryoradiolysis (**Figure 60** below). Using this approach, which was pioneered by Martyn Symons (1980s) and refined and used extensively by Hoffman, Sligar[38] and coworkers (1990-present), the intermediates along the catalytic cycle can be studied. The method is based on preparing the precursor (oxy-ferrous complex) at -20°C for CYP119 and quickly freezing at 77 K. At ambient or moderately low temperatures, oxy-ferrous complex is easily protonated and cannot be studied, but at 77 K, it is stable for several months[38, 110] and can be studied by UV-vis, rR, EPR and other methods. This is followed by one-electron (from water and glycerol) reduction of the frozen (77 K or lower) oxy-ferrous complex using ionizing γ-irradiation (from ^{60}Co source). Such an approach allows accumulation of the peroxo intermediate, as only electrons are mobile and migrate while other movements including proton transport, are generally restricted at 77 K. Annealing at different temperatures allows accumulation of the ferric-hydroperoxo intermediate. Further warming can permit delivery of a second proton followed by O-O bond cleavage and formation of the Compound I intermediate which reacts quickly with a suitable substrate. As in previous approach that takes advantage of peroxide shunt (*vide supra*), in this work the perfluorinated substrate will be also used to prolong the lifetime of Compound I and hopefully permit RR characterization of this intermediate.

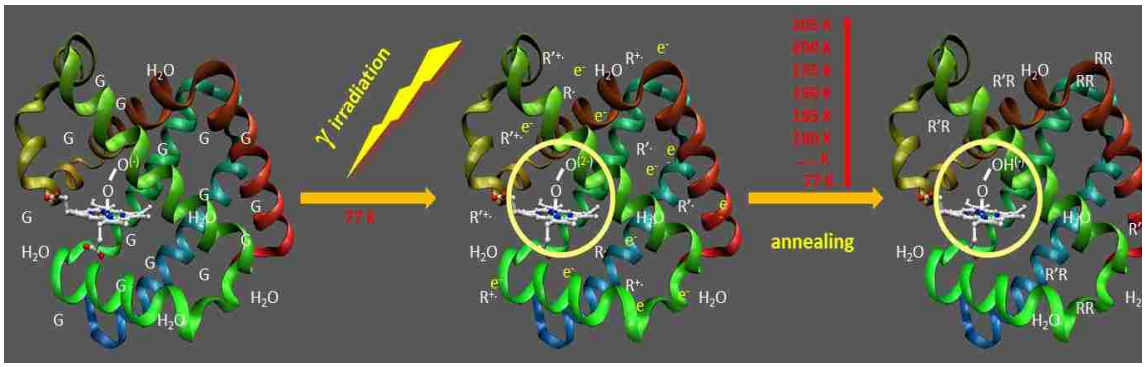

Figure 60 The scheme of cryoradiolytic reduction of ferrous dioxygen adduct (left), to form peroxo (center) and hydroperoxo (right) intermediates upon γ irradiation and annealing, respectively

As mentioned above, the use of very low temperatures is key to trapping CYP's intermediates; e.g., even the relatively stable oxygen adduct often needs to be generated at low temperature, such as -20 °C (Figure 61 below).[110] In order to generate the oxy complex at lower temperatures the protein samples need to be prepared in glycerol/ water solutions to prevent the samples from freezing. Furthermore, the glycerol is also required for cyoradiolysis since is the major source of electrons and radicals during the γ-irradiation.[110] Fortunately, the enzyme remains folded and active even at low temperatures in cryosolvents

A very important aspect in stabilizing the oxy complexes is to control the pH of the sample solution. Volker Ullrich[111] and co-workers performed a pH dependence study of oxy-ferrous complexes which showed that a proton assisted decomposition of oxy-cytochrome C occurs in acidic medium[111]. However, for cytochrome CYP119, the substrate binding seems to be better at low pH values like 6.0. Therefore, to get excellent quality spectra for oxy-complexes a compromise must be reached, giving adequate substrate binding while suppressing autoxidation of the complex, this task is undertaken

in this report. In these studies, oxy-samples were prepared by hooking the sample tube to the vacuum line as shown in Figure 64 below

Other key factors to consider in successfully making oxy-complexes include proper degassing of the sample using vacuum and argon. Typically, this is repeated three times to ensure complete degassing. Reduction of CYP119 is another big challenge and takes sometimes up to an hour to achieve complete reduction.[80] Optimization of the reduction procedure will be discussed in this work and best conditions to ensure the best reduction in the best possible time are deduced in this work.

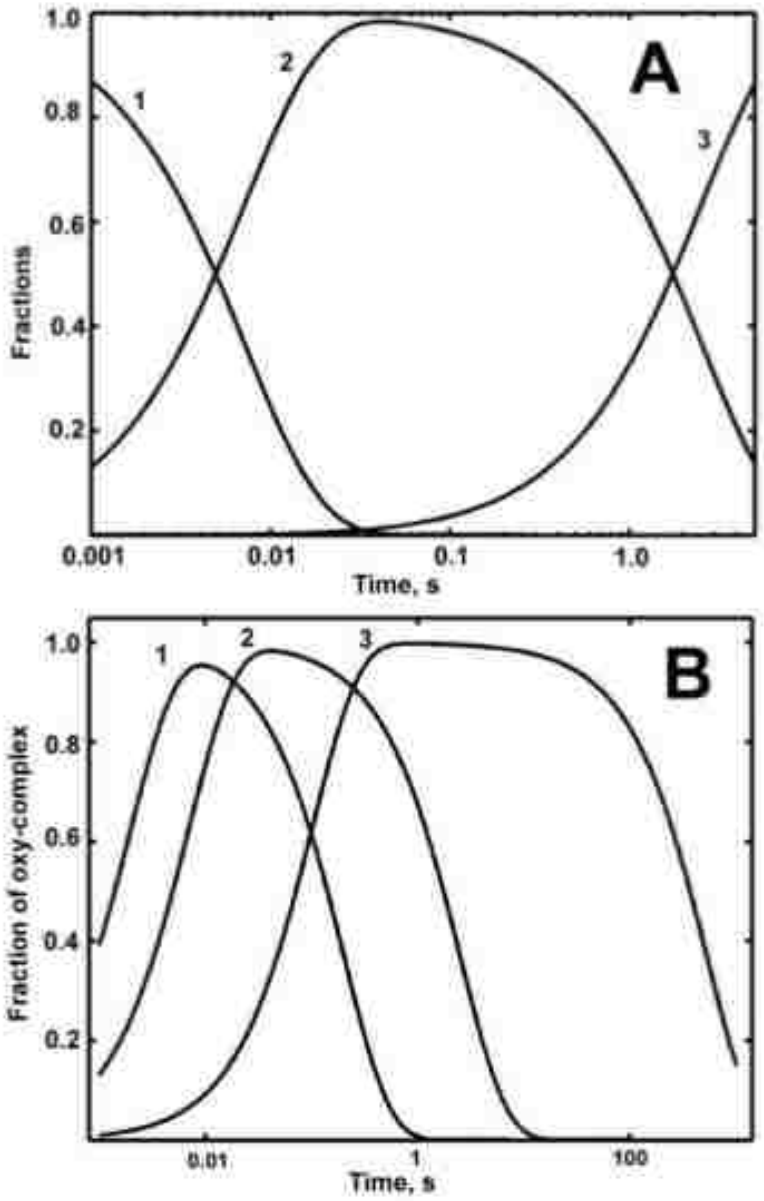

Figure 61 The kinetics of formation and decay of oxy-ferrous complex of cytochrome P450 3A4[110]. (A) Fractions of ferrous (1), oxy-ferrous (2), and ferric (3). At 279 K against time. (B) Fractions of oxy-ferrous complex as a function of time at three different temperatures: (1) 300 K; (2) 279 K; (3) 243 K.

Summary for oxygen sensitive modes studied for cytochrome P450cam and it's D251N mutant.

The data presented in Figure 62 below summarise previous studies of the wild type CYP101 and it's D251N mutant. The v(O-O) stretching mode shows two conformers, one sensitive to hydrogen/deuterium (H/D) shift occurring around 1125 cm^{-1} and the other showing no H/D shift around 1136 cm^{-1}. These conformers show $^{16/18}O_2$ isotope shifts of around 65-66 cm^{-1}. Notice that the conformers are observed after deconvolution of the v(O-O) band. The $^{16}O_2$ - $^{18}O_2$ difference traces are typically deconvoluted using the following procedure.

First, well isolated bands of the absolute trace are fitted with functions that are allowed to have varying bandwidths, intensities, frequencies and Gaussian/Lorenzian percentage contributions. The optimal fit gives two parameters that are then kept constant during deconvolution procedure, that is: functions composition; e.g, 50/50 % Gaussian/Lorenzian, and bandwidths; usually 10.0 cm^{-1}.

In the next step, the bandwidths of the positive and negative peaks of the difference traces are measured. If these bandwidths are wider than the bandwidths of the isolated bands, it is reasonable to assume that they are composed of two or more components. Furthermore, the second derivative of the trace can be run using Grams software to further confirm the presence of multiple conformers. The positive and negative peaks in the difference traces are then fitted with two (or more) peaks of fixed bandwidth and function. The usual practice is to perform the fitting in a manner that restricts the number of peaks to the minimum. The intensities and frequencies of ^{16}O - ^{16}O and ^{18}O -^{18}O modes are then allowed to change during iteration cycles.

The deconvoluted traces of samples prepared in H_2O buffers are compared with these prepared in D_2O buffer. Typically, the D_2O traces exhibit expected $^{16}O_2$ - $^{18}O_2$ shifts that are equal in value to that seen in the spectra of H_2O samples. Quite often the frequencies of the positive and negative bands of the D_2O traces are slightly, but clearly, shifted with respect to corresponding bands seen in H_2O differences. These up-shifts usually reflect the formation of H-bonding interactions between Fe-O-O fragments and the heme pocket amino acid residues or water molecules. It is noted that these H/D shifts are usually small, 1-3 cm^{-1}, however, if present, they can be easily detected and evaluated.

As will be seen later, one of the bands can be very weak and if the weak band is seen and with the correct H/D shift then it is considered a valid peak rather than just ignored. On forming the peroxo intermediate the O-O bond weakens yielding a ν(O-O) frequency of 792 cm^{-1}, whereas the Fe-O bond strengths exhibiting a ν(Fe-O) of 553 cm^{-1}, as shown going from oxo to hydroperoxo intermediate. Protonation to form the hydroperoxo intermediate further weakens the O-O bond, ν(O-O) = 774 cm^{-1}, while strengthening the corresponding Fe-O bond, ν(Fe-O) = 564 cm^{-1}, these shifts reflecting the overall progress in transitioning between the dioxygen adduct through O-O bind cleavage to formation of Compound I. It should be noted that for wild type CYP101, the proton transfer is so efficient that upon cryoreduction of the oxo intermediate, only the hydroperoxo form is formed. This behaviour was also seen for CYP119 as will be discussed in chapter 3. However, the mutant D251N slows down the proton transfer and the peroxo intermediate is observed for the mutant. Also, the hydroperoxo intermediate for wild type is 25 cm^{-1} different than that of the mutant D251N. This

observation demontrates that even a small structural change in the pocket can cause a drastic shift, validating the utility of resonance Raman in studying these catalytic intermediates.

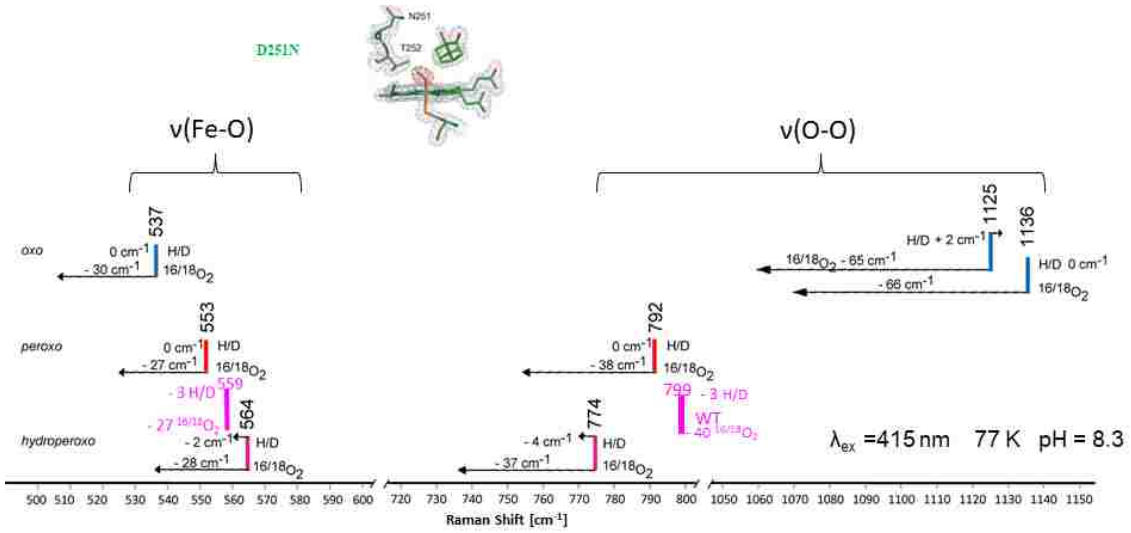

Figure 62 Oxygen sensitive modes for superoxo-, peroxo- and hydroperoxo- forms of heme proteins. The figure shows the utility of rR for studying Cytochromes P450.

3.2 Materials and Methods

To carry out the studies on CYP119 as outlined in the goals and introduction, expression and purification of CYP119 was done as outlined in the methods below. The process helped us understand the biochemistry concepts including transformations, expressions and use of various columns for purification.

3.2.1 Materials

The plasmid encoding the CYP119 gene was kindly provided by the Sligar group (University of Illinois at Urbana-Champaign) and competent BL21 *E. coli* cells were purchased from Biolabs. Tryptone, yeast extract and Luria-Bertani (LB) agar, used in the expression procedure described below, were purchased from Mo Bio Laboratories Inc. obtained from Sigma Aldrich. Perfluorodecanoic acid (PFDA) was purchased from Alfa

Aesar and used without further purification. Lauric acid, β-D glucose, m-Chlorobenzoyl chloride, dioxane were purchased from Sigma Aldrich.

3.2.2. Instrumentation

UV measurements were done using a Hewlett-Packard, Model 8452 Diode Array Spectrometer. For checking the substrate binding same instrument was used but equipped with a temperature controlled cuvette compartment.

RR measurements were obtained using a Spec 1269 spectrometer equipped with a Spec-10 liquid nitrogen cooled detector (Spec 10 from Princeton Instruments, NJ), at liquid nitrogen (N_2) temperatures (77 K). The excitation lines employed for oxy samples before and after irradiation were 413 nm (Coherent Sabre Kr ion laser) and 441.6 nm (Kimmon Model IK4153RC He: Cd laser), respectively. The measurements of ferric protein were performed using 406 nm excitation line (Coherent Sabre Kr ion laser). Resonance Raman measurements of ferrous CO adducts were acquired using 441.6 nm excitation line provided by a He-Cd laser (IK Series He Cd laser, Kimmon Koha Co., Ltd.) The laser power was kept below 1.4 m to minimize photodissociation. The power at the oxy samples and irradiated forms was approximately 1.5 mW, and for the ferric protein was kept at ~ 10 mW. The NMR tube containing the sample was spun and the RR spectra collected at liquid N_2 temperature using 180° (back scattering) geometry in combination with a cylindrical lens, which focusses the laser beam on the sample as a line, to avoid local heating. Temperature during temperature dependence RR measurements of ferric and ferrous CO adducts was controlled by adding hot or icy water to the Dewar and monitoring the temperature changes every 5 minutes. Fenchone was

used to calibrate all spectra, which were processed using Grams 32/ AI (Galactic Industries, Salem, NH). Rayleigh scattering discussed earlier was removed by use of an appropriate Notch filter from Kaiser Optical.

3.2.1 CYP119 expression and purification

Transformation and expression of CYP119

This method is adapted from Sligar's method[112] of purifying CYP119 with some minor modifications. CYP119 plasmid kindly provided by Sligar's group from was transformed into BL21 cells as described before for CYP 101. A single well separated colony was selected and inoculated into a starter culture of 10 mL LB broth supplemented with 100 mg/mL ampicillin and grown overnight at 37 °C and 250 rpm. 1% of the overnight starter culture was inoculated into 80 mL 2YT medium with 100 mg/L ampicillin and grown at 37 °C, 250 rpm until OD_{600} reached 0.3 (early log phase ≈ 2-3 hours). 1% of the early log phase culture was inoculated into 1 L of $2YT_{amp}$ medium also 100 mg/mL ampicillin. A total of 8 L was grown in one of my best trials. The solutions were grown at 37°C/250 rpm for 20 hours. Cells were harvested by centrifugation at 7000 rpm for 15 minutes at 4 °C. A typical yield was 8.5 g/L of wet cells. The cells were stored in the freezer at -80 °C until needed.

Purification of CYP119

Cells were thawed and resuspended in 4 volumes (4 mL/g cell paste) of lysis buffer (50 mM Tris/HCl pH 8.0, 1mM EDTA, 4 mg/mL lysozyme, 16 U/ mL DNase, 4 U/mL RNase) and stirred gently for 4 hours at 4°C followed by centrifugation at 20000 rpm for 1 hour to remove cell debris. The supernatant was incubated at 75 °C for 15 minutes to remove some of the contaminating bacterial proteins followed by centrifugation at 8000 rpm for 30 minutes.

The supernatant was saturated to 40 % $(NH_4)_2SO_4$ and shaken gently for 30 minutes at 4 °C. The precipitated proteins were removed by centrifugation at 8000 rpm for 30 minutes. The supernatant was saturated to 60 % $(NH_4)_2SO_4$ and shaken gently at 4 °C for 30 minutes. The pellet was recovered by centrifugation at 8000 rpm, 4 °C for 30 minutes. The pellet was resuspended in a minimum volume (≈ 5 mL) of 10 mM Phosphate buffer (PB), pH 7.2.

The protein was loaded onto a Bio-gel P100 column equilibrated in 10 mM PB, pH 7.2. Several fractions were collected each with a volume of about 2 mL. All fractions with Rz values > 0.5 were pooled and concentrated and used in the next purification step. The concentrated protein was loaded onto a DEAE 53 anion exchange column equilibrated in 10 mM PB, pH 7.2. The protein was washed with 6 column volumes of 10 mM PB, pH 7.2 and eluted using a 10-100 mM PB gradient at pH 7.2. Fractions with Rz values > 1.5 were pooled and concentrated. Protein purity was monitored using mainly UV-vis determination of Rz values at each stage, checking P450 content of the Ferrous-CO complex and SDS PAGE

P450 content was checked by taking a blank (1.5 mL buffer, ≈20 μL of protein, ≈5 mg dithionite) in a cuvette with rubber sealed stopper. The UV range was adjusted to 400-500 nm. Carbon monoxide gas was bubbled through the solution for two minutes and a spectrum was acquired. A band around 450 nm indicates good and active protein. (see Figure 63. However, a shoulder or a band near 420 nm indicates P420, the inactive form. This process was important throughout my studies, checking for P450 content during expression, purification, and before making samples to ensure protein is still intact.

Protein concentration of CYP119 was calculated based on the extinction coefficient of 104 cm^{-1} mM^{-1} at 415 nm.[98]

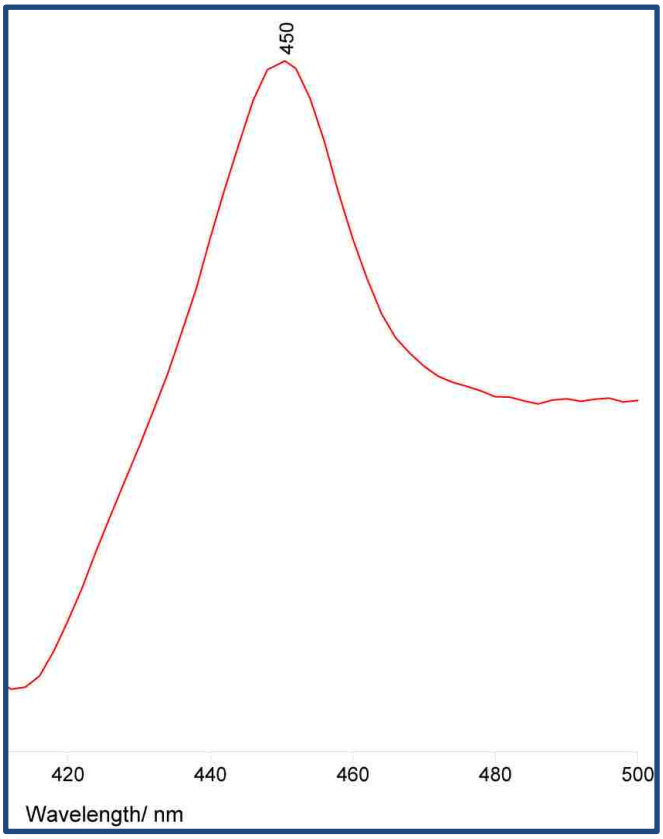

Figure 63 Absorption spectrum of Cytochrome P450-CO complex for CYP119 showing characteristic Soret peak at about 450 nm.

3.2.2 Purification of H_3 glycerol and deuteration of H_3 glycerol to form D_3 glycerol

It has been reported previously in our lab that commercial glycerol at 77 K exhibits significant fluorescence[113]. Hence to remove the fluorescence impurities, a purification method is employed which involves treatment of glycerol with charcoal followed by a vacuum distillation. The methods will be reported here with some slight modifications and simplicity to help future experimenters.

A) Treatment with charcoal

35 mL of spectrophotometric grade glycerol ≥ 99.5%, (Sigma-Aldrich) was mixed with 22.4 mg of charcoal (activated charcoal, decolorizing Sigma-Aldrich) in a round bottomed flask and slowly heated while stirring to 55-60 °C for 3 hours. Charcoal was removed by vacuum filtration assembly consisting of a 100 mL-round bottom flask, 50 mL funnel top, fritted glass funnel support with PTFE membrane filters 0.2 µm pore size. All glassware was cleaned and dried to avoid introducing more impurities during the entire process. Integrity of the sample was checked by RR spectroscopy and GC/MS. The fluorescence level was monitored using RR spectroscopy at 77 K.

B) Vacuum Distillation of glycerol

10 mL glycerol purified in previous step was placed in a small round bottomed flask and connected to a vacuum system and degassed. The temperature of the silicone oil bath was increased to 150 °C and pressure was set to about 6 mTorr.[114] The distilled glycerol samples were collected in 4 fractions.

C) Deuteration of glycerol

This reaction was carried out under nitrogen atmosphere. A mixture of 10 mL commercial glycerol and 74.50 mL (20 M excess) of deuterium oxide was refluxed at 100 °C for 30 minutes. The temperature was increased to 130 °C to distill off the H_2O/ D_2O by-product. The apparatus was covered with aluminum foil to minimize heat loss to the surroundings. The product remaining after distillation was checked by RR spectroscopy to ascertain the extent of deuteration. Toluene was used to calibrate the spectra. The broad OH stretch at around 3340 cm^{-1} levels off in D_3-glycerol. D_3-glycerol was treated with charcoal under vacuum distillation as done for H_3-glycerol above.

3.2.3 Iodometric titrations of *m*CPBA

Iodometric titration[115] is being used to determine the purity of commercial *m*CPBA and the samples of ^{18}O-labeled *m*CPBA prepared as described later on page 143. A 200 mg sample of commercial *m*CPBA was dissolved in 10 mL of 10% KI (w/v), followed by dropwise addition of 5 mL of 1 M acetic acid and dilution to 50mL with water. The dark red solution was titrated against 0.01 M $S_2O_3^{2-}$ to a pale-yellow color and 1 mL of 1% starch solution (w/v) (freshly prepared) was added and the titration was continued until the dark blue solution turned to clear.

The procedure was validated by checking % ^{16}O mCPBA commercial sample and there was good agreement between the values obtained and the manufacturer's values. The procedure above used a lot of sample and was modified especially when ^{18}O mCPBA was purified since the initial amount was mg quantities. About 5 mL of 0.03 M potassium iodide and 10 mL of 2 M sulfuric acid were added to a 250 mL conical flask with 5.0 mL of mCPBA (5.02 mg dissolved in 3-5 mL acetonitrile) and stirred for about 1 hour. The liberated iodine was titrated with the standard solution of sodium thiosulfate, 0.0100 M and a small amount of starch indicator was added when solution turned pale yellow towards the endpoint of the titration. The endpoint was determined by the change of color from blue to colorless.

3.2.4 Preparation of ferrous-CO adducts of CYP119 for RR studies

A 100 μL aliquot of 100 μM sample of substrate free or substrate bound CYP119 was placed in an NMR tube (WG-5 Economy, Wilmad) and sealed with a rubber septum (Sigma-Aldrich, Milwaukee, WI). The tube was saturated with the CO gas for about 30

minutes by passing through the CO gas applied through a long needle. The ferrous CO adducts were prepared by addition of an excess amount of the reducing agent, sodium dithionite ($Na_2S_2O_4$) dissolved in an argon degassed buffer using a needle. The tube was further sealed by adding layers of parafilm on top of the rubber seal.

3.2.5 Preparation of oxy complexes

The buffers were prepared as outlined for CYP101 in Chapter 2. A special note is hereby brought to the reader's attention when preparing D_2O buffers, since we need pH=pD and pH is related to pD by: pD = pH meter reading + 0.40. This relationship was discussed extensively elsewhere[116] and was taken into consideration in preparation of good samples. Each sample was prepared in the same manner and an 80 µL sample of 200 µM CYP119 in 100 mM Phosphate buffer, 0.3 M NaCl, pH 8.0 were prepared with 30 % glycerol. The samples were prepared in clearly labeled, shortened NMR tubes (to ensure tubes fit in the liquid nitrogen Dewar for irradiation setup).

The NMR tube containing protein was mounted carefully on the vacuum line and evacuated followed by addition of argon gas. This is illustrated in Figure 64. This degassing was repeated 3 times to ensure sample is saturated with Argon gas and there is no oxygen remaining. This was followed by protein reduction using 2 µL 7-9 mg/ mL of freshly prepared sodium dithionite which was titrated into the ferric protein using a gas tight syringe through a rubber septum on the vacuum line system, with gentle tapping to mix sample. The sample was titrated with small amount (< 2.5 µL) of sodium dithionite while monitoring the rising of the sharp band at 550 nm that indicates the formation of ferrous form and disappearance of the band at 645 nm, characteristic of high spin ferric protein. Sodium dithionite was introduced using a long needle through the rubber septum. Sample was warmed up to 50 °C (for relatively quicker reduction ≈10 minutes) followed by cooling to -20 °C for 2 minutes. The reduction was studied extensively during this work. The reduction was monitored by UV-visible spectroscopy (Figure 65). The absorption spectrum shows the best temperature for reduction of CYP119 of about 50 °C.

Higher temperature may lead to heme degradation and lower temperatures reduction is too slow and may take up to 2 hours. After cooling the reduced protein for about 2 minutes, ^{16}O or ^{18}O gas was quickly added and mixed for 3-5 s by vortexing or tapping with finger and then quickly (less than 2 s) frozen in liquid nitrogen.

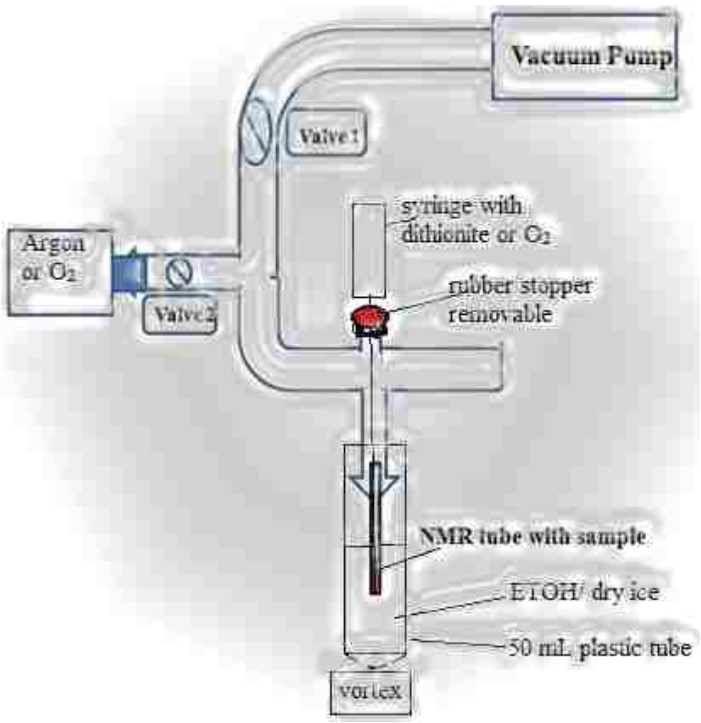

Figure 64 The schematics of vacuum line for preparation of oxy-CYP119 samples.

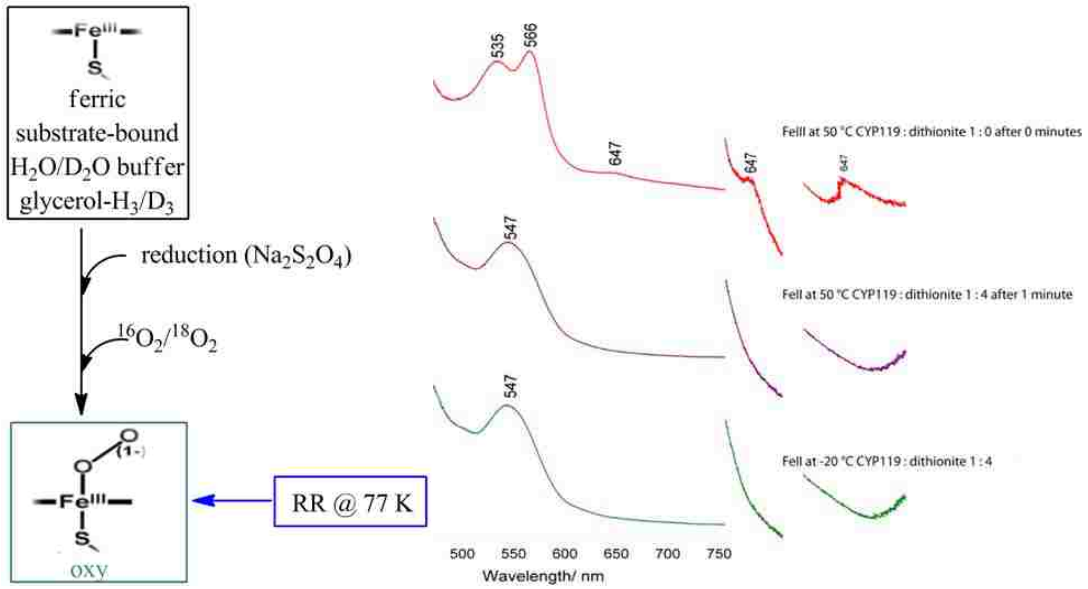

Figure 65 Making oxy complexes involves reduction of ferric SB sample and addition of dioxygen. The absorption spectrum of ferric (top right trace), ferrous (bottom traces) for LA bound CYP 119. The insert shows the expanded Q band region to show complete reduction of sample.

RR measurements of the frozen sample were performed at 77 K, using 413 nm excitation line. The choice of excitation line was based on the Soret of oxy adducts of cytochromes P450cam which is around 415nm (Figure 66 below).[117]

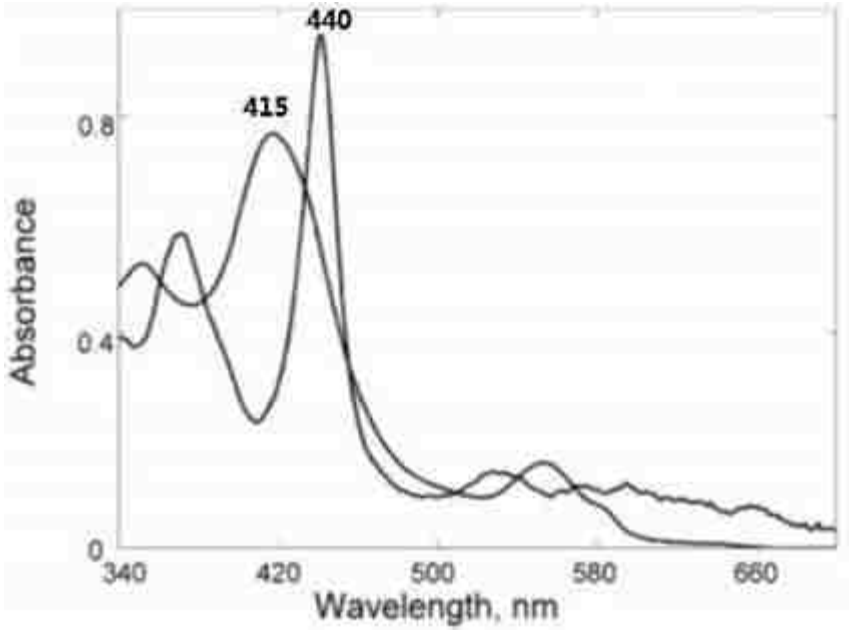

Figure 66 Absorption Spectra for P450cam before (oxy 415 nm) and after (peroxo, hydroperoxo 440 nm) cryoradiolysis[117]

3.2.6 Cryoradiolytic reduction and annealing studies of oxyCYP119 complexes

Cryoradiolytic reduction of the oxy complexes of CYP119 was performed as reported earlier[118] with minor modifications. Specifically, frozen samples of oxy-ferrous CYP119 were irradiated with ^{60}Co γ rays at 77 K at Notre Dame Radiation Laboratory (University of Notre Dame, South Bend, IN). The samples were exposed to 3.5 megarads of γ-irradiation from a 60Co source. During irradiation the samples were contained in a modified Dewar vessel and continuously immersed in the liquid nitrogen. Samples were kept in liquid N_2 before, during and after irradiation. RR measurements were performed on irradiated samples using 442 nm and 1.4 mW power for 6 hours each sample. RR measurements were acquired using 442 nm because the Soret of both peroxo and hydroperoxo is near 440 nm, see Figure 66.

Annealing was carried out by immersing the irradiated CYP119 samples (2 sets at the same time eg. LA ^{16}O and LA ^{18}O) into pentane/ liquid nitrogen bath at desired temperatures (142- and 185 K) for 1 minute.[119] Samples were quickly (less than 2 s) placed back into liquid nitrogen.

3.2.7 Rapid mixing of substrate bound CYP119 with *m*CPBA

20 µM CYP119 ferric protein solution (buffered to 100 mM PB, pH 6) was mixed with PFDA (15-fold excess) incubated overnight to ensure substrate binding. The UV-vis spectra were calibrated using 1.5 mL of 100 mM PB in a 1 cm cuvette. The blank solution was discarded and replaced with 1.5 mL of about 20 µM CYP 119 PFDA bound was added and a spectrum was acquired for the ferric CYP119.

The UV-visible was set up to acquire automatically 15 spectra in a total time of 50 s. A 5-fold excess of 98 % (purified according to previously published procedures)[120] ^{16}O mCPBA was added using a 5 µL syringe, quickly mixed with a small glass rod and the spectra acquired about a couple of seconds after addition of 5-fold mCPBA at 4 °C. A total of 15 spectra were acquired to monitor the accumulation and decomposition of Compound I. The process was repeated with LA and SF CYP119 maintaining all other conditions the same.

3.2.8 Purification of ^{18}O *m*CPBA

^{18}O *m*CPBA was synthesized more than two decades ago in our lab and most likely decomposed over the years; e.g., the % of peracid was as low as 12 %. The sample was purified by dissolving the *m*CPBA in 50g/L toluene and washed with 100 mM phosphate buffer, pH 7.5 (5 x 10 mL)[120, 121]. The organic layer was dried over $MgSO_4$ and carefully evaporated under reduced vacuum. The solution was recrystallized from dichloromethane and stored in a plastic container in the freezer at 4°C

A very high pure sample is required (>90 %).[35] High % of ^{18}O *m*CPBA was needed, hence we decided to synthesize it using the steps outlined below.

3.2.9 Preparation of ^{18}O *m*CPBA

Step 1 Synthesis of Hydrogen peroxide ($H_2{}^{18}O_2$)

The ^{18}O-labeled hydrogen peroxide was synthesized by the glucose oxidase method.[122, 123] 20 mL of reaction mixture containing 0.1 M β-D-glucose and 1 mM EDTA in 10 mM potassium phosphate buffer at pH 5.1 was placed in a 100 mL round bottomed flask, which was then connected to the vacuum line. The flask was evacuated and filled with argon three times (degassing) to remove oxygen followed by addition of 2 mg of glucose oxidase (dissolved in 100 μL of same buffer). The flask was then evacuated and immediately frozen in liquid nitrogen to inactivate the catalase activity and to facilitate transfer of ≈80 cm^3 of $^{18}O_2$ (3.57 mmol) The mixture was stirred for three hours at 37 °C. The reaction was terminated by addition of 0.2 mL of 2 M HCl. The solution was carefully neutralized to pH 7.0 by addition of 2 N KOH and then passed through a 2x3 cm column packed with Dowex 1-X_2 ion exchange resin. The concentration of H_2O_2 was checked by iodometric titration and obtained about 20 mL of 73 mM (1.46 mmol). The yield of hydrogen peroxide was ~40 %.

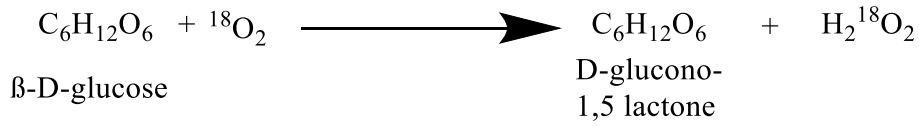

Step 2 Synthesis of *m*CPBA

The synthesis was based on a previously published procedure[118]. 1.5 mL of 3.6 M NaOH was added to a 20 mL-plastic vial equipped with a magnetic stirrer. 15 mg of MgSO4, chilled (0º C) solution of $H_2{}^{18}O_2$ (1 mL of 73 mM or 73 μmoles) and 5 mL

dioxane was added to the vial. The reaction mixture was placed in an ice bath and stirred vigorously. Then 3-chlorobenzoyl chloride (0.41g or 2.3 mmol) was injected with a syringe under the surface of the solution and stirring was continued for 30 minutes. The reaction mixture was transferred to a separatory funnel and 10 mL of 20 % sulfuric acid was added. The *m*CPBA was extracted with 4 volumes (5 ml) of chilled dichloromethane. The extract was dried over $MgSO_4$, filtered, evaporated under reduced pressure and dried under vacuum. The white solid (0.25 g) was checked using iodometric titration and GC/MS. The expected yield of mCPBA synthesized using this method (from iodometric titration was 1.2 mmol (52 % with respect to benzoyl chloride and 12 % based on available oxygen). The ratio of H_2O_2:mCPBA was 1 : 2. This method will need to be refined and optimized to get higher yield of mCPBA.

3.3 Results and Discussion

3.3.1 CYP119 expression and purification

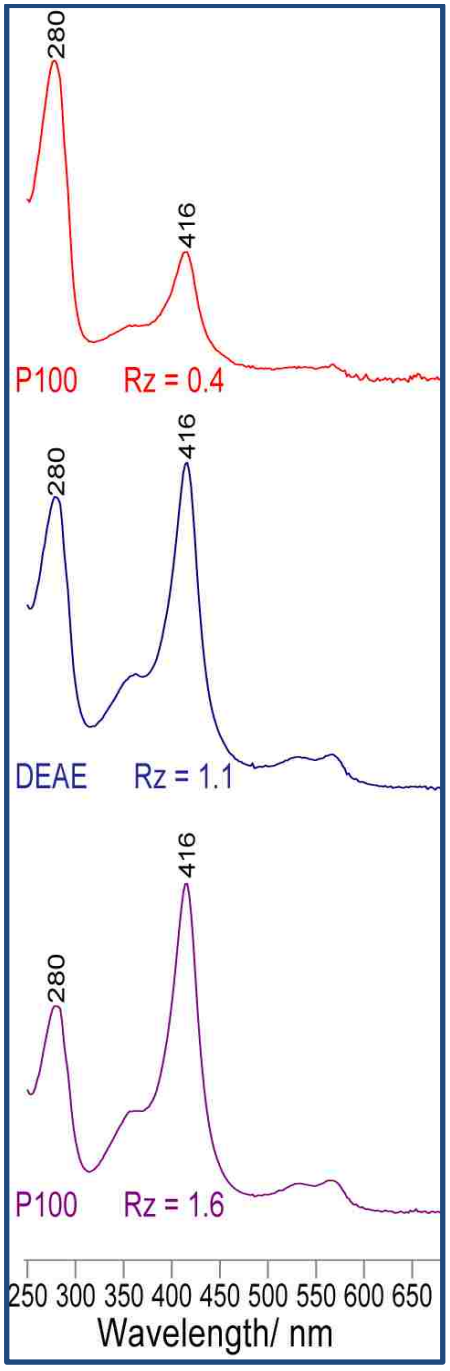

Figure 67 UV-visible spectra of protein from various stages of purification by size exclusion P100 (top) and anion exchange (DEAE) (middle spectrum) and another P100 (bottom spectrum) columns. Pure protein with Rz ≈ 1.6 (purple spectrum) was used for experiments.

As shown in Figure 67, the purification of CYP119 was monitored mainly using UV-visible spectroscopy which allowed us to calculate protein purity by checking Rz values (ratio of A_{416}/A_{280}). After the first column, the protein contained a lot of impurity protein and Rz was about 0.4. Purification with an anion exchange column DEAE greatly improved the purity of the protein and Rz ≈1.1. The final column, also P100, used in experiments was for polishing and improving the purity, with a final Rz of about 1.5-1.6 being obtained.

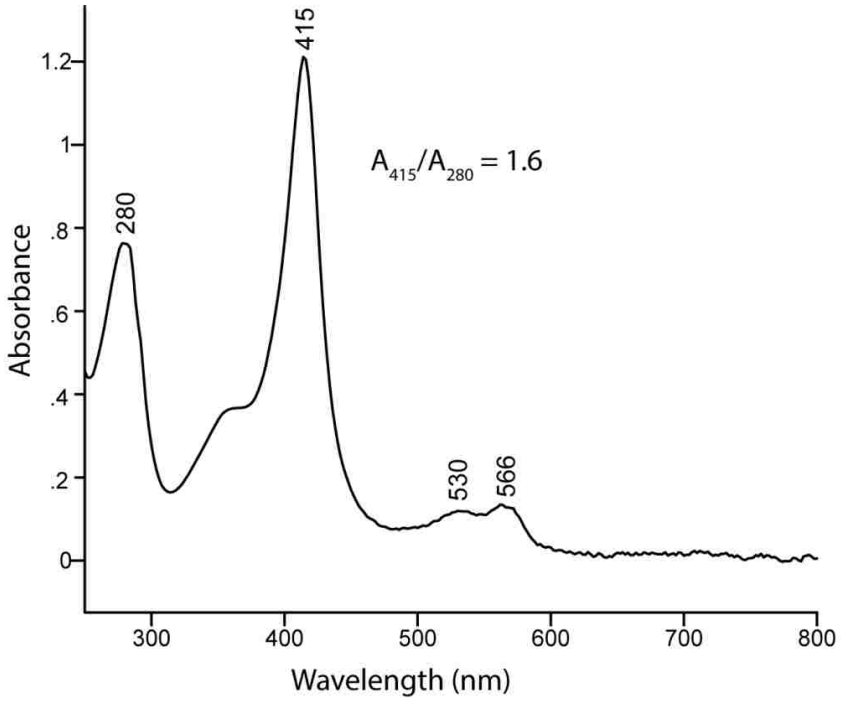

Figure 68 Absorption spectrum of pure SF CYP119

The absorption spectrum displayed in Figure 68 above shows a purified substrate-free samples of CYP119 with Rz = 1.6; only high purity protein was used for the rR

measurements. The protein was stored in -80 °C freezer until required. UV-visible spectroscopy played a key role in following the purity of the protein.

Protein purity was also checked using SDS PAGE and as expected purity improved with subsequent columns used. The expected molar mass of CYP119 was estimated to be about 43 kDa in agreement with previously published data on this enzyme[25].

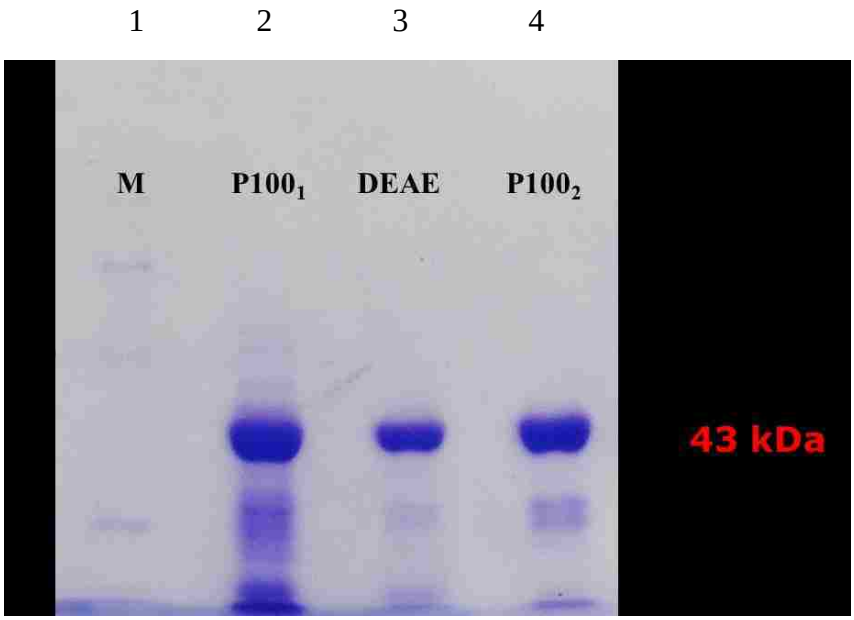

Figure 69 SDS-PAGE results showing protein purity after P100 and DEAE columns. Lane 1, M markers, Lane 2 protein after first P100 size exclusion column, Lane 3 after anion exchange DEAE column, Lane 4 after a second P100 column which was necessary for polishing and improving the purity of the protein.

3.3.2 Purification of H_3 glycerol and deuteration of H_3 glycerol to form D_3 glycerol

Glycerol was purified according to the published procedures. There was good agreement between the results observed and the previously published results.[113, 124] The deuteration was estimated to be about 95 % by comparing the intensity of the broad OH

band at 3340 cm^{-1} in H_3 glycerol and that same band in d_3 glycerol which now exhibited a broad OD band at 2471 cm^{-1} (Figure 70 below). All other bands remained were same in commercial H_3 glycerol and d_3 exchanged glycerol confirming the glycerol was still intact.

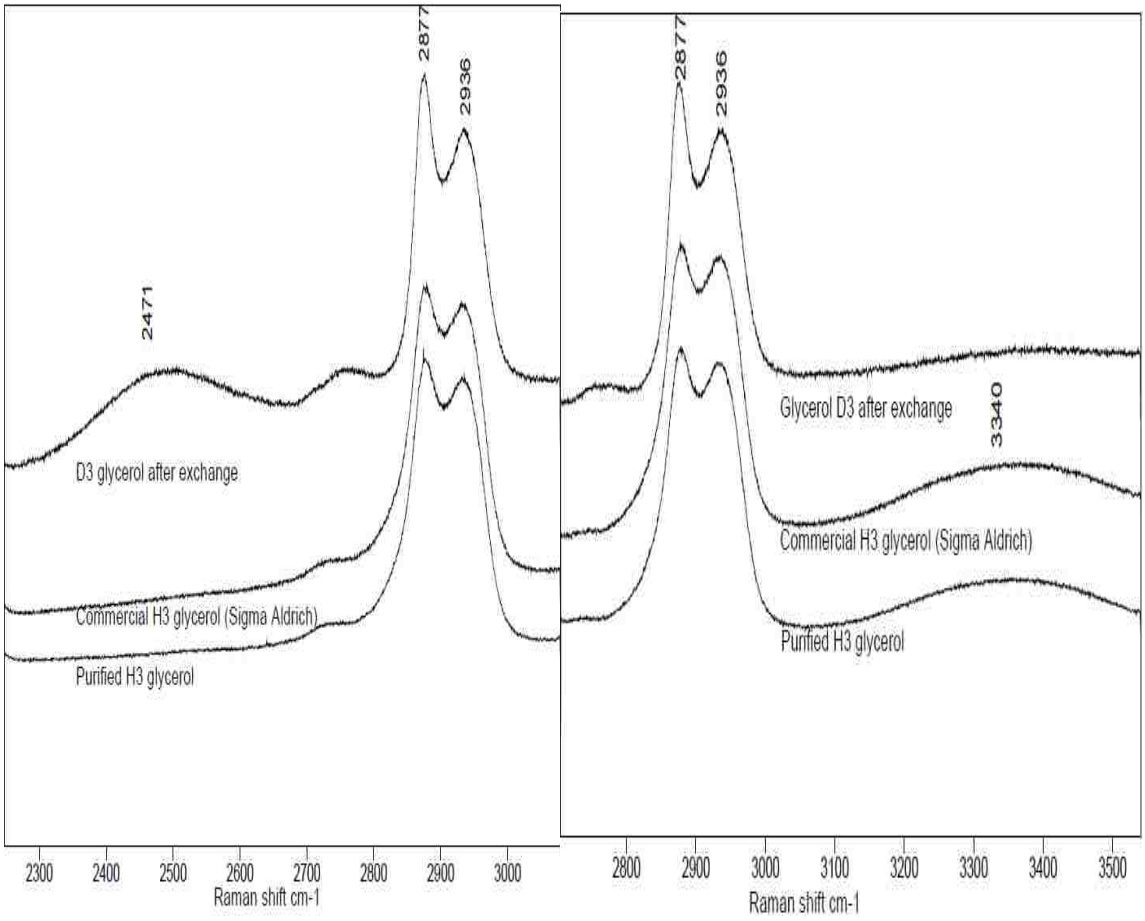

Figure 70 Purification and deuteration of glycerol

3.3.3 Iodometric titrations

Table 8 shows some results of iodometric titration of mCPBA for validation of the method, average 77.7 %. The specified value is 77 % from Sigma Aldrich. The calculation was based on previous publication.[115] The important points here are the precision of the values and the accuracy. The mCPBA was purified as shown in the methods and purity improved to 98 %, which was used in experiments for stabilization of Compound I generated by reacting ferric CYP119 PFDA bound with pure ^{16}O mCPBA.

Table 8 Results from iodometric titrations

Commercial m-CPBA

Initial buret reading/ mL	0.00	14.00	11.10
Final buret reading/ mL	28.80	42.20	39.20
Volume of $S_2O_3^{2-}$ used/ mL	28.80	28.20	28.10
Moles of $S_2O_3^{2-}$	0.001833	0.001795	0.001789
Moles of I_3^-	0.000917	0.000898	0.000894
Moles m-CPBA	0.000917	0.000898	0.000894
Mass m-CPBA/ g	0.1582	0.1549	0.1544
% mCPBA	79.1	77.4	77.2
Average		78	

Note moles I_3^- =0.5 x moles of $S_2O_3^{2-}$ and 0.2 g of thiosulfate was used

Pure mCPBA

Initial buret reading/ mL	13.10	18.80	13.95
Final buret reading/ mL	18.80	24.45	19.60
Volume of $S_2O_3^{2-}$ used/ mL	5.70	5.65	5.65
Moles of $S_2O_3^{2-}$	0.00057	0.000565	0.000565
Moles of I_3^-	0.000285	0.000283	0.000283
Moles m-CPBA	0.000285	0.000283	0.000283
Mass m-CPBA/ g	0.049	0.049	0.049
% mCPBA	98	98	98
Average		98	

Equation 4 Reaction of *m*CPBA with KI[125] The equation shows reaction of mCPBA with iodide ions in an acidic medium to form hypoiodous acid.

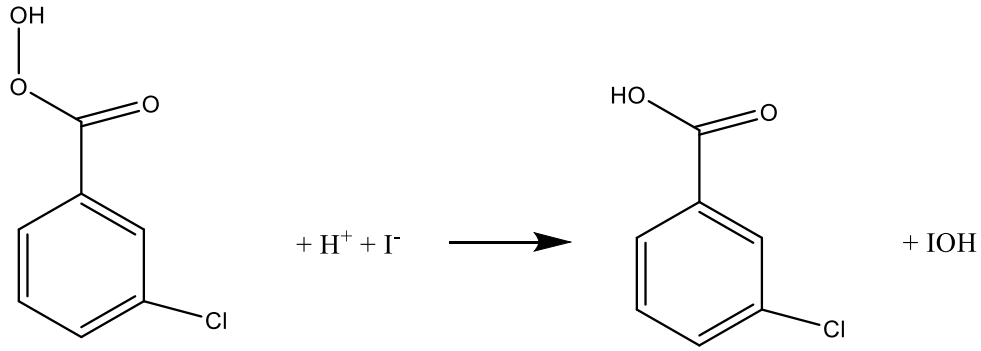

Equation 5 Reaction of iodine with excess iodide.[125] The hypoiodous acid reacts with excess iodide to form triiodide ions which is titrated against thiosulfate as shown in **Equation 6** below

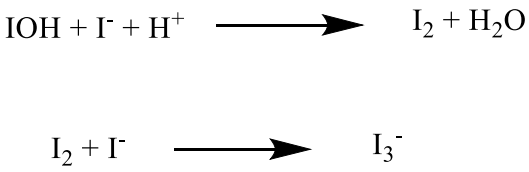

Equation 6 Reaction for the titration of iodine with thiosulfate solution. The progress of the titration and its equivalence point monitored by starch indicator turning from blue to colorless when all triiodide ions are used up in the reaction.

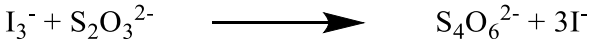

3.3.4 Ferric and ferrous CO complexes of CYP119

Temperature and pH studies of CYP119 in the presence of substrates

UV-Vis spectroscopy was used to study binding of the lauric acid (LA) and perfluorinated decanoic acid (PFDA). The Figure 71 below shows UV-Vis spectra of CYP119 in the presence of PFDA at pH 6 (left) and pH 7 (right) at 4 °C (blue) and 65 °C (red). It is clear, that in both pH cases the UV-Vis spectra of CYP119 in the presence of PFDA at low temperatures (blue spectra) resemble the spectral features of substrate free protein; e.g., the low spin state (Figure 71). The Soret band is observed at 415 nm and the Q bands are seen at 530 nm and 566 nm. Interestingly, when temperature was increased to 65 °C (red spectra), the Soret band of these samples shifted to about 392 nm indicating presence of a significant high spin components characteristic for substrate bound CYP (Figure 71 below); e.g., besides that Soret band at around 390 nm, the Q band is seen near 540 nm and a charge transfer band is seen at 647 nm. The comparison of the UV-Vis data of samples at 65 °C, but different pH, clearly indicates that the sample prepared in slight acidic buffer (pH 6) exhibits larger percentage of spin state conversion (80 %) than that prepared at neutral pH (60%).

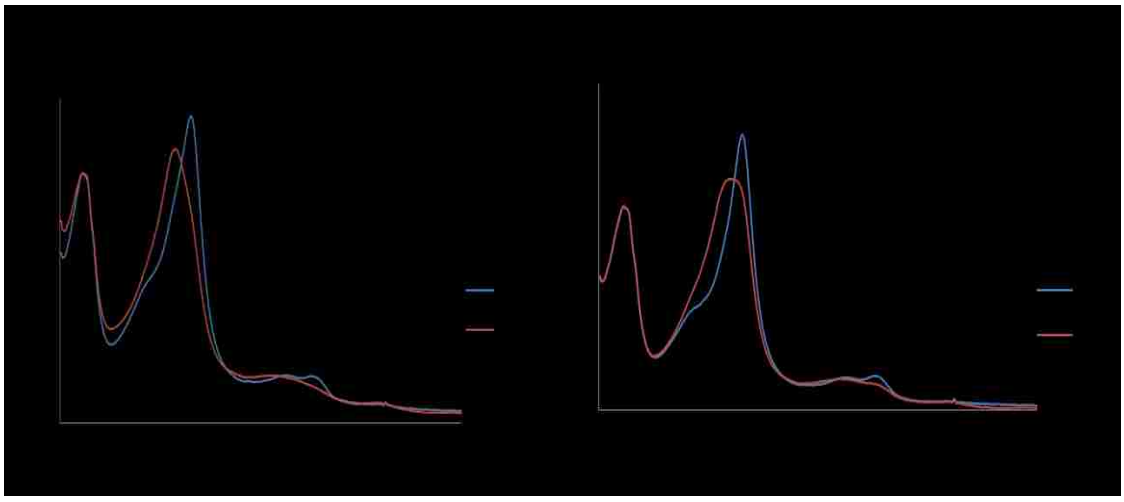

Figure 71 Effect of Temperature on spin state for PFDA bound CYP119 in 100 mM PB, pH 6 (left) and 7 (right). There is better binding at pH 6 giving rise to more high spin form (red trace) than at pH 7

It is noted that when the experiment was repeated with substrate-free CYP119 no shift of the Soret band was observed from the low spin state (417 nm) to the 392 nm, characteristic of the high spin state (Figure 71 **Error! Reference source not found.**).

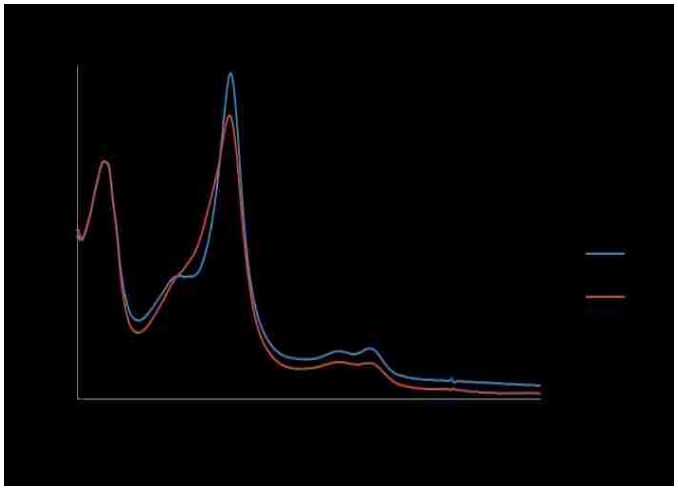

Figure 72 Effect of Temperature on spin state for substrate free CYP119 in 100 mM PB at pH 7

Similar studies were performed for LA bound CYP119 samples showing around 80 % spin state conversion of to the high spin state LA binding at pH 6, in agreement with previously published data.[108, 109]

Based on these studies, it can be concluded that substrate binding by CYP119 is affected by pH. Substrate binds better in acidic medium. The possible explanation for this is the fact that the isoelectric point (PI) of CYP119 is 6.08. This is the pH at which the protein charge is zero, hence the hydrophobic substrate LA or PFDA readily accesses the active site. The question that needs to be addressed however, is whether the substrate is in the active site at low temperatures or only enters the active site at higher temperatures. This issue will be addressed by studies of the ferrous CO adducts that are excellent probes of the changes happening in the active site (*vide infra*).

The RR studies of PFDA bound CYP119 in ferric and ferrous states

Figure 73 below shows the comparison of the high frequency RR spectra of camphor bound CYP101 and PFDA bound CYP119 at room temperature and at 77 K in their ferric and ferrous states. This data was collected as a reference for the RR measurements of oxy adducts prepared later; e.g., during initial steps of preparation of the oxy adducts, often happens that not enough oxygen was added and the sample contains some ferrous forms. Also, when the sample is mixed with oxygen for too long, the autoxidation might happen, leading to formation of the ferric state. Therefore, the RR spectra of frozen ferrous and frozen ferric samples will help in elucidating the presence of possible unreacted ferrous or autoxidized ferric forms in the oxy samples. Furthermore, the data are also helpful to ensure the integrity of the CYP119 protein and to confirm

whether the RR spectra of PFDA bound protein exhibit low spin or high spin spectral pattern.

As expected, the SB CYP101 sample, at room temperature as well as at 77 K, exhibits Raman bands characteristic for the high spin state, that is a ν_3, ν_2 and ν_{10} modes at 1486 cm^{-1}, 1569 cm^{-1} and 1625 cm^{-1}, respectively. The corresponding spectra of the ferric CYP119 with PFDA present at room temperature and at 77 K show spectral pattern characteristic of the low spin state; e.g., the ν_3, ν_2 and ν_{10} modes, are seen at 1502 cm^{-1}, 1584 cm^{-1} and 1641 cm^{-1}, respectively. The RR spectra of ferrous CYP101 and CYP119 at both temperatures shows the ν_4 mode at around 1342 cm^{-1} and the ν_3 mode near 1465 cm^{-1} indicating the five-coordinated high spin form. It is noted that lowering of the temperature causes slight upshifts of the Raman bands as well as their narrowing, an observation in line with previous studies.[126–128]

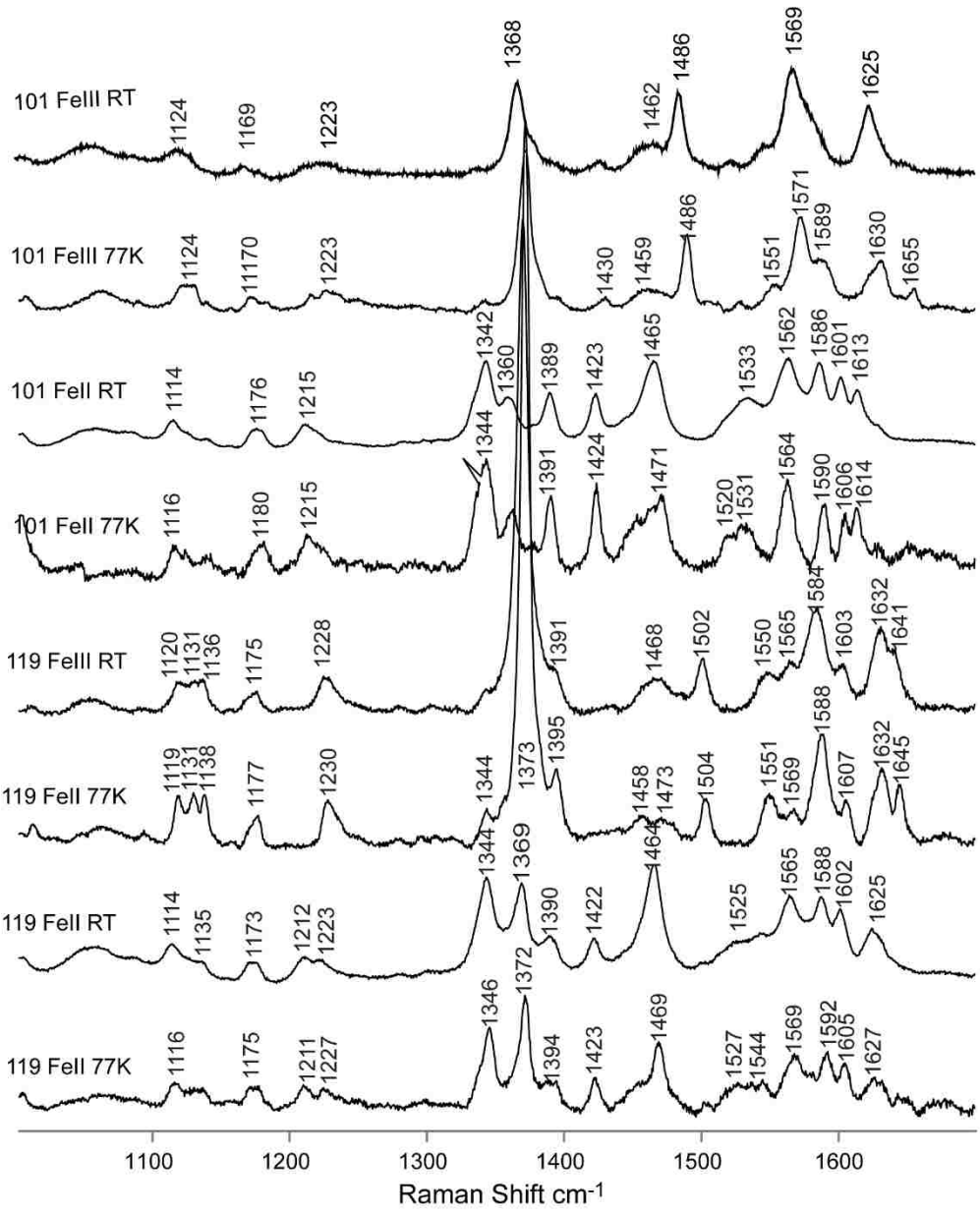

Figure 73 The high frequency RR spectra of camphor bound CYP101 and PFDA bound CYP119 in their ferric and ferrous states, at room temperature and at 77 K.

The RR studies of LA-bound CYP119 at different temperatures

To further evaluate the substrate binding to CYP119 the RR studies of substrate-free and LA-bound samples were performed at different temperatures. Figure 74 shows LA-bound (left) and substrate-free (right) RR spectra at 10, 20, 40 and 65 °C; the corresponding low frequency data are shown in Figure 75 . The high frequency spectrum of LA-bound at 10 °C (top left spectrum, Figure 74) exhibit a ν_3 mode characteristic exclusively for low spin complex (1503 cm^{-1}) even though the substrate was added. Increase in temperature results in a gradual shift to high spin, achieving ≈80 % high spin at 65 °C, in a good agreement with the UV-Vis data. The corresponding data for substrate-free sample (Figure 74, right) shows only modest increase of a 5 % high spin component at elevated temperatures, and observation consistent with the previously published data.[25] One possibility is that the LA substrate is not in the active site at low temperatures, but enters the active site when temperature is increased, an issue that will be addressed in the next section dealing with ferrous CO adducts.

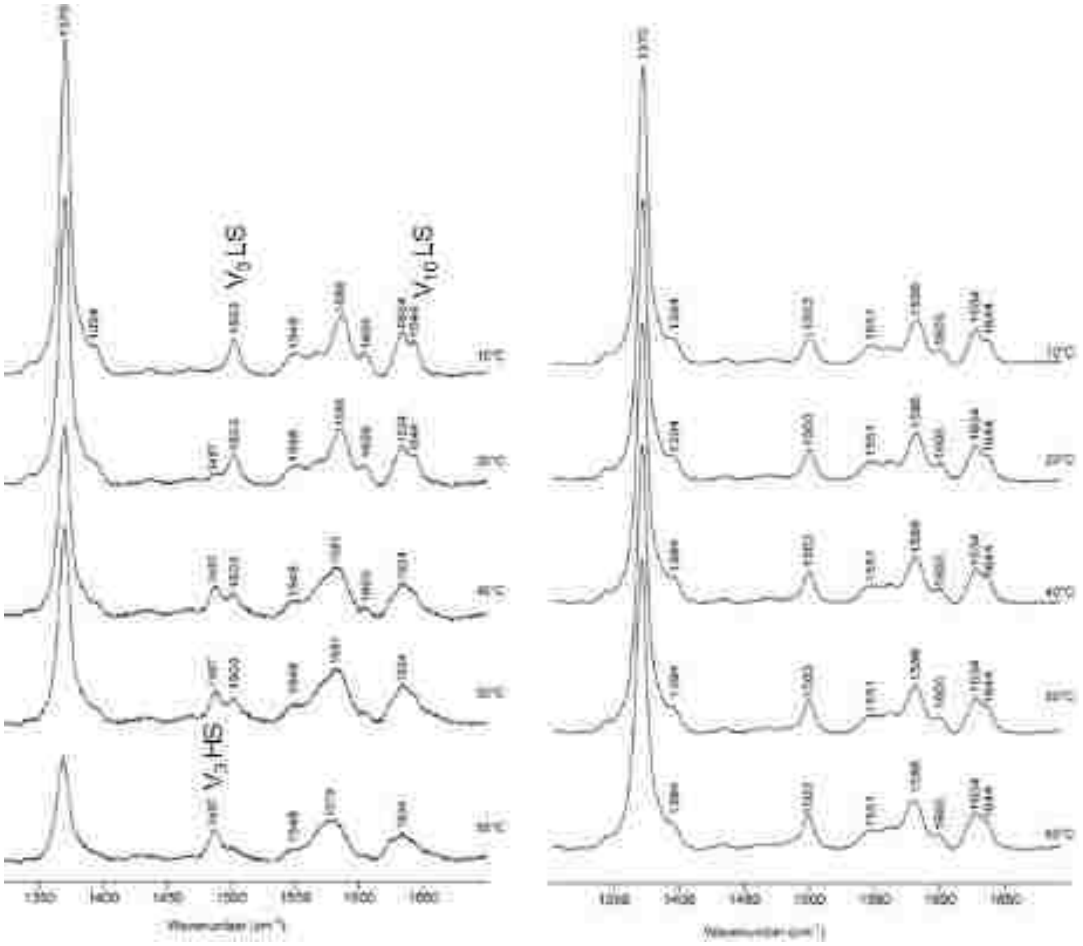

Figure 74 High frequency resonance Raman spectra showing effect of temperature on binding of lauric acid (left) (≈ 80 % high spin formed at 65 °C and effect of temperature on substrate free CYP119 (right) (≈3-5 % high spin formed at 65 °C)

The corresponding data in the low frequency region (Figure 75) shows that the increase of temperature in the LA-bound sample causes the spectral changes usually associated with the increase of the high spin state, e.g., activation of out of plane modes at 319 (γ_7) and 496 cm^{-1}, activation of the lower frequency propionate bending mode at 369 cm^{-1} and activation of the lower frequency vinyl bending mode at 408cm^{-1}. There is no temperature associated spectral changes observed for the substrate-free sample.

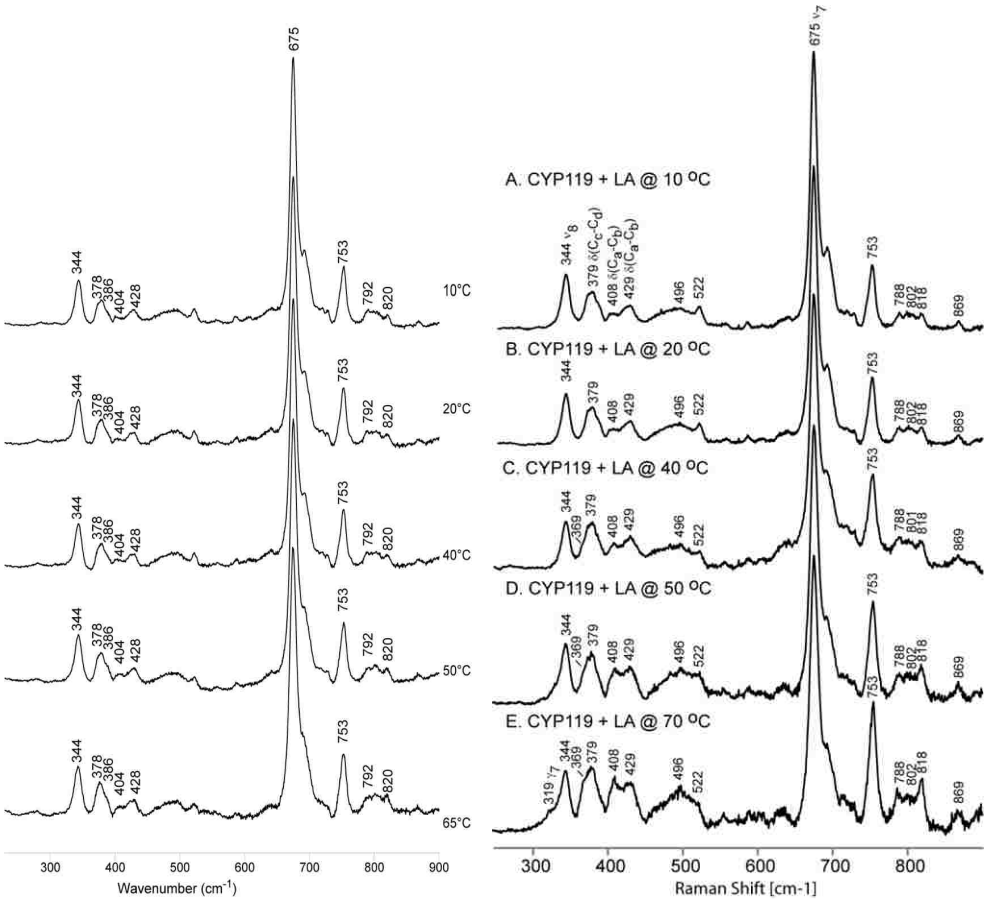

Figure 75 Low frequency resonance Raman of substrate free (left) and LA-bound (right) CYP119

The RR studies of the CO adducts of CYP119

The CO adduct of cytochromes P450 are often used and a way to probe the distal side of the heme pocket; e.g., the Fe-C-O fragment is very sensitive to changes in its polarity such as presence of H-bonding interactions with distal amino acid residues, water molecules or substrates. The ν(Fe-C) stretching modes are usually observed in the region of 460-490 cm^{-1}, while the ν(C-O) stretching modes are seen in the 1920 - 1970 cm^{-1} region. This experiment was carried out to address the question of whether the substrate is in active site at low temperature or only enters when the temperature is increased.

Figure 76 shows low and high frequency regions of CO adducts of substrate-free, LA-bound and PFDA-bound samples at 10 °C. The ν(Fe-C) mode of substrate-free sample is observed at 476 cm^{-1}, with corresponding ν(C-O) mode seen at 1945 cm^{-1}. Binding of LA do not affect the frequency of the ν(Fe-C) or ν(C-O) modes, however, these modes clearly become sharper and exhibit increase in intensity; e.g., the carefully applied deconvolution of the ν(Fe-C) envelopes revealed that the bandwidth of the ν(Fe-C) mode is substrate-free sample is ~ 24 cm^{-1} and in the LA-bound protein is ~ 17 cm^{-1}. Such effects are usually associated with crowding of the heme pocket caused by some steric effect, in this case, presence of LA in the heme pocket. It is noted that these changes are slight which is likely because the substrate is small and does not kick out the water molecule from the cluster at low temperature. More convincing evidence is obtained for the samples containing PFDA substrate. The bottom spectra of Figure 76 clearly shows that PFDA binding causes a clear 2 cm^{-1} downshift of the ν(Fe-C) stretching mode and a corresponding 6 cm^{-1} upshift of the ν(C-O) mode. The downshift of the ν(Fe-O) mode and corresponding upshift of the ν(C-O) mode are usually indicators of the less positive environment of the Fe-C-O fragment, and behavior entirely consistent with the presence of a chemically neutral substrate, such as PFDA. These data provide direct evidence that the substrates are bound in the heme pocket even at the lower temperatures.

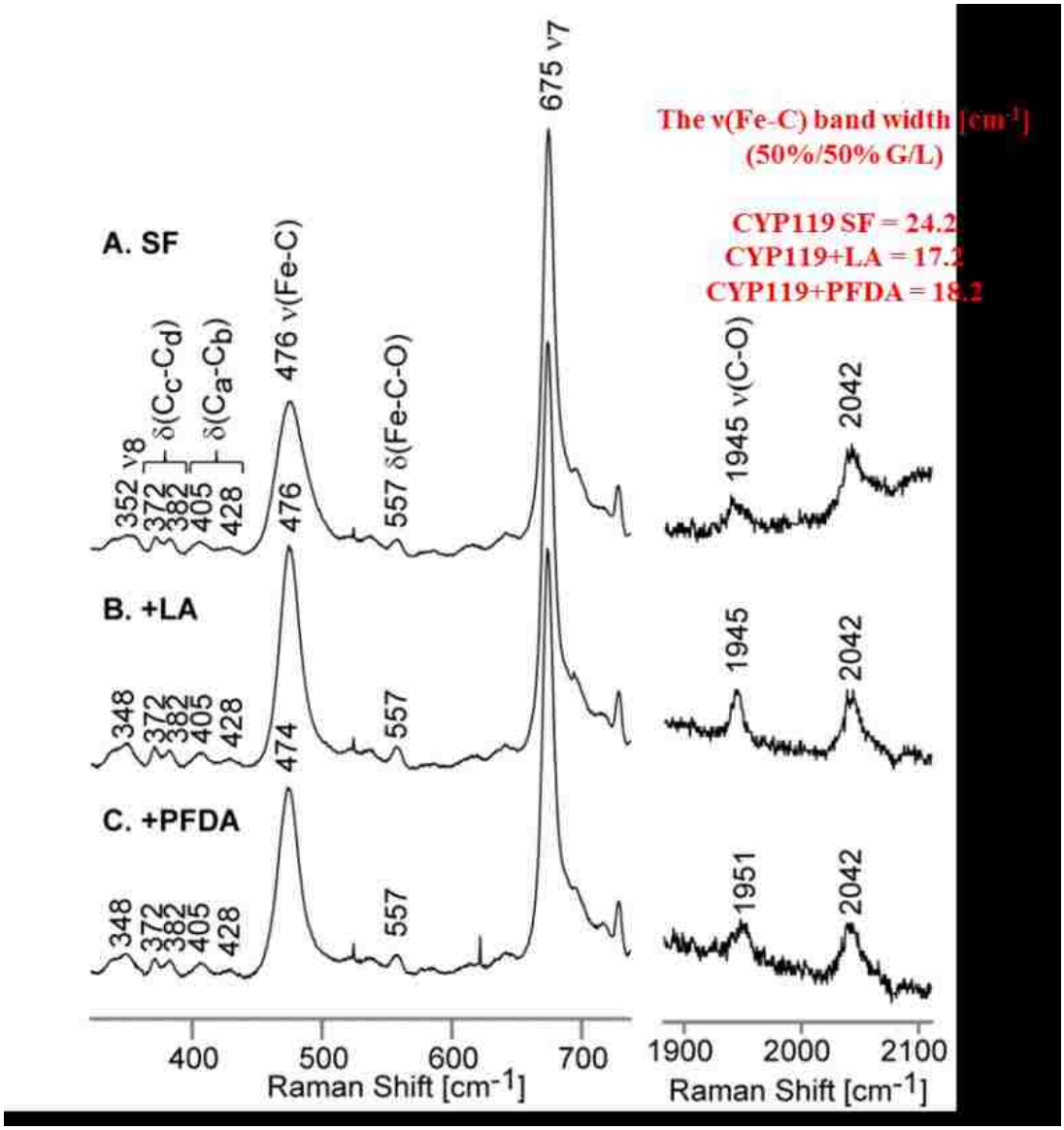

Figure 76 Low frequency (left) and high frequency (right) resonance Raman spectra of ferrous CO adducts of CYP119 and effect of substrates LA and PFDA at 10 °C.

3.3.5 RR characterization of CYP119 dioxygen adducts

The formation of oxy ferrous complex of LA and PFDA bound CYP119 was confirmed by RR spectroscopy at 77 K. The medium frequency spectra which allow simultaneous observation of the ν(Fe-O) and ν(O-O) regions are shown in Figure 77 for the LA-bound samples. The spectra were measured for $^{16}O_2$ and $^{18}O_2$ samples in H_2O buffer (A and B, respectively), and for $^{16}O_2$ and $^{18}O_2$ samples in D_2O solutions (C and D, respectively. Furthermore, the $^{16}O_2$ - $^{18}O_2$ difference traces were generated and are shown at the bottom of Figure 77. To get better insight into the O-O modes distribution, careful deconvolution was performed using 50/50% Gaussian/Lorentzian functions of 11.0 cm^{-1} ± 0.5 cm^{-1} bandwidth, and the results of this band fitting are shown in Figure 78. Inspection of Figure 78 clearly indicates that the asymmetric envelope of O-O bands can be deconvoluted into two modes, a lower frequency one at 1130 cm^{-1} that is much less populated and a higher frequency, dominant mode at 1139 cm^{-1}. These modes exhibit expected $^{16/18}O$ shifts of 66 and 65 cm^{-1}, respectively. The inspection of difference pattern in the D_2O buffer (Figure 78, B) indicates that the lower frequency mode is H/D sensitive and is upshifted by 2 cm^{-1} in buffer prepared in D_2O. Even though this mode is relatively weak, the fact that it is indeed present and exhibits the correct frequency and, also $^{16/18}O_2$ isotope shifts, then it is considered a valid peak as discussed earlier for Figure 62. It is apparent that these two ν(O-O) modes correspond to two Fe-O-O conformers. The frequency of the 1139 cm^{-1} mode and its lack of H/D sensitivity indicate that this Fe-O-O conformer doesn't participate in any substantial H-bonding interactions with active side residues or water molecules. On the other hand, the 9 cm^{-1} downshift of the less populated, lower frequency mode and its H/D sensitivity clearly indicate that this mode is

H-bonded. It is noted that these rR data are like those of CYP101 and its D251N mutant, where also multiple Fe-O-O conformers were observed. The ν(Fe-O) stretching mode is seen at 535 cm^{-1} (Figure 77) and exhibits 28 cm^{-1} shift upon $^{18}O_2$ substitution and no H/D sensitivity. This is also like ν(Fe-O) modes seen for other oxygenated P450s; i.e., 537 cm^{-1} in D251N mutant and ~ 540 cm^{-1} in CYP101.

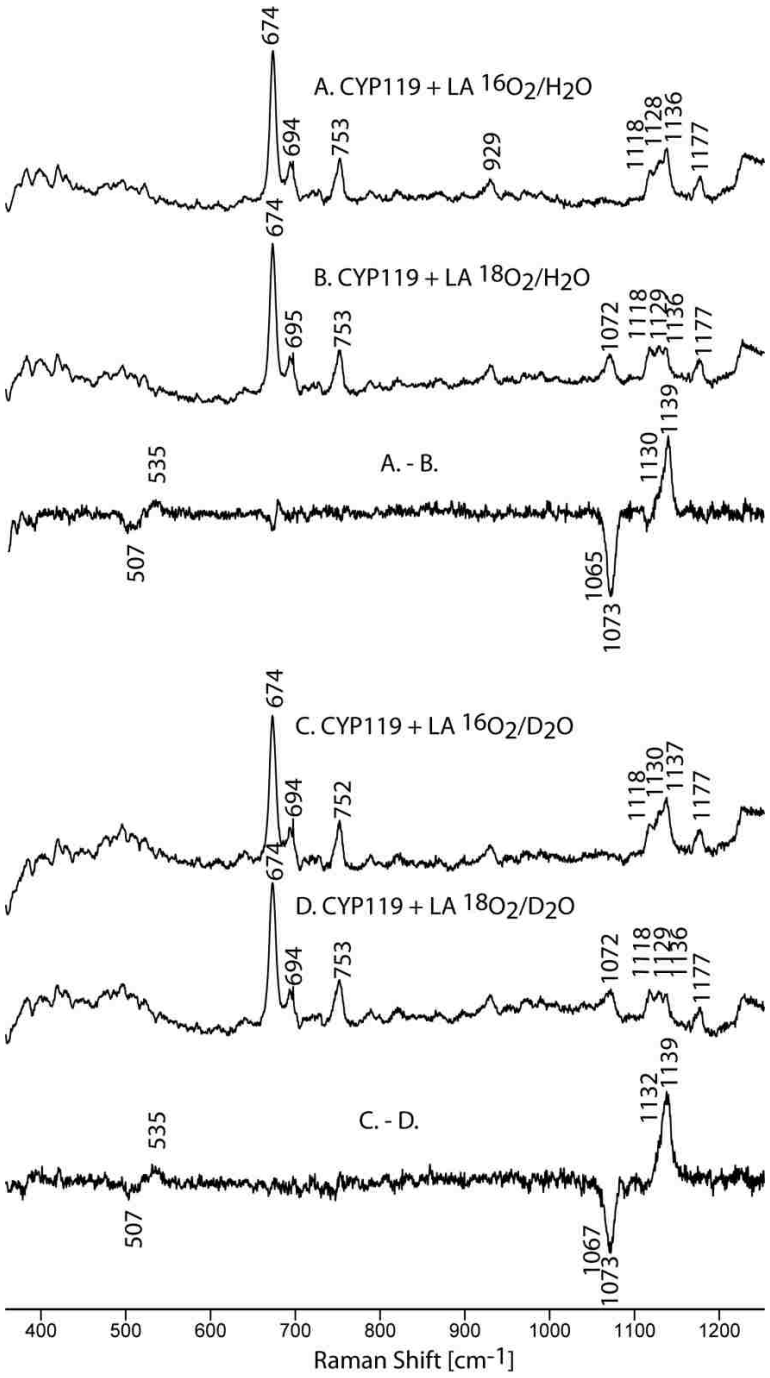

Figure 77 Medium frequency rR spectra of CYP119 with LA in H_2O buffer, A) $^{16}O_2/H_2O$, B) $^{18}O_2/H_2O$, C) $^{16}O_2/D_2O$, D) $^{18}O_2/D_2O$, and their difference traces.

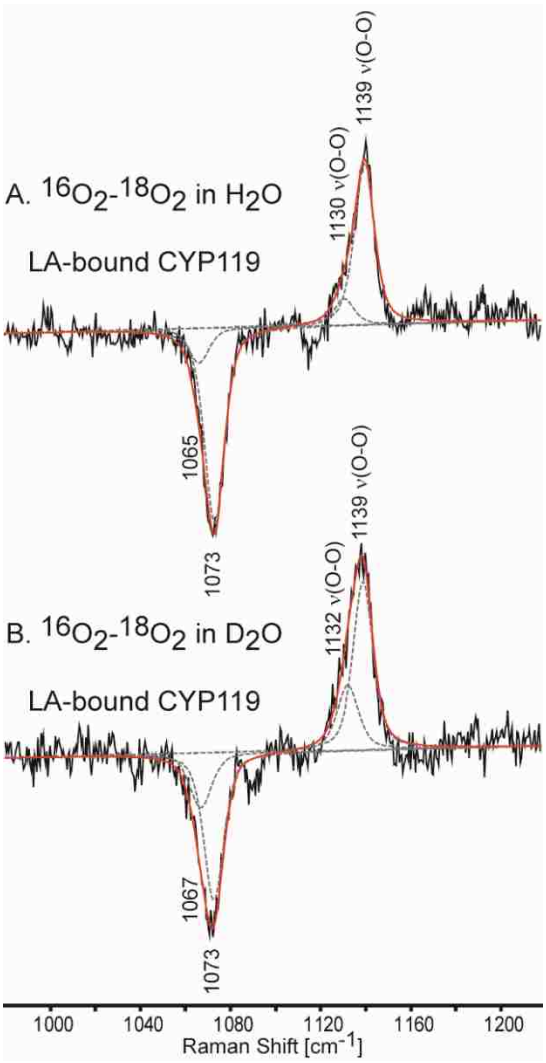

Figure 78 The deconvoluted $^{16}O_2$- $^{18}O_2$ traces in H_2O (A) and D_2O (B) buffers for the LA-bound oxyCYP119.

Similar studies were done for CYP119 bound with PFDA and corresponding RR data of isotopically labeled oxy adducts are presented in Figure 79, along with their difference traces, where clear positive and negative features are seen. The deconvolution procedure, shown in Figure 80, revealed the presence of two Fe-O-O conformers, like LA bound samples. Thus, two ν(O-O) modes are seen, one at 1130 cm^{-1} (1065 cm^{-1} upon $^{18}O_2$ exchange) and the second one at 1139 cm^{-1} (1073 cm^{-1} with $^{18}O_2$ isotopomer).

Interestingly, the lower frequency mode is now a dominant one, and exhibits stronger H/D sensitivity; e.g., it shifts up by 4 cm^{-1} in the D_2O buffer, and the higher frequency, non-H/D sensitive mode, is less intense. It is obvious that these changes in the H-bonding interactions with the Fe-O-O fragments reflect alteration in H-bonding network in the distal side caused by binding of perfluorinated substrate. It seems reasonable to conclude that such changes might affect formation and stability of the Compound I intermediate. The ν(Fe-O) mode is seen at 534 cm^{-1} and shifts down by 29 cm^{-1} upon $^{18}O_2$ substitution.

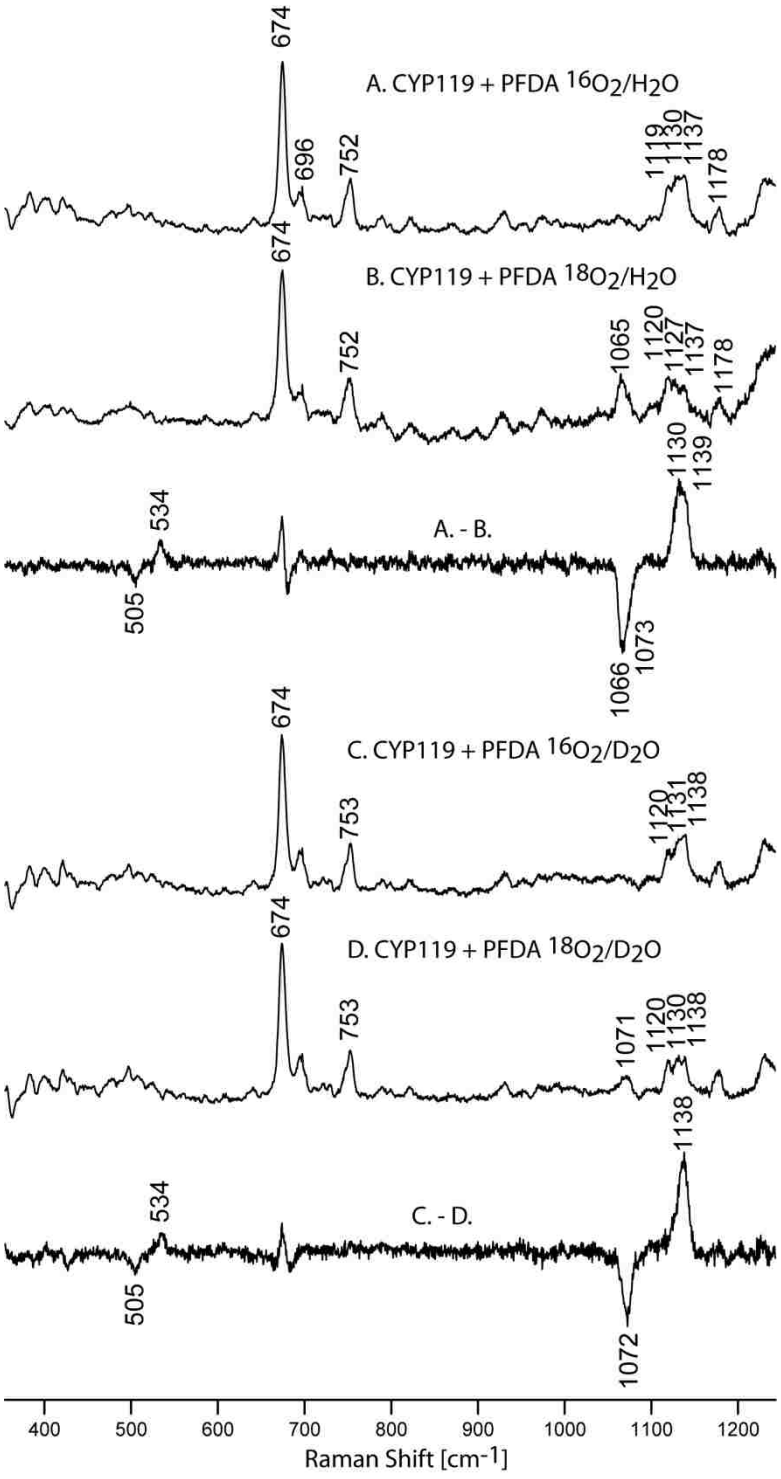

Figure 79 Medium frequency rR spectra of oxy CYP119 with PFDA; A) $^{16}O_2/H_2O$, B) $^{18}O_2/H_2O$, C) $^{16}O_2/D_2O$, D) $^{18}O_2/D_2O$, and their difference traces.

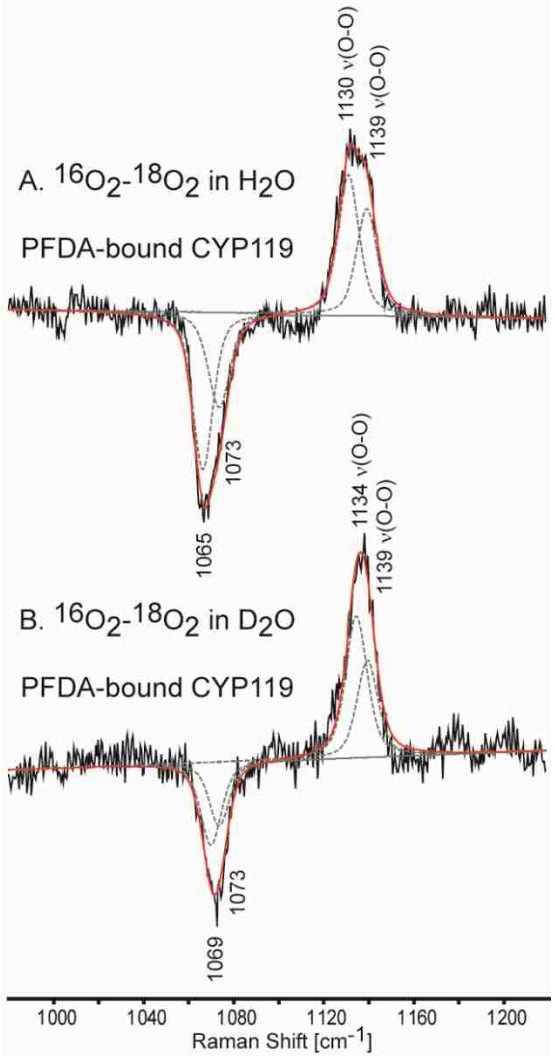

Figure 80 The deconvoluted $^{16}O_2$- $^{18}O_2$ traces in H_2O (A) and D_2O (B) buffers for the PFDA-bound oxyCYP119.

In summary, the oxy complexes of LA- and PFDA-bond samples of CYP119 were successfully prepared and characterized by RR spectroscopy. The careful deconvolution studies revealed that these two adducts exhibit two Fe-O-O conformers, a H-bonded and a non-H-bonded form. The H-bonded conformer is dominant in the PFDA bound sample. The ν(Fe-O) mode was detected in spectra of samples containing both substrates, and was seen at 534-535 cm^{-1}.

3.3.6 Resonance Raman studies of cryoradiolytically reduced samples of oxyCYP119

The oxygenated samples of CYP119 bound to LA and PFDA were irradiated and handled according to previously published procedures.[128, 129] The spectra of $^{16}O_2$ and $^{18}O_2$ samples in H_2O and D_2O buffers, as well as their difference traces are shown in Figure 81. These RR data are for irradiated oxy adducts of CYP119 bound with LA and were obtained directly after irradiation at 77 K without annealing to higher temperature. The oxygen sensitive mode seen at 772 cm^{-1} shifts to 733 cm^{-1} in $^{18}O_2$ sample and exhibit 5 cm^{-1} downshift in D_2O buffer; the frequency and H/D sensitivity allows for confident assignment of this mode to the ν(O-O) stretching mode of the hydroperoxo intermediate. Those data are consistent with the previously published RR results for CYPs hydroperoxo intermediates and the weakening of the O-O bond relative to the oxygenated complex confirms substantial weakening of this bond. The corresponding ν(Fe-O) mode is seen at 569 cm^{-1}, shifting by 27 cm^{-1} upon $^{18}O_2$ substitution and exhibit small H/D shift of ~ 1 cm^{-1}. This apparent strengthening of the Fe-O bond, as compared to the Fe-O bond of the oxy adduct (535 cm^{-1}), is consistent with the eventual formation of the hydroperoxo form, which converts to Compound I upon further protonation.

It is also important to mention that the failure to observe the peroxo intermediate indicates that the heme active site of this enzyme is designed in such a way that the proton shuttle for this system is very efficient and transfers a proton even at 77 K.[117] Such observation was previously made also for WT CYP101.[130] It is also noted that EPR studies of irradiated oxy adducts of substrate-free CYP119 also showed formation of hydroperoxo intermediate immediately after irradiation.[131]

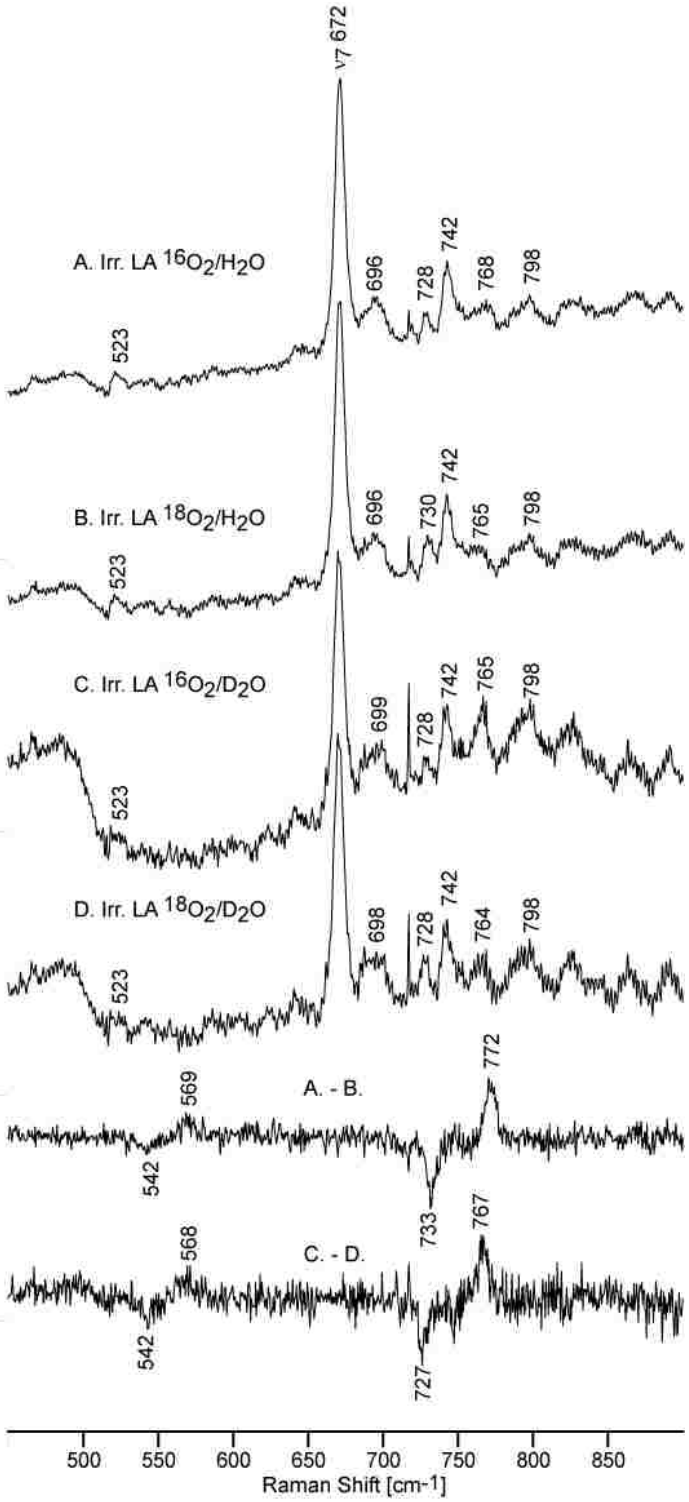

Figure 81 Middle frequency rR spectra of oxy CYP119 with LA after irradiation; A) $^{16}O_2/H_2O$, B) $^{18}O_2/H_2O$, C) $^{16}O_2/D_2O$, D) $^{18}O_2/D_2O$, and their difference traces. Total collection time was 6 hours for each spectrum using 442 nm excitation line at 77 K.

The corresponding studies of PFDA-bound CYP119 were also conducted and the results are shown in Figure 82. The mode assigned to ν(O-O) stretching of hydroperoxo intermediate is seen at 775 cm^{-1} and shifts by 40 cm^{-1} upon $^{18}O_2$ substitution. This mode also exhibits a 5 cm^{-1} downshift in D_2O, securing its assignment to the Fe-O-O-H fragment. The corresponding ν(Fe-O) mode is seen at 570 cm^{-1}, and shifts by 25 cm^{-1} upon $^{18}O_2$ substitution (small H/D shift of ~ 1 cm^{-1}).

The PFDA bound irradiated samples in H_2O buffer were annealed at 190 K in an attempt to generate compound-I, and measurements of the RR spectra were done using the 356 nm excitation line, since the Soret band of compound I occurs at around 360 nm. It is anticipated that the RR spectra of annealed LA-bound samples would simply show formation of ferric form, owing to efficient reaction of Compound I with this reactive substrate. On the other hand, it is possible that the inert substrate, PFDA, would allow Compound I to persist and be observed by RR spectroscopy. However, while the PFDA samples showed a possible peak at 754 cm^{-1}, possibly due to the ν(Fe-^{16}O) mode of compound I, there is no clear negative peak assignable to a ν(Fe-^{16}O) counterpart. Consequently, the resonance Raman data on Compound-I are inconclusive and we see no clear evidence of compound I (see Figure 83 below). The sample could not be measured for longer times owing to photodecomposition after 80 minutes at 1.4 mW and the signal was lost and background was quite noisy and unusual. Further studies will include measuring the PFDA samples with rapid mixing/ detection. Specifically, a platinum sphere mixing device will be used.[132] Stopped flow methods will also be used on CYP119, PFDA and the putidaredoxin (redox partner)[109] to attempt to generate and detect the fleeting intermediate CYP119-I.

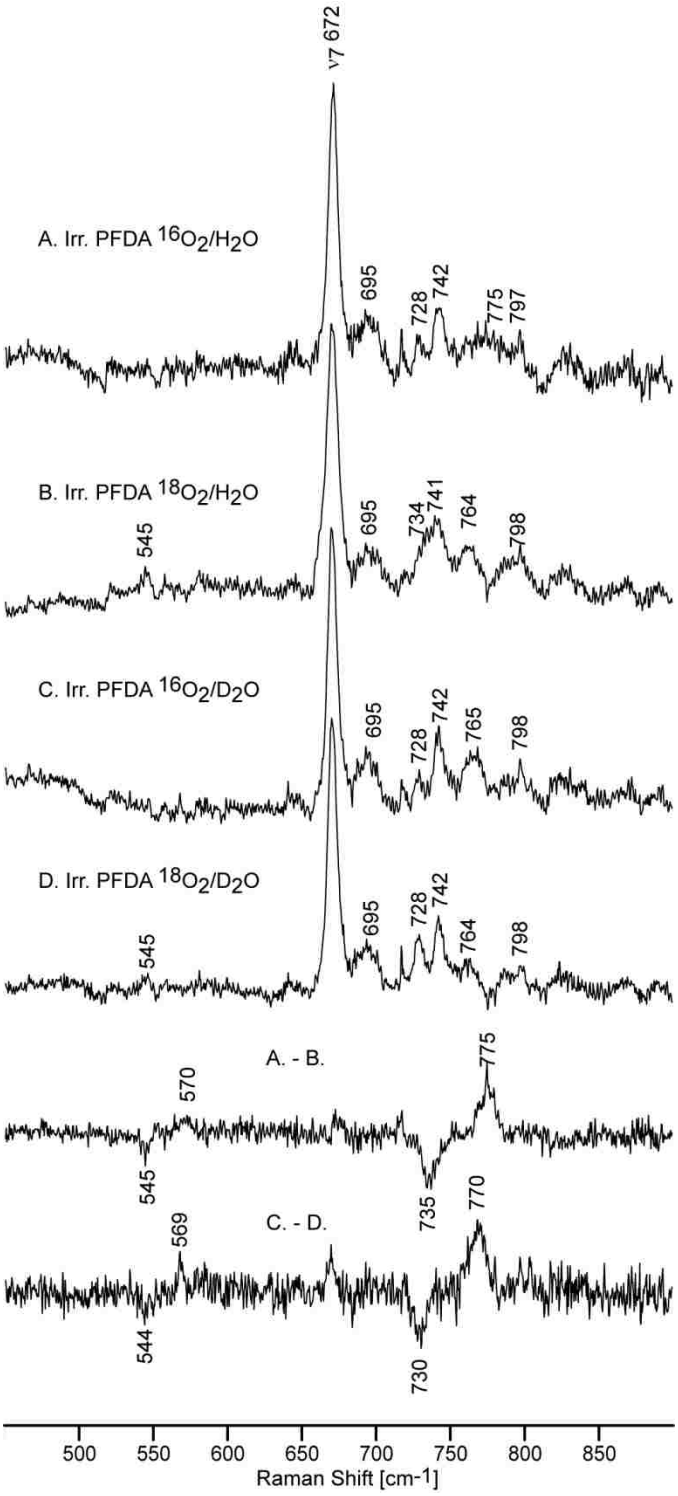
672
A. Irr. PFDA $^{16}O_2/H_2O$
695
728
742
775
797
B. Irr. PFDA $^{18}O_2/H_2O$
545
695
734
741
764
798
C. Irr. PFDA $^{16}O_2/D_2O$
695
728
742
765
798
D. Irr. PFDA $^{18}O_2/D_2O$
545
695
728
742
764
798
A. - B.
570
545
775
735
C. - D.
569
544
770
730
500
550
600
650
700
750
800
850
Raman Shift [cm-1]

Figure 82 Middle frequency rR spectra of oxy CYP119 with PFDA after irradiation; A) $^{16}O_2/H_2O$, B) $^{18}O_2/H_2O$, C) $^{16}O_2/D_2O$, D) $^{18}O_2/D_2O$, and their difference traces. Total collection time was 6 hours for each spectrum using 442 nm excitation line at 77 K.

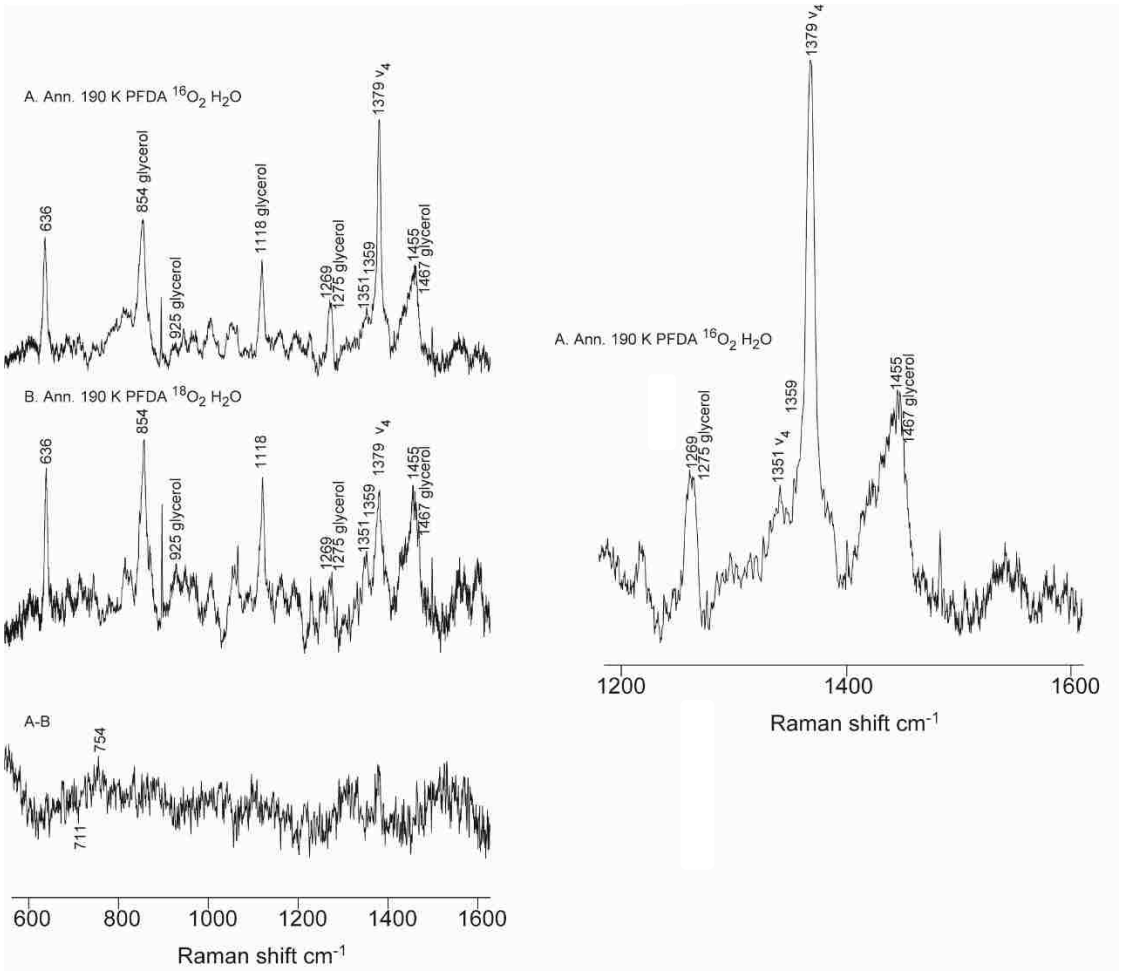

Figure 83 Middle frequency rR spectra of oxy CYP119 with PFDA after annealing at 190 K; A) $^{16}O_2/H_2O$, B) $^{18}O_2/H_2O$ and the difference trace. Total collection time was 1 hour 20 minutes for each spectrum using 356 excitation line at 77 K.

3.3.7 Generation of Compound I, using mCPBA in the presence of fluorinated substrate PFDA

The experiment was conducted to determine if fluorinated substrates can prolong the lifetime of Compound I. The inability of researchers "to see compound-I in action" has led to some doubts in its existence as the most potent oxidizing species. This experiment reinforces what was observed using stopped flow methods[35] by Green and co-workers. They reported Compound I maximized in about 35 ms using stopped flow technique. In this present study, it was observed that CYP119-I can be captured, and characterized with PFDA present. The UV-visible spectroscopy revealed that the the absorption spectrum of compound I is detectable for about 45 s in the presence of PFDA. Figure 84 (left) shows spectra collected 3.3, 10.0, 16.7, 23.3, 30.0, 36.7, 43.3 and 50.0 s after addition of mCPBA (green spectra). As can be seen, there is no evidence for formation of the Compound I in this substrate-free CYP119. On the contrary, an identical experiment with samples containing PFDA (Figure 84, right) exhibit clear bands at 366 nm and 690 nm characteristic of the Compound I intermediate. These results agree with previously published spectra of compound I in CYP119-I using m-chloroperoxybenzoic acid by Green and coworkers.[35] However, some portion of the protein degraded (31 % loss due to heme degradation) owing to side reactions of compound I.

Resonance Raman studies of compound I generated using *m*CPBA on PFDA bound CYP119 have not been attempted, owing to difficulties in getting pure ^{18}O mCPBA with >90 % active oxygen as the purified commercial ^{16}O mCPBA. In the near future, such studies will be conducted with isotopically labeled mCPBA, using a rapid mixing device which will soon be refurbished.[132]

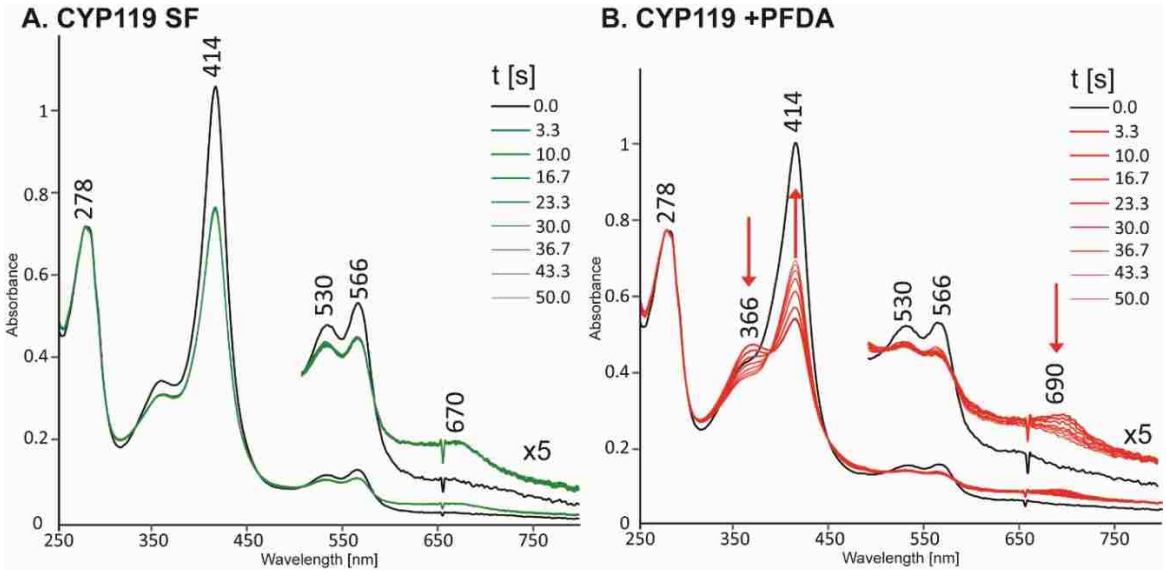

Figure 84 UV-visible spectra for substrate free (left) and PFDA bound CYP119 (right) showing the generation and stabilization of CYP119-I using 5-fold excess mCPBA. CYP119-I lifetime prolonged for up to 45 s. A portion of the protein was also degraded from using excess mCPBA.

3.4 Summary

The present work employed PFDA as an inert substrate for the thermophilic protein CYP119, to capture, generate and spectroscopically characterize Compound I intermediate. CYP119 was shown for the first time to bind LA and PFDA with up to 80 % spin state conversion at elevated temperature, by UV-visible spectroscopy and rR spectroscopy temperature dependence studies. Further studies on ferrous CO complexes of CYP119 provided evidence that the substrate is in the active site even at low temperatures, even though the RR spectra of the ferric enzyme at low temperatures exhibit spectral pattern characteristic of low spin form. This is in agreement with previous studies[25] of CYP119 with styrene by T1 NMR relaxation studies which proved the substrate is bound in the active site of the protein even at low temperatures. In one approach, we planned to generate Compound I by following the normal catalytic pathway. This involved making oxy complexes of CYP119 with LA and PFDA and RR measurement of oxy adduct and their reduced forms generated by irradiation. We report for the first time, high quality data for oxy samples in the presence of LA and PFDA substrates, revealing the presence of multiple Fe-O-O conformers. It is shown that the non-H-bonded conformer is dominant in the sample containing LA, while both (H-bonded and non-H bonded) conformers are comparable in intensity in the samples with PFDA substrate. Both, LA and PFDA bound, cryoradiolytically reduced samples quickly form hydroperoxo intermediates, indicative of very efficient proton delivery network in the CYP119 active site. In another approach, we have shown using UV-Vis spectroscopy, for the first time, that the Compound I can be generated and its half-life prolonged by a factor of more than 10 using fluorinated substrate PFDA. With this technique, a

Compound I spectrum persisted for up to about 45 s in contrast with stopped flow method which showed a rapidly decaying compound I[35]. The future plan is to generate Compound I using this approach and characterize it by RR spectroscopy.

BIBLIOGRAPHY

(1) Katsumi Iida and Masahiro Kajiwara. *J. Label. Compd. Radiopharm.* **2002**, *45*, 139–143.

(2) Kellner, D. G.; Hung, S. C.; Weiss, K. E.; Sligar, S. G. *J. Biol. Chem.* **2002**, *277*, 9641–9644.

(3) De Ropp, J. S. Proton NMR studies of horseradish peroxidase, University of Carlifornia, Davis, 1981.

(4) Parish, D. W. Syntheses of isotopically labeled porphyrins and hemins, University of Carlifornia, Davis, 1984.

(5) Reedy, C. J.; Gibney, B. R. *Chem. Rev.* **2004**, *104*, 617–649.

(6) Les, A. M.; Lecomte, J. T. J. In *Protein Families*; Orengo, C.; Bateman, A., Ed.; 2014; pp. 207–235.

(7) Oohora, K.; Hayashi, T. *Curr. Opin. Chem. Biol.* **2014**, *19*, 154–161.

(8) Sigel, A. Sigel, H. Sigel, R. K. O. *The Ubiquitous Roles of Cytochrome P450 proteins*; John Wiley & Sons, Ltd, 2007.

(9) Axelrod, J. *J. Pharmacol. Exp. Ther.* **1955**, *114*, 430–438.

(10) Brodie, B. B.; Axelrod, J.; Cooper, J. R.; Gaudette, L.; La Du, B. N.; Mitoma, C.; Udenfriend, S. *Science* **1955**, *121*, 603–604.

(11) Garfinkel, D. *Arch. Biochem. Biophys.* **1958**, *77*, 493–509.

(12) Klingenberg, M. *Arch. Biochem. Biophys.* **1958**, *75*, 376–386.

(13) Estabrook, R. W. *Drug Metab. Dispos.* **2003**, *31*, 1461–1473.

(14) Stern, J. O.; Peisach, J. *J. Biol. Chem.* **1974**, *249*, 7495–7498.

(15) Groves, J. T.; McClusky, G. A.; White, R. E.; Coon, M. J. *Biochem. Biophys. Res. Commun.* **1978**, *81*, 154–160.

(16) Ortiz de Montellano, P. R. *Chem. Rev.* **2010**, *110*, 932–948.

(17) Makris, T. M.; von Koenig, K.; Schlichting, I.; Sligar, S. G. *J. Inorg. Biochem.* **2006**, *100*, 507–518.

(18) Nelson, D. R. *Hum. Genomics* **2009**, *4*, 59–65.

(19) Bernhardt, R. In *Reviews of Physiology Biochemistry and Pharmacology, Volume 127*; Springer-Verlag: Berlin/Heidelberg, 1995; pp. 137–221.

(20) Lewis, D. F. V; Ito, Y. *Cytochromes P450 Role Metab. Toxic. Drugs other Xenobiotics* **2008**, 3–45.

(21) Mak, P. J. *Handb. Porhyrin Sci.* **2016**, 1–120.

(22) Harris, D.; Loew, G. *J. Am. Chem. Soc.* **1993**, *115*, 8775–8779.

(23) Ortiz de Montellano, P. R. *Cytochrome P450 : structure, mechanism, and biochemistry*; Ortiz de Montellano, P. R., Ed.; 4th editio.; Springer: Switzerland, 2015.

(24) Truan, G.; Peterson, J. A. *Arch. Biochem. Biophys.* **1998**, *349*, 53–64.

(25) Koo, L. S.; Tschirret-Guth, R. A.; Straub, W. E.; Moënne-Loccoz, P.; Loehr, T. M.; Ortiz De Montellano, P. R. *J. Biol. Chem.* **2000**, *275*, 14112–14123.

(26) Poulos, T. L. *Drug Metab. Dispos.* **2005**, *33*, 10–18.

(27) Hrycay, E. G.; Bandiera, S. M. Hrycay, E. G.; Bandiera, S. M., Eds.; Springer International Publishing: Switzerland, 2015; pp. 1–61.

(28) Zhou, S.-F.; Liu, J.-P.; Chowbay, B. *Drug Metab. Rev.* **2009**, *41*, 89–295.

(29) Ortiz de Montellano, P. R. *Cytochrome P450 : structure, mechanism, and biochemistry*; Kluwer Academic/Plenum Publishers, 2005.

(30) Spolitak, T.; Dawson, J. H.; Ballou, D. P. *J. Biol. Chem.* **2005**, *280*, 20300–20309.

(31) Schünemann, V.; Jung, C.; Trautwein, A. X.; Mandon, D.; Weiss, R. *FEBS Lett.* **2000**, *479*, 149–154.

(32) Egawa, T.; Shimada, H.; Ishimura, Y. *Biochem. Biophys. Res. Commun.* **1994**, *201*, 1464–1469.

(33) Spolitak, T.; Dawson, J. H.; Ballou, D. P. *J. Biol. Chem.* **2005**, *280*, 20300–20309.

(34) Kellner, D. G.; Hung, S.-C.; Weiss, K. E.; Sligar, S. G. *J. Biol. Chem.* **2002**, *277*, 9641–9644.

(35) Rittle, J.; Green, M. T. *Science (80-.).* **2010**, *330*, 933–937.

(36) Raner, G. M.; Thompson, J. I.; Haddy, A.; Tangham, V.; Bynum, N.; Ramachandra Reddy, G.; Ballou, D. P.; Dawson, J. H. *J. Inorg. Biochem.* **2006**, *100*, 2045–2053.

(37) Raner, G. M.; Hatchell, A. J.; Morton, P. E.; Ballou, D. P.; Coon, M. J. *J. Inorg. Biochem.* **2000**, *81*, 153–160.

(38) Denisov, I. G.; Makris, T. M.; Sligar, S. G. *Methods Enzymol.* **2002**, *357*, 103–115.

(39) Kincaid, J. R. *Porphyr. Handb.* **2000**, *7*, 225.

(40) Spiro, T. G. *Inorg. Chem.* **2007**, *46*, 10968–10980.

(41) Dolphin, D. *The Porphyrins V3 : Physical Chemistry, Part A.*; Elsevier Science, 1978.

(42) Gardiner, D. I. *Practical Raman spectrosopy*; Springer-Verlag, 1989.

(43) Raman, C. V. *Science (80-.).* **1929**, *69*, 267–275.

(44) Kincaid, J. R. In *Porphyrin Handb.*; Academic Press, 2000; Vol. 7, pp. 225–291.

(45) Spiro, T. G.; Li, X.-Y. *Biological Applications of Raman Spectroscopy, Vol. 3*; Spiro, T. G., Ed.; John Wiley and Sons: New York, 1988.

(46) Champion, P. M. *Biological Applications of Raman Spectroscopy*; John Wiley and Sons: New York, 1988.

(47) Li, X. Y.; Czernuszewicz, R. S.; Kincaid, J. R.; Spiro, T. G. *J. Am. Chem. Soc.* **1989**, *111*, 7012–7023.

(48) Hu, S.; Morris, I. K.; Singh, J. P.; Smith, K. M.; Spiro, T. G. *J. Am. Chem. Soc.* **1993**, *115*, 12446–12458.

(49) Choi, S.; Spiro, T. G.; Langry, K. C.; Smith, K. M.; Budd, D. L.; La Mar, G. N. *J. Am. Chem. Soc.* **1982**, *104*, 4345–4351.

(50) Li, X-Y.; Czernuszewicz, R. S.; Kincaid, J. R.; Stein, P.; Spiro, T. G. *J. Phy. Chem.* **1990**, *13*, 47–61.

(51) Partners, R.; Mak, P. J.; Im, S.; Zhang, H.; Waskell, L. A.; Kincaid, J. R. **2008**, 3950–3963.

(52) Hildebrandt, P.; Greinert, R.; Stier, A.; Taniguchi, H. *Eur. J. Biochem.* **1989**, *186*, 291–302.

(53) Wells, A. V.; Li, P.; Champion, P. M.; Martinist, S. A.; Sligar, S. G. *Biochemistry* **1992**, 4384–4393.

(54) Yu, N. T, Kerr, E. A. In *Biological Applications of Raman Sectroscopy*; 1988; pp. 39–95.

(55) Yu, N.-T. *Enzyme Structure Part K*; Methods in Enzymology; Elsevier, 1986; Vol. 130.

(56) Wuthrich, K. *NMR of Proteins and Nucleic acids*; John Wiley & Sons: New York, 1986.

(57) Keizers, P. H. J.; Schraven, L. H. M.; de Graaf, C.; Hidestrand, M.; Ingelman-Sundberg, M.; van Dijk, B. R.; Vermeulen, N. P. E.; Commandeur, J. N. M. *Biochem. Biophys. Res. Commun.* **2005**, *338*, 1065–1074.

(58) Rivera, M.; Caignan, G. a. *Anal. Bioanal. Chem.* **2004**, *378*, 1464–1483.

(59) Jacobsen, N. E. *NMR spectroscopy explained : simplified theory, applications and examples for organic chemistry and structural biology*; Wiley-Interscience, 2007.

(60) Butts, C. P.; Jones, C. R.; Towers, E. C.; Flynn, J. L.; Appleby, L.; Barron, N. J. *Org. Biomol. Chem.* **2011**, *9*, 177–184.

(61) Alontaga, A. Y.; Bunce, R. a; Wilks, A.; Rivera, M. *Inorg. chem.* **2006**, *45*, 8876–8881.

(62) Bryson, D.; Lim, P.-L.; Lawson, A.; Manjunath, S.; Raner, G. M. *Biotech. lett.* **2011**, *33*, 2019–2026.

(63) Li, J.; Deslouches, B.; Cosloy, S. D.; Russell, C. S. *Biochim. Biophys. Acta - Gene Struct. Expr.* **2003**, *1626*, 102–105.

(64) Poulos, T. L.; Finzel, B. C.; Howard, A. J. *J. Mol. Biol.* **1987**, *195*, 687–700.

(65) Campbell, J. B.; Johnston, J. S. *J. Label. Compd. & Radiopharm.* **1989**, *XXVII*, 1353–1358.

(66) Fedorov, R.; Ghosh, D. K.; Schlichting, I. *Arch. Biochem. Biophys.* **2003**, *409*, 25–31.

(67) Wang, A.; Savas, U.; Hsu, M.-H.; Stout, C. D.; Johnson, E. F. *J. Biol. Chem.* **2012**, *287*, 10834–10843.

(68) Takara Bio. Inc. Chaperone plasmid set- Takara.

(69) Nishihara, K.;Kanemori, M.; Kitagawa, M.; Yanagi, H.; Yura, T. *Appl. Environ. Microbiol.* **1998**, *64*, 1694.

(70) Maeng, B. H.; Nam, D. H.; Kim, Y. H. *World J. Microbiol. Biotechnol.* **2011**, *27*, 1392–1398.

(71) Amrein, K. E.; Takacs, B.; Stieger, M.; Molnos, J.; Flint, N. a; Burn, P. *Proc. Natl. Acad. Sci. U. S. A.* **1995**, *92*, 1048–1052.

(72) Goenka, S.; Rao, C. M. *Protein Expr. Purif.* **2001**, *21*, 260–267.

(73) Gordon, A. J., Ford, R. A. *The chemist's companion: a handbook of practical data, techniques, and references (Gordon, A.J.)*; John Willey & Sons,: New York, 1972.

(74) Davydov, R.;Dawson, J. H. .; Roshan, P,; Hoffman, B. M. *Biocemistry* **2013**, *52*, 667–671.

(75) Furrow, M. E.; Myers, A. G. *J. Am. Chem. Soc.* **2004**, *126*, 5436–5445.

(76) Kolb, V. M.; Kuffel, A. C.; Spiwek, H. O.; Janota, T. E. *J. Org. Chem.* **1989**, *54*,

2771–2775.

(77) McCullough, C. R.; Pullela, P. K.; Im, S.-C. C.; Waskell, L.; Sem, D. S. *J. Biomol. NMR* **2009**, *43*, 171–178.

(78) Li, X. Y.; Czernuszewicz, R. S.; Kincaid, J. R.; Su, Y. O.; Spiro, T. G. *J. Phys. Chem.* **1990**, *94*, 31–47.

(79) Li, X. Y.; Czernuszewicz, R. S.; Kincaid, J. R.; Stein, P.; Spiro, T. G.; Su, Y. O.; Li, X. -Y, Spiro, T. G.; Kitagawa, T.; Abe, M.; Ogoshi, H.; Kyogoku, Y. *J. Chem. Phys.* **1978**, *69*, 47–61.

(80) Kaluka, D. Spectral Characterization of Cytochromes P450 Active Site and Catalytic Intermediates, 2012.

(81) Wakasugi, K.; Ishimori, K.; Morishima, I. *Biochimie.* **1996**, *78*, 763–770.

(82) Rivera, M.; Qiu, F.; Bunce, R. A.; Stark, R. E. **1999**, 87–98.

(83) Zabell, A. P. R.; Post, C. B. *Proteins Struct. Funct. Genet.* **2002**, *46*, 295–307.

(84) Bazeley, P. S.; Prithivi, S.; Struble, C. A.; Richard J. Povinelli, A.; Sem, D. S. *J. Chem. Inf. Model.* **2006**, *46*, 2698–2708.

(85) Abraham, R. J.; Ainger, N. *J. Chem. Soc., Perkin Trans. 2*, **1999**, 441–448.

(86) Abraham, R. J. .; Mobli, M. *Modelling 1H NMR spectra of organic compounds : theory, applications and NMR prediction software*; Wiley, 2008.

(87) Sanders, J. K. M.; Hunter, B. K. *Modern NMR spectroscopy : a guide for chemists*; Oxford University Press, 1993.

(88) Ainger, N. J. The theoretical prediction of proton chemical shifts in carbonyl compounds., University of Liverpool, 1999.

(89) Abraham, R. J.;Barlow, A. P.; Rowan, A. E. *Magn. Reson. Chem.* **1989**, *27*, 1024.

(90) Wolff, L. *Justus Liebig's Ann. Chem.* **1912**, *394*, 86–108.

(91) Barton, D. H. R.; O'Brien, R. E.; Sternhell, S. *J. Chem. Soc.* **1962**, 470.

(92) Raag, R.; Poulos, T. *Biochemistry* **1991**, *30*, 2674–2684.

(93) Brünger, a T. *Nat. Struct. Biol.* **1997**, *4 Suppl*, 862–865.

(94) Denisov, I. G.; Hung, S.-C.; Weiss, K. E.; McLean, M. A.; Shiro, Y.; Park, S.-Y.; Champion, P. M.; Sligar, S. G. *J. Inorg. Biochem.* **2001**, *87*, 215–226.

(95) Kellner, D. G.; Hung, S.-C.; Weiss, K. E.; Sligar, S. G. *J. Biol. Chem.* **2002**, *277*, 9641–9644.

(96) Puchkaev, A. V.; Koo, L. S.; Ortiz de Montellano, P. R. *Arch. Biochem. Biophys.*

2003, *409*, 52–58.

(97) Sheng, X.; Horner, J. H.; Newcomb, M. *J. Am. Chem. Soc.* **2008**, *130*, 13310–13320.

(98) McLean, M. a; Maves, S. a; Weiss, K. E.; Krepich, S.; Sligar, S. G. *Biochem. Biophys. Res. Commun.* **1998**, *252*, 166–172.

(99) Tschirret-Guth, R. A.; Koo, L. S.; Gaston Hui Bon Hoa, A.; Paul R. Ortiz de Montellano. *J. Am. Chem. Soc.* **2001**, *123*, 3412–3417.

(100) Kincaid, J. R.; Zheng, Y.; Al-mustafa, *J. Biol. Chem.*; Czarnecki, K. **1996**, *271*, 28805–28811.

(101) Egawa, T.; Proshlyakov, D. A.; Miki, H.; Makino, R.; Ogura, T.; Kitagawa, T.; Ishimura, Y. *J. Biol. Inorg. Chem.* **2001**, *6*, 46–54.

(102) Sitter, A. J.; Reczek, C. M.; Terner, J. *Biochim. Biophys. Acta - Protein Struct. Mol. Enzymol.* **1985**, *828*, 229–235.

(103) Felton, R. H.; Roman, A. Y.; Nai-Teng, Y.; Schonbaum, G. R. *Biocimica Biophys. Acta* **1976**, *434*, 82–89.

(104) Terner, J.; Palaniappan, V.; Gold, A.; Weiss, R.; Fitzgerald, M. M.; Sullivan, A. M.; Hosten, C. M. *J. Inorg. Biochem.* **2006**, *100*, 480–501.

(105) S.D. Burke and R.L Danheiser. Handbook of Reagents for Organic Synthesis Oxidizing and Deducing Agents. *Journal of the American Chemical Society*, 1980, *2*, 1–6.

(106) Stone, K. L.; Behan, R. K.; Green, M. T. *Proc. Natl. Acad. Sci. U. S. A.* **2006**, *103*, 12307–12310.

(107) Davydov, D. R.; Fernando, H.; Halpert, J. R. *Biophys. Chem.* **2006**, *123*, 95–101.

(108) Koo, L. S.; Immoos, C. E.; Cohen, M. S.; Farmer, P. J.; Ortiz de Montellano, P. R. *J. Am. Chem. Soc.* **2002**, *124*, 5684–5691.

(109) Lim, Y. R.; Eun, C. Y.; Park, H. G.; Han, S.; Han, J. S.; Cho, K. S.; Chun, Y. J.; Kim, D. *J. Microbiol. Biotechnol.* **2010**, *20*, 574–578.

(110) Denisov, I.; Grinkova, Y.; Sligar, S. *Methods Mol. Biol* **2012**, *875*, 375–391.

(111) KUTHAN, H.; ULLRICH, V. *Eur. J. Biochem.* **1982**, *126*, 583–588.

(112) McLean, M. A.; Maves, S. A.; Weiss, K. E.; Krepich, S.; Sligar, S. G. *Biochem. Biophys. Res. Commun.* **1998**, *252*, 166–172.

(113) Manyumwa, M. E. Resonance Raman Spectroscopy of Isotopically Labeled Cytochrome P450cam and Low Temperature Measurements, 2005.

(114) Segur, J. *Aciscience.Org* **1953**, 1–27.

(115) Richard, M.; McDonald, R. N.; Steppel, R. N.; Dorsey, J. E. *Org. Synth.* **1970**, *50*, 15–16.

(116) Glasoe, P.; Long, F. *J. Phys. Chem.* **1960**, *64*, 188–190.

(117) Sjodin, T.; Christian, J. F.; Macdonald, I. D. G.; Davydov, R.; Unno, M.; Stephen G. Sligar; Brian M. Hoffman,and; Paul M. Champion,. *Biochemistry* **2001**, *40*, 6852–6859.

(118) Jankowski, S.; Kamiński, R. *J. Label. Compd.* **1995**.

(119) Gordon, A. J.; Ford, R. A. *The Chemist's Companion*, John Wiley & Sons, London. 1972; 451.

(120) Perrin, D. D.; Armarego, W. L. F. *Purification of Laboratory chemicals*; 2014.

(121) Schwartz, N. N.; Blumbergs, J. H., *J. Org. Chem.* **1964**, *29*, 1976–1979.

(122) Asada, K.; Badger, M. *Plant cell Physiol.* **1984**.

(123) Hu, S. Resonance Raman structural characterization of cytochrome P450cam and lactoperoxidase, 1991.

(124) Mendelovici, E.; Frost, R. L.; Kloprogge, T. *J. Raman Spectrosc.* **2000**, *31*, 1121–1126.

(125) Deary, M. E.; Mousa, S. M.; Martin Davies, D. *J. Incl. Phenom. Macrocycl. Chem.* **2014**, *78*, 127–136.

(126) Denisov, I. G.; Mak, P. J.; Makris, T. M.; Sligar, S. G.; Kincaid, J. R. *J. Phys. Chem. A* **2008**, *112*, 13172–13179.

(127) Piotr J. Mak; Ilia G. Denisov; Doreen Victoria; Thomas M. Makris; Tianjing Deng; Stephen G. Sligar, and; Kincaid, J. R. *J. Am. Chem. Soc.* **2007**, *129*, 6382–6383.

(128) Ibrahim, M.; Denisov, I. G.; Makris, T. M.; James R. Kincaid, A.; Stephen G. Sligar. *J. Am. Chem. Soc.* **2003**, *125*, 13714–13718.

(129) Piotr J. Mak; Ilia G. Denisov; Doreen Victoria; Thomas M. Makris; Tianjing Deng; Stephen G. Sligar, and; Kincaid, J. R. **2007**.

(130) Davydov, R.; Makris, T. M.; Kofman, V.; Werst, D. E.; Sligar, S. G.; Hoffman, B. M. *J. Am. Chem. Soc.* **2001**, *123*, 1403–1415.

(131) Denisov, I. G.; Hung, S. C.; Weiss, K. E.; McLean, M. A.; Shiro, Y.; Park, S. Y.; Champion, P. M.; Sligar, S. G. *J. Inorg. Biochem.* **2001**, *87*, 215–226.

(132) Paeng, K.; Kincaid, R. *Analytical Sciences*, **1994**, *10*, 1993–1995.

APPENDIX

List of Abbreviations

ν(Fe-O)	iron-oxygen stretching mode
δ(Fe-C-O)	iron-carbon-oxygen bending mode
Cam	Camphor
CCD	Charge coupled device
CYP	Cytochrome P450
CPO	Chloroperoxidase
HRP	Horseradish peroxidase
EPR	Electron paramagnetic resonance
NMR	Nuclear magnetic resonance
rR	resonance Raman
LA	Lauric acid
PFDA	perfluorodecanoic acid
mCPBA	m-Chloroperoxybenzoic acid
SB	Substrate bound
SF	Substrate free
P450cam	Cytochrome P450cam (CYP101)
PDB	Protein data bank
HF	High frequency
HS	High spin
LS	Low spin
LF	Low frequency

Solution preparations and recipes

LB Medium

Per Liter

- 10 g Tryptone
- 5 g Yeast extract
- 10 g NaCl

For LB Plate, 35g bacto-agar was dissolved in 1L of highly polished water and 40 plates made from this solution.

2YT Medium

Per Liter

- 16 g Tryptone
- 10 g Yeast extract
- 5 g NaCl

Terrific broth (TB) Medium

Per Liter

- 12 g Tryptone
- 24 g Yeast extract
- 4 mL glycerol

Dissolve in 900 mL of highly polished water- autoclave

- 12.54 g K_2HPO4
- 2.32 g KH_2PO4

Dissolve in 100 mL of water-autoclave

Mix after autoclave and add 50mg ampicillin and 50mg chloramphenicol after cooling.

50x TAE buffer

Per Liter

- 242 g Tris base
- 57.1 mL of 100% acetic acid
- 100 mL of 0.5 M sodium EDTA
- Make up to the mark with DI water

To make 1x TAE buffer dilute 20mL of 50x TAE with 980mL of DI water.

2D6 Running buffer (500 mM PB, pH 7.4)

250 mL……. Highly polished water

3.9 g……. Monosodium phosphate monohydrate

25.9 g……. Disodium phosphate, heptahydrate

20 % glycerol (v/v)

195mg……β-mercaptoethanol (10 mM)

2.15 g……. CHAPS (14 mM)

43.5 mg……phenylmethylsulfonylfluoride (PMSF)

2D6 Elution buffer (10 mM PB, pH 7.4)

250 mL……. Highly polished water
0.078 g……. Monosodium phosphate monohydrate
0.519…… Disodium phosphate, heptahydrate
20 % glycerol (v/v)
1.16 g……. Histidine (30 mM)
14.61 g……NaCl (1 M)
2.15 g……. CHAPS (14 mM)
195 mg……. β-mercaptoethanol (10 mM)
43.5 mg……phenylmethylsulfonylfluoride (PMSF)

1.5 **Stock Solutions**

- 1 M Tris Chloride (157.56)- dissolve 157.6 g of Tris-HCl and make up to 1 L
- 1 M Tris base (121.14 g/mol)- dissolve 121.14 g of tris base and make up to 1 L with highly polished water
- 1 mM Camphor (152.23 g/mol)- dissolve 152.23 g in 1L water
- 1 M IPTG (238.3 g/mol)- dissolve 11.91 g IPTG in 50 mL of water
- 10 mM PMSF (174.19 g/mol)- dissolve 87 mg in 50 mL of propanol
- 100 mg/mL ampicillin (349.406)- dissolve 1 g of ampicillin in 10 mL of water
- 100 mg/mL Chloramphenicol (323.13)- dissolve 1 g chloramphenicol in 10 mL of ethanol
- 20 mg/mL ALA- dissolve 200 mg of ALA in 10 mL of water
- 5 mg/mL antipain- dissolve the 5 mg in 5 mL of highly polished water
- 1 M Aminolevulinic acid (167.59 g/mol) - dissolve 1.006 g of ALA and make up to 6 mL.